Titre: Title:	Modélisation et simulation de pyrolyse de pneus usagés dans des réacteurs de laboratoire et industriel
Auteur: Author:	Jean-Rémi Lanteigne
Date:	2014
Type:	Mémoire ou thèse / Dissertation or Thesis
Référence: Citation:	Lanteigne, J.-R. (2014). Modélisation et simulation de pyrolyse de pneus usagés dans des réacteurs de laboratoire et industriel [Ph.D. thesis, École Polytechnique de Montréal]. PolyPublie. https://publications.polymtl.ca/1456/

UNIVERSITÉ DE MONTRÉAL

MODÉLISATION ET SIMULATION DE PYROLYSE DE PNEUS USAGÉS DANS DES RÉACTEURS DE LABORATOIRE ET INDUSTRIEL

JEAN-RÉMI LANTEIGNE

DÉPARTEMENT DE GÉNIE CHIMIQUE

ÉCOLE POLYTECHNIQUE DE MONTRÉAL

THÈSE PRÉSENTÉE EN VUE DE L'OBTENTION

DU DIPLÔME DE PHILOSOPHIAE DOCTOR

(GÉNIE CHIMIQUE)

JUIN 2014

UNIVERSITÉ DE MONTRÉAL

ÉCOLE POLYTECHNIQUE DE MONTRÉAL

Cette thèse intitulée :

MODÉLISATION ET SIMULATION DE PYROLYSE DE PNEUS USAGÉS DANS DES RÉACTEURS DE LABORATOIRE ET INDUSTRIEL

présentée par : LANTEIGNE Jean-Rémi

en vue de l'obtention du diplôme de : Philosophiae Doctor

a été dûment acceptée par le jury d'examen constitué de :

M. TAVARES Jason-Robert, Ph.D., président

M. CHAOUKI Jamal, Ph.D., membre et directeur de recherche

M. DOUCET Jocelyn, Ph.D., membre

M. BRIENS Cédric Louis, Ph.D., membre

DÉDICACE

À ma merveilleuse épouse, Katia

et à mes deux enfants chéris, Benjamin et Juliette.

REMERCIEMENTS

Je voudrais tout d’abord remercier mon directeur de recherche, le professeur Jamal Chaouki. Il m’a toujours poussé à me dépasser, à sortir de ma zone de confort. Durant les méandres de mon parcours doctoral, il a fait preuve d’une grande compréhension. Je lui suis reconnaissant et je me considère privilégié d’avoir pu faire partie de son équipe de recherche.

Je tiens à souligner la grande collaboration de Jean-Philippe Laviolette. Jean-Philippe m’a conseillé judicieusement au cours de la rédaction et a travaillé très fort pour assurer la qualité des publications. Merci pour ta patience et ton temps précieux.

RÉSUMÉ

La présente thèse couvre une étude appliquée sur la pyrolyse des pneus. L'objectif global est de développer des outils pour permettre la prédiction de la production et de la qualité de l'huile de pyrolyse des pneus.

Le premier objectif de recherche consistait à modéliser la cinétique de pyrolyse des pneus dans un réacteur, en l'occurrence un tambour rotatif industriel opérant en mode batch. Une revue de littérature effectuée ultérieurement a démontré que la quasi-totalité des modèles cinétiques développés pour représenter la pyrolyse des pneus ne parvenait pas à représenter avec suffisamment de précision le procédé industriel à l'étude.

Parmi les familles de modèles cinétiques pour la pyrolyse, trois ont été identifiées : modèle à une seule réaction globale, modèle à plusieurs réactions parallèles combinées linéairement et modèle à plusieurs réactions en série et/ou en parallèle. Il a été remarqué que ces modèles ont des limites. Dans les modèles à réaction globale et à plusieurs réactions en parallèle, la production de chaque produit pyrolytique individuel ne peut être prédite, mais seulement pour les volatiles combinés. De plus, le terme massique de la cinétique se réfère à la quantité de char finale (W_∞), qui varie en fonction des conditions de pyrolyse, ce qui rend ces modèles beaucoup moins robustes. Aussi, malgré le fait que les modèles à plusieurs réactions en série et/ou parallèle puissent prédire le taux de production de chaque produit de la pyrolyse, les sélectivités sont déterminées pour des températures d'opération et non des températures réelles de masse, ce qui génère des modèles dont l'ajustement des paramètres fait défaut lorsqu'utilisé à l'échelle industrielle.

Un nouveau modèle cinétique a été développé, permettant de prédire le taux de production de gaz non-condensable, d'huile et de char provenant de la pyrolyse des pneus. La nouveauté de ce modèle est la considération des sélectivités intrinsèques de chaque produit en fonction de la

température. Cette hypothèse a été considérée valide assumant que dans le procédé industriel de pyrolyse, la cinétique de pyrolyse est limitante.

Le modèle développé considère des cinétiques de production individuelles pour chacun des trois produits pyrolytiques proportionnelles à une cinétique de décomposition globale des pyrolysables. Les simulations avec des données obtenues en opération industrielle ont démontré la robustesse du modèle à prédire avec précision en régime transitoire, la pyrolyse des pneus, à l'aide de paramètres du modèle obtenus à l'échelle du laboratoire, nommément en ce qui a trait au début de la production, le temps de résidence des pneus (production dynamique) et de la quantité d'huile produite (rendement cumulatif). Il s'agit d'une toute nouvelle façon de modéliser la pyrolyse qui pourrait être extrapolée à de nouvelles matières premières.

Le deuxième objectif de cette recherche doctorale était de déterminer l'évolution de la chaleur spécifique des pneus pendant la pyrolyse et l'enthalpie de pyrolyse. L'origine de cet objectif provient d'une contradiction primaire. Outre quelques exceptions, il est admis que la pyrolyse des matières organiques est globalement un phénomène endothermique. À l'opposé, toutes les expériences menées à l'aide d'appareils de laboratoire tels la DSC (Differential Scanning Calorimetry) ont montré des pics exothermiques durant les expériences dynamiques (rampe de température constante). Cela a été confirmé par les résultats obtenus à l'échelle industrielle, où aucune trace d'exothermicité n'a été observée. La loi de Hess a aussi confirmé ces résultats, à savoir que globalement, la pyrolyse est bel et bien un processus entièrement endothermique. Un bilan d'énergie précis est requis pour prédire la température des pneus durant la pyrolyse, paramètre indissociable de la cinétique.

Une investigation approfondie du char a permis dans un premier temps de démontrer que la chaleur spécifique des solides au cours de la pyrolyse décroît en fonction de la température jusqu'à l'atteinte du pic de perte de masse en décomposition, vers 400°C, pour ensuite remonter. Ce constat, combiné au fait que l'échantillon perd de sa masse au cours de la pyrolyse est

considéré comme la principale cause de l'apparition du pic exothermique dans les expériences de laboratoire. C'est-à-dire que le système de contrôle de ces appareils provoque un biais et une surchauffe involontaire des échantillons leur conférant un comportement exothermique. Il s'agirait donc d'un artéfact.

Sur la base des nouvelles données sur l'évolution de la chaleur spécifique globale en pyrolyse, un modèle du bilan d'énergie a été développé à l'échelle industrielle pour déterminer l'enthalpie de pyrolyse. La simulation a montré que la majeure partie de la chaleur transférée à la masse décomposée servait à augmenter sa température. Ensuite, une enthalpie de pyrolyse dépendante de la perte de masse a été obtenue. Enfin, deux autres termes d'enthalpie ont été trouvés, nommément une enthalpie pour le bris des ponts soufrés et une enthalpie pour la stabilisation du char lorsque la conversion approche la complétion.

Cette recherche aura permis d'établir une nouvelle méthodologie générale pour déterminer l'enthalpie de pyrolyse. Plus particulièrement, de nouveaux éclaircissements ont été obtenus quant à l'évolution de la chaleur spécifique de la masse lors de la pyrolyse et de nouvelles enthalpies de pyrolyse, toutes endothermiques, ont pu être obtenues, en accord avec les attentes théoriques.

Le troisième objectif de recherche concernait le comportement du soufre lors de la pyrolyse des pneus. Avec comme prémisse que le soufre est un contaminant intrinsèque de plusieurs résidus à valoriser, il est critique d'en clarifier le devenir lors de la pyrolyse, dans le cas présent des pneus usagés. De la littérature est ressorti que certaines analyses quantitatives avaient été présentées, mais de façon généralisée, les mécanismes de distribution du soufre parmi les produits pyrolytiques demeurent flous. Ainsi, il n'était pas possible de prédire le transfert du soufre vers chacun des produits de la pyrolyse des pneus.

Les résultats tirés de la littérature ont été complémentés par une série d'expériences en TGA, suivies d'analyses élémentaires complètes pour les résidus solides. Des bilans de matière ont été effectués afin de caractériser la distribution des différents éléments parmi les trois produits (gaz non-condensable, huile et char). Un tout nouveau paramètre a été créé lors de cette recherche : la sélectivité pour la perte du soufre. Cette sélectivité intrinsèque est une prédiction de la répartition du soufre dans les produits de la pyrolyse en fonction de la température.

Trois phénomènes ont été identifiés pouvant affecter la sélectivité pour la perte du soufre. Tout d'abord, la volatilisation naturelle du soufre due à la pyrolyse. Ensuite, la volatilisation du soufre due à la désulfuration de la matrice solide par l'hydrogène et enfin, la séquestration du soufre à l'état solide due à la sulfuration des métaux (zinc et fer). Les résultats ont démontré que cette sélectivité atteint la valeur limite de 1 dans des conditions où la pyrolyse est limitée par la cinétique et en l'absence de métaux. Lorsque le transfert de matière est limitant à faible température (<350°C), la sélectivité dépassera 1. À une température supérieure à 350°C en présence de métaux, la sélectivité sera inférieure à 1.

Il s'agit d'un outil très utile pour les procédés de pyrolyse industrielle, étant un nouvel indicateur pour la distribution des contaminants lors de la pyrolyse des résidus. Une meilleure compréhension de ces mécanismes permet d'élaborer une meilleure stratégie lors du design de ces procédés industriels. Par exemple, à la lumière de cette recherche, il pourrait être préférable de prétraiter les pneus à basse température pour éliminer une quantité significative du soufre avant de les soumettre à une pyrolyse à température élevée. Les produits pyrolytiques résultants nécessiteraient alors un post-traitement de purification moins intensif, plus efficace et plus économique.

ABSTRACT

The present thesis covers an applied study on tire pyrolysis. The main objective is to develop tools to allow predicting the production and the quality of oil from tire pyrolysis.

The first research objective consisted in modelling the kinetics of tires pyrolysis in a reactor, namely an industrial rotary drum operating in batch mode. A literature review performed later demonstrated that almost all kinetics models developed to represent tire pyrolysis could not represent the actual industrial process with enough accuracy. Among the families of kinetics models for pyrolysis, three have been identified: models with one single global reaction, models with multiple combined parallel reactions, and models with multiple parallel and series reactions. It was observed that these models show limitations. In the models with one single global reaction and with multiple parallels reactions, the production of each individual pyrolytic product cannot be predicted, but only for combined volatiles. Morevoer, the mass term in the kinetics refers to the final char weight (W_∞) that varies with pyrolysis conditions, which yields less robust models. Also, despite the fact that models with multiple parallels and series reactions can predict the rate of production for each pyrolysis product, the selectivities are determined for operating temperatures instead of real mass temperatures, giving models for which parameters tuning is not adequate when used at the industrial scale.

A new kinetics model has been developed, allowing predicting the rate of production of non-condensable gas, oil, and char from tire pyrolysis. The novelty of this model is the consideration of intrinsic selectivities for each product as a function of temperature. This hypothesis has been assumed valid considering that in the industrial pyrolysis process, pyrolysis kinetics is limiting.

The developed model considers individual kinetics for each of the three pyrolytic products proportional to the global decomposition kinetics of pyrolysables. The simulation with data obtained in industrial operation showed the robustness of the model to predict with accuracy in

transient regime, tires pyrolysis, with the help of model parameters obtained at laboratory scale, namely in regards of the trigger of production, the residence time of tires (dynamic production) and the amount of oil produced (cumulative yield). It is a novel way to model pyrolysis that could be extrapolated to new waste materials.

The second objective of this doctoral research was to determine the evolution of specific tires specific heat during pyrolysis and the enthalpy of pyrolysis. The origin of this objective comes from a primary contradiction. With few exceptions, it is acknowledged that organic materials pyrolysis is globally an endothermic phenomenon. At the opposite, all experiments led with laboratory apparatuses such as DSC (Differential Scanning Calorimetry) showed exothermic peaks during dynamic experiments (constant heating rate). It has been confirmed by results obtained at the industrial scale, where no sign of exothermicity has been observed. The Hess Law has also confirmed these results, that globally, pyrolysis is indeed a completely endothermic process. An accurate energy balance is required to predict mass temperature during pyrolysis, this parameter being unbindable from kinetics.

An advanced investigation of char first allowed demonstrating that specific heat of solids during pyrolysis decreases with increasing temperature until the weight loss peak is reached, around 400°C, and then starts increasing again. This observation, combined with the fact that the sample loses weight during pyrolysis is considered as the major cause of the apparition of an exothermic peak in laboratory scale experiments. That is, the control system of these apparatuses generates a bias and an unavoidable overheat of the samples producing this exothermic behavior. It would thus be an artifact.

On the base of new data on the evolution of global specific heat during pyrolysis, a model of the energy balance has been developed at the industrial scale to determine the enthalpy of pyrolysis. The simulation has shown that a major part of the heat transferred to the pyrolized mass would make its temperature increase. Next, an enthalpy of pyrolysis dependent of weight loss was

obtained. Finally, two other terms of enthalpy have been found, namely an enthalpy for the breakage of sulfur bridges and an enthalpy for the stabilization of char when conversion approaches completion.

This research will have allowed establishing a novel general methodology to determine the enthalpy of pyrolysis. More particularly, new clarifications hasve been obtained in regards to the evolution of specific heat of solids during pyrolysis and new enthalpies of pyrolysis, all endothermic, could be obtained, in agreement with the theoretical expectations.

The third research objective concerned the behavior of sulfur during tires pyrolysis. With as a premise that sulfur is an intrinsic contaminant of many types of waste, it is critical to clarify its fate during pyrolysis, in the present case for waste tires. It has been observed in the literature that some quantitative analyses had been presented, but generally, the mechanisms for the distribution of sulfur within the pyrolytic products remain unclear. Thus, it was then not possible to predict the transfer of sulfur to each of the tire pyrolysis products.

The results taken form literature have been complemented with a series of TGA experiments followed by complete elemental analyses of the residual solids. Mass balances have been performed in order to characterize the distribution of elements within the three products (non-condensable gas, oil, and char). A novel parameter has been created during this research: the sulfur loss selectivity. This intrinsic selectivity is a prediction of the distribution of sulfur within the pyrolysis products as a function of temperature.

Three phenomena has been identified that could affect the sulfur loss selectivity. First, the natural devolatilization of sulfur due to pyrolysis. Next, the sulfur devolatilization due to the desulfurization of the solid matrix by hydrogen and finally, the clustering of sulfur in the solid state due to metal sulfidation (zinc and iron). The results have shown that this selectivity reach a limit value of 1 when pyrolysis is limited by the kinetics and in the absence of metal. When the

mass transfer is limiting at low temperature (<500°C) the selectivity will be greater than 1. At a temperature over 350°C with the presence of metals, the selectivity will be lower than 1.

It is a useful tool for industrial pyrolysis processes, being a novel indicator for the distribution of contaminants during the pyrolysis of waste. A better comprehension of these mechanisms allows elaborating a better strategy when designing these industrial processes. For example, in light of this research, it could be preferable to pre-treat the tires at lower temperature to eliminate a significant part of sulfur before pyrolyzing them at high temperature. The resulting pyrolytic products would then necessitate a lighter purification post-treatment, being more efficient and more economical.

TABLE DES MATIÈRES

LISTE DES TABLEAUX

LISTE DES FIGURES

LISTE DES SIGLES ET ABRÉVIATIONS

CHAPITRE II

A = Pre-exponential factor [=] s-1 for a 1st order reaction

d = Diameter

E = Activation energy [=] Jmol-1

Fr = Froude number

g = Standard gravity [=] m*s-2

h = Heat transfer constant [=] Wm-2K-1

k = Thermal conductivity [=] Wm-1K-1

m = Dimensional & non-dimensional weight

n = Order of reaction, non-dimensional

Nu = Nusselt number

Pr = Prandtl number

R = Universal gas constant OR Radius [=] Jmol-1K-1 OR m

Re = Reynolds number

t = Time

T = Temperature

U = Velocity [=] m*s-1

Symbols

μ = Viscosity [=] Pa*s

ρ = Density [=] kgm-3

ω = Angular velocity [=] s-1

Subscripts

bed = Fluidized bed

bp = Bed of particles (in rotary drums)

g = Gas phase

p = Particle

t = Terminal (velocity)

CHAPITRE III

A	Pre-exponential factor (min^{-1})
C_{Pbed}	Tire shred bed specific heat ($J^{1}kg^{-1}K^{-1}$)
C_{Pchar}	Char heat capacity ($J^{1}kg^{-1}K^{-1}$)
C_{Psteel}	Steel heat capacity ($J^{1}kg^{-1}K^{-1}$)
C_{Ptire}	Tire heat capacity ($J^{1}kg^{-1}K^{-1}$)
E_a	Activation energy ($J^{1}mol^{-1}$)
Fr	Froude number
g	Gravity constant ($m^{1}s^{-2}$)
h	Average thermal convection coefficient ($W^{1}m^{-2}K^{-1}$)
H_{pyr}	Heat consumed by pyrolysis ($J^{1}min^{-1}$)
k	Kinetics constant (min^{-1})
m	Mass (kg)
m_{bed}	Mass of bed (kg)
m_{char}	Mass of char (kg)
m_o	Initial mass (kg)

$m_{pyrolysis}$ Mass of converted pyrolysables (kg)

m_{steel} Mass of steel (kg)

m_{tire} Mass of tire sample (kg)

$m_{tire\_initial}$ Mass of initial tire sample (kg)

$m_{volatiles}$ Mass of generated volatiles (kg)

m_{∞} Mass of residual solids at 100% conversion (kg)

$M_{reactant}$ Dimensionless weight

n Order of reaction

r_{char} Reaction rate (min^{-1})

$r_{devolatilization}$ Rate of devolatilization (min^{-1})

r_{gas} Rate of formation of pyrolysis gas (min^{-1})

r_i Rate of formation of pyrolysis product *i* (min^{-1})

r_{oil} Rate of formation of pyrolysis oil (min^{-1})

$r_{products}$ Rate of formation of pyrolysis products (min^{-1})

$r_{pyrolysis}$ Rate of pyrolysis (min^{-1})

$r_{volatiles}$ Rate of production of volatiles (min^{-1})

R Perfect gas constant ($J^1mol^{-1}K^{-1}$)

S_{char} Instantaneous char selectivity

S_{gas} Instantaneous gas selectivity

S_i Instantaneous product *i* selectivity

S_{oil} Instantaneous oil selectivity

t Time (min)

T Temperature (K or °C)

T_{wall} Wall temperature (K or °C)

T_{bed} Bed temperature (K or °C)

W_{exp} Tire shred bed surface exposed the drum wall (m^2)

Greek letters

ω Rotational speed (s^{-1})

CHAPITRE IV

c_{pan} Heat capacity of the pan in DSC

C_{Pbatch} Tire batch specific heat ($J^1kg^{-1}K^{-1}$)

C_{Pchar} Char heat capacity ($J^1kg^{-1}K^{-1}$)

C_{Psteel} Steel heat capacity ($J^1kg^{-1}K^{-1}$)

C_{Ptire} Tire heat capacity ($J^1kg^{-1}K^{-1}$)

C_r Reference side heat capacitance in DSC

C_s Sample side heat capacitance in DSC

h Average thermal convection coefficient

$\dot{H}_{charring}$ Heat consumed by the charring reactions (J^1min^{-1})

$H^3_{charring}$ Constant heat of pyrolysis for the charring reactions (kJ^1kg^{-1})

$\dot{H}_{crosslink}$ Heat consumed by the sulfur crosslinks breakage (J^1min^{-1})

$H^2_{crosslink}$ Constant heat of pyrolysis for the sulfur crosslinks breakage (kJ^1kg^{-1})

$H^0_{formation}$ Standard enthalpy of formation (kJ^1kg^{-1})

$\dot{H}_{pyrolysis}$ Heat consumed by pyrolysis (J^1min^{-1})

$H^1_{pyrolysis\_dmdt}$ Constant heat of pyrolysis (kJ^1kg^{-1})

$m_{active\text{-}sites}$ Mass of active sites for charring (kg)

m_{batch} Mass of batch (kg)

m_{char} Mass of char (kg)

$m_{crosslink}$ Mass of sulfur crosslinks (kg)

m_o Initial mass (kg)

m_{out} Mass of material exiting a system (kg)

m_{pr} Mass of pan on reference side in DSC (mg)

m_{ps} Mass of pan and sample combined (mg)

m_{steel} Mass of steel (kg)

m_{tire} Mass of tire sample (kg)

$\dot{q}_{convection}$ Convection heat flow

$\dot{Q}_{input}$ Heat flow input in a system

$\dot{q}_r$ Heat flow through the reference side in DSC

$\dot{q}_s$ Heat flow through the sample side in DSC

$\dot{q}_{sam}$ Heat flow through the sample in a DSC

$\dot{q}_{sensible\_heat}$ Sensible heat flow

R_p Thermal resistance of pan in DSC

R_r Thermal resistance of reference side in DSC

R_s Thermal resistance of sample side in DSC

t Time (min)

T Temperature (K or °C)

T_{wall} Wall temperature (K or °C)

T_{bed} Bed temperature (K or °C)

T_{ps} Pan and sample temperature in DSC

T_{pr} Reference side pan temperature in DSC

T_r Reference side temperature in DSC

T_s Sample side temperature in DSC

W_{exp} Tire shred bed surface exposed the drum wall (m^2)

CHAPITRE V

A Pre-exponential factor (min^{-1})

E_a Activation energy (J^1mol^{-1})

k Kinetics constant (min^{-1})

m Mass (kg)

$m_{pyrolysis}$ Mass of converted pyrolysables (kg)

m_{tire} Mass of tire sample (kg)

$m_{tire\_initial}$ Mass of initial tire sample (kg)

M_{H2} Hydrogen molecular weight

M_{H2S} Hydrogen sulfide molecular weight

$M_{reactant}$ Dimensionless weight

m_{sulf_0} Initial weight of sulfur

n Order of reaction

P_{H2} Partial pressure of hydrogen

P_{H2S} Partial pressure of hydrogen sulfide

$r_{pyrolysis}$ Rate of pyrolysis

r_{SL} Rate of sulfur loss

r_{TWL} Rate of total weight loss

R Perfect gas constant ($J^{1}mol^{-1}K^{-1}$)

s_{gas} Intrinsic gas selectivity

s_{H2} Intrinsic hydrogen selectivity in non-condensable gas

s_{H2S} Intrinsic hydrogen sulfide selectivity in non-condensable gas

s_{oil} Intrinsic oil selectivity

$s_{SL/TWL}$ Intrinsic sulfur loss selectivity

$S_{SL/TWL}$ Global sulfur loss selectivity

$s^{0}_{SL/TWL}$ Reference intrinsic sulfur loss selectivity

S_{ZnO} Surface of active sites available for sulfidation

t Time (min)

T Temperature (K or °C)

V_{cp} Characteristic pore volume

INTRODUCTION

Le XXIe siècle est ponctué par des niveaux de surconsommation très élevés. Que ce soit au point de vue alimentaire, matériel, technologique ou autre, le fait est que les sites d'enfouissement des déchets se saturent. Les déchets organiques, outre le constat de leur surconsommation, sont bien assimilés par les sols. Pour une majorité d'autres types de résidus, toutefois, on cherche souvent des moyens de leur donner une nouvelle vie, par exemple en tentant d'exploiter leur potentiel chimique et énergétique.

Le XXe siècle a vu des milliers de projets naître et disparaître, motivés par ces problématiques, espérant en tirer profit, de faire d'une pierre, deux coups. Pourtant, la plupart de ces initiatives n'ont pas eu de succès et sont même souvent mortes dans l'œuf. Les causes sont innombrables : défis techniques et technologiques, problèmes de rentabilité dus à la sous-performance, présence importante d'éléments indésirables dans les résidus et donc, dans les produits, etc. Parfois même le choix de technologie était inapproprié pour l'application visée.

Néanmoins, ces difficultés sont facilement justifiables. Les déchets, peu importe leur provenance ou leur nature, ont certains points en commun : composition, taille et format hétérogènes, présence de contaminants (halogénés, métaux, etc.) importante, faible densité géographique, sont des caractéristiques intrinsèques aux résidus qu'il faut considérer lors de la conception de nouvelles technologies visant à les valoriser.

Parmi les candidats résidus notables, les pneus usagés cadrent très bien avec cette description. Intrinsèquement, les pneus contiennent du soufre et du zinc. Ils sont récoltés entiers et doivent souvent être réduits en charpie pour être récupérés. Dû à leur utilisation sur des véhicules, plusieurs contaminants inorganiques peuvent s'ajouter à cela, suite à leur contact prolongé avec le sol et les routes : alcalins, alcalino-terreux, halogénés et autres. Malgré le fait que certaines

nouvelles technologies permettent de nos jours de retirer la structure d'acier des pneus, il peut être, dans certaines circonstances, souhaitable de ne pas le faire.

Il existe dans le monde des centaines de dépotoirs à pneus usagés, à ciel ouvert, dont plusieurs sont ont été ou sont actuellement la proie d'incendies permanents. De tels événements ont été répertoriés depuis les années 1980, où parfois plus de 10 millions de pneus sont brûlés. Cela a été le cas en 1999, où dans l'état Américain de l'Ohio, un incendie de plus de 25 millions de pneus a causés d'importants dommages environnementaux[1]. De ces accidents ont émané des quantités importantes d'oxydes de soufre et d'azote, ainsi que des particules fines. Les températures élevées ont favorisé la volatilisation de métaux lourds, tels l'arsenic et le plomb. Les pneus ayant été brûlés avec peu d'oxygène, des goudrons issus de la pyrolyse des pneus ont été libérés dans le sol.

Ces situations demeurent difficiles à éviter principalement à cause de la génération accrue de ces pneus usagés. En effet, il était estimé en 2009 que 5 millions de tonnes de pneus usagés étaient produits aux États-Unis seulement, comme le rapportait la Rubber Manufacturers Association. Environ 15 % de ces pneus se retrouvent dans ces dépotoirs, 12 % des pneus sont enfouis dans le sol, approximativement 30 % sont réutilisés dans des applications commerciales, alors que plus de 40 % des pneus usagés deviennent un carburant dérivé (Tire Derived Fuel, TDF).

Parmi les consommateurs de pneus comme TDF, les cimenteries les alimentent entiers dans des incinérateurs rotatifs, dont les longueurs dépassent parfois les 100 m. Les pneus y sont brûlés à très haute température, générant des niveaux de polluants, tels ceux mentionnés plus haut, au-delà des normes environnementales.

---

[1] Site web de l'EPA, url : http://www.epa.gov/region5/waste/solidwaste/tires/miforum/large.pdf.

Pour remédier à cette réalité, l'alternative la plus intéressante, pour des applications énergétiques, est la pyrolyse. Le but de cette opération est de produire un combustible plus propre et plus facile à transporter. La pyrolyse des pneus génère essentiellement trois produits : un gaz combustible non-condensable, une huile combustible, possédant des caractéristiques communes avec certaines coupes du raffinage du pétrole, et enfin une poudre de carbone, souvent appelée char. La pyrolyse est une décomposition purement thermique se déroulant en l'absence d'oxygène. Elle se produit à des températures plus basses que l'incinération et la gazéification. Par conséquent, les risques d'évaporation ou de sublimation des métaux, en particulier du zinc, sont grandement réduits.

Puisqu'il n'y a pas d'air présent en pyrolyse, on pourrait la qualifier de prétraitement visant à transformer les pneus afin de purifier et concentrer leur contenu énergétique. Cependant, il a aussi été démontré que la pyrolyse des pneus pouvait, dans certaines situations, produire des quantités significatives de limonène, de toluène, de styrène, de xylène et autres composés chimiques d'intérêt, conférant à la pyrolyse des pneus usagés le potentiel élevé de devenir une application à haute valeur ajoutée.

Toutes ces avenues de valorisation ont captivé l'intérêt des chercheurs et des industriels, qui ont fait de la pyrolyse des pneus un véritable pôle de recherche scientifique et appliquée durant la seconde moitié du XXe siècle.

Dans les premiers temps, les rendements de pyrolyse et la composition chimique des produits pyrolytiques étaient le plus souvent étudiés, en fonction des différents paramètres et facteurs pouvant les influencer. Depuis les années 1990, avec l'avènement des technologies informatiques et la volonté de passer efficacement à l'échelle industrielle, les efforts de recherche ont été dirigés vers la modélisation numérique de la pyrolyse.

La présente recherche doctorale est née dans ces réalités. Un client industriel avait déjà solidement démontré le potentiel de sa technologie de pyrolyse des pneus usagés, conçue dès les

années 1970. Néanmoins, la commercialisation de leur procédé pilote s'est vue ralentie par plusieurs défis techniques. Ce projet doctoral a été lancé dans l'optique de faciliter la progression de son développement commercial.

CHAPITRE 1 PRÉSENTATION DES ÉTAPES DE LA RECHERCHE

Afin d'optimiser l'opération et d'automatiser l'usine, un modèle cinétique de la pyrolyse a été requis. Dès ce premier objectif, il a été possible de détecter de façon généralisée, l'écart notable entre les recherches réalisées en laboratoire et les besoins de cette industrie naissante.

Entre autres constats, la très grande majorité des modèles cinétiques sont développés pour des conditions très peu similaires au contexte industriel. De ce fait, les modèles tirés de la littérature n'ont pas permis de représenter adéquatement l'opération du procédé pilote de pyrolyse des pneus usagés. D'autres recherches dans la littérature ont mis en évidence les mêmes problématiques pour le bilan d'énergie de la pyrolyse et le comportement du soufre.

Pour un procédé énergétique où la connaissance précise de la température est critique, et de surcroît vu la normalisation étroite dont font l'objet les combustibles hydrocarbures pouvant être issus de la pyrolyse quant à leur teneur en soufre, les deuxième et troisième objectifs de ce doctorat sont devenus plus évidents et d'une continuité naturelle avec le premier.

De façon plus globale, le but de ce projet de doctorat a été de produire des outils appliqués pour prédire la production et la qualité de l'huile de pyrolyse des pneus.

En résumé, les objectifs spécifiques de cette thèse sont :

1. Modéliser la cinétique de la pyrolyse des pneus pour un procédé industriel en mode batch, afin de prédire quantitativement et dynamiquement la production de char, d'huile pyrolytique et de gaz non-condensable.

2. Étudier le comportement thermodynamique des pneus en pyrolyse pour caractériser l'évolution de la capacité calorifique et de déterminer l'enthalpie de pyrolyse des pneus, en s'appuyant sur des données de laboratoire et des données industrielles.
3. Investiguer le comportement du soufre lors de la pyrolyse des pneus afin de comprendre et les mécanismes et phénomènes derrière sa migration au sein des trois produits pyrolytiques et de déterminer un état de référence pour la distribution du soufre.

Cette thèse de doctorat est présentée en cinq chapitres, le premier étant celui-ci présentant les étapes de la recherche. Le Chapitre 2 expose une revue de littérature complète ayant été révisée par un comité de pairs ainsi qu'une revue critique de la littérature centrée sur les trois objectifs spécifiques. Le Chapitre 3 présente le modèle cinétique de pyrolyse appliqué à un procédé industriel et concerne donc le premier objectif spécifique. Le Chapitre 4 montre un nouveau bilan d'énergie pour la pyrolyse des pneus et concerne le deuxième objectif spécifique. Le Chapitre 5 discute le comportement du soufre lors de la pyrolyse des pneus et couvre le troisième objectif spécifique.

Le Chapitre 6 contiendra une discussion générale sur les résultats obtenus dans le cadre de ce projet doctoral.

CHAPITRE 2 REVUE DE LA LITTÉRATURE : ACQUISITION D'UNE BASE DE CONNAISSANCES

Ce chapitre de livre intitulé « Pyrolyis », a été publié dans le livre « Biomass Pre-treatments for Biorefinery Applications » en 2013, aux Éditions Springer, pages 197-227. Cette publication a été révisée par un comité de pairs.

2.1 PRÉSENTATION DE LA PUBLICATION

Puisque cette recherche se fait de concert avec l'étude d'un procédé industriel, une revue de littérature complète est requise. Un livre portant sur les prétraitements de la biomasse pour les bioraffineries nécessitait un chapitre couvrant la pyrolyse. Celui-ci a été révisé par un comité de pairs, comptant donc comme une publication officielle dans le cadre actuel de ce doctorat. Ce chapitre de livre a été structuré de façon à présenter à la fois l'état de la recherche scientifique.

La première section expose les propriétés des différents types de biomasse. La deuxième section montre les familles de modèles cinétiques retrouvés dans la littérature scientifique ainsi que leurs avantages et inconvénients. La troisième section explique les sortes de pyrolyse en fonction de leur vitesse caractéristique. La quatrième section présente des technologies de réacteur sélectionnées pour la pyrolyse de la biomasse ainsi que des exemples de procédés commerciaux en développement. Enfin, la cinquième section discute de points clés à considérer pour l'optimisation des procédés industriels de pyrolyse.

BIOMASS PRE-TREATMENTS FOR BIOREFINERY APPLICATIONS: PYROLYSIS

Chapter 11 - Biomass Pre-Treatments for Biorefinery Applications: Pyrolysis

Jean-Remi Lanteigne, Jean-Philippe Laviolette and Jamal Chaouki*

Chemical Engineering Department, École Polytechnique de Montréal, C.P. 6079, succ. Centre-Ville, Montréal, Qc, Canada H3C 3A7

*Corresponding Author (jamal.chaouki@polymtl.ca)

2.2 BIOMASS PRE-TREATMENTS FOR BIOREFINERY APPLICATIONS: PYROLYSIS

2.2.1 ABSTRACT

Biorefineries are small integrated plants aiming at the recovery of specific biomass wastes via their conversion to high-value biofuels and chemicals. Pyrolysis is among the promising technologies to achieve this goal. Three major factors influence the development of a pyrolysis process: the type of biomass, the process operating conditions and the choice of reactor technology. In this chapter, pyrolysis as a solution to sustain biorefineries is reviewed. The chapter first discusses the various biomass feedstock and their important characteristics. Secondly, the pyrolysis concepts and kinetics are reviewed in light of their importance in process design and modelling. The chapter also discusses the influence of several process conditions and reactor technologies on the pyrolysis reaction and pyrolysis products behaviour. Finally, strategies for product optimization and to avoid purity issues are analyzed. The emphasis of this chapter is put on technologies that have been developed at commercial scale.

Keywords: Biomass, Pyrolysis, Biorefinery, Pre-treatments, Bio-oil, Bio-char, Kinetics, Hydrodynamics.

2.2.2 INTRODUCTION

At the present day, various technologies are presented as feasible to sustain biorefineries [1, 2]. Two main pathways are often highlighted: the thermochemical [3, 4] and the biochemical pathways [5]. Thermochemical pathways involve the decomposition of matter at high temperature in the absence (pyrolysis) or presence (gasification) of oxygen. On the other hand, single and multi-step alcoholic fermentation are the main focus of biochemical process development and involve the digestion of matter by microorganisms.

The development of both thermochemical and biochemical processes face many challenges. Cellulose fermentation processes are characterized by slow reaction rates and low overall yield for non-genetically modified microorganisms [5]. On the other hand, reaching high yield and selectivity remains an issue for both gasification and pyrolysis [4]. However, the thermochemical pathway offers a significant advantage over biochemical processes: reactions rates are high and offer the potential for high product throughput, which is essential to develop a commercially viable industry. Nevertheless, there is an increasing interest in using both pathways in biorefineries such that their respective advantages are exploited.

Gasification is a multi-step process in the context of biorefineries: it yields a synthesis gas rich in hydrogen and carbon monoxide that requires further synthesis to produce “biorefinables” [6]. The second recombination process is performed at mild temperatures with patented catalysts [3, 6] and achieving high conversion as well as high selectivity remains a challenge to this day.

On the other hand, pyrolysis potentially offers interesting techno-economic advantages over gasification since it is a single-step process operating at lower temperature that yields three products: non-condensable gas, condensable gas (oil) and char. [6]. Pyrolysis processes may therefore require significantly less process equipment compared to gasification. Produced from biomass pyrolysis, bio-char have direct applications as activated carbon [7]. Furthermore, bio-oil can be further refined to produce specialty chemicals and/or biofuels in dedicated plants (biorefineries) that this chapter will discuss in more details.

Together with products market value, the operating scale also determines the feasibility of biomass pyrolysis and gasification pathways for biomass pre-treatments for biorefineries. It has been repeatedly demonstrated that gasification is sustainable at very large scale. However, considering that biomass availability is geographically limited, pyrolysis may be better suited for smaller distributed biorefineries. This chapter will discuss biomass pre-treatments for pyrolysis processes as well as pyrolysis as a pre-treatment for further biorefining. The pyrolysis process products and operability depend on several factors including (1) the type of biomass (chemical and physical characteristics), (2) the pyrolysis process operating conditions and (3) the type of reactor (gas/solid hydrodynamics and heat/mass transfer).

2.2.3 TYPES OF BIOMASS

Most of the biomass feedstocks can be classified in three families as defined by the U.S. Department of Energy [8]: Forestry, Agriculture and Municipal. Table 2.2.1 summarizes key chemical and physical characteristics of the main feedstocks that are considered for biorefineries.

Table 2.2.1 Summary of available biomass feedstock for biorefineries

	Biomass family	**Forestry/Pulp & Paper**			**Agriculture**			**Municipal**	
	Feedstock	Bark & wood residue	Black liquor	Perennial crops	Corn & grains	Oilseeds & plants	Manures	MSW (RDF)	Municipal biosolids
Elemental composition (dry wt%)	C	50-55	30-35	40-55	N/A	60-65	35-40	40-45	40-50
	H	5-7.5	4-6	5-7.5	N/A	7.5-10	5-7.5	5-7.5	5-7.5
	O	40-45	35-40	30-45	N/A	20-25	30-35	35-40	25-35
	N	0.5-1	trace	3-5	N/A	3-5	2-5	<1	<1
	S	trace	1-2	<1	N/A	trace	<1	<1	<1
	Inorganics/trace	3.5-4 (bark)	20-25 (sodium)	3-6	N/A	5-7.5	20-25	10-15	25-35
Molecular composition (dry wt%)	Cellulose	40-45	N/A	30-35	4-5	10-20	N/A	60-70	N/A
	Hemicellulose	25-35	N/A	20-40	4-5	10-20	N/A	10-15	N/A
	Lignin	25-35	N/A	5-20	-	-	N/A	2-5	N/A
	Starch	-	N/A	-	75-77	10-20	N/A	-	N/A
	Extractibles	3-15	N/A	10-20	12-15	40-50	N/A	2-5	N/A
	Inorganics/trace	3.5-4 (bark)	N/A	3-6	1.5-2.5	5-10	N/A	10-15	N/A
	Moisture (wt%)	20-80	40-50	10-70	10-20	5-15	20-70	15-20	5-98
	References	[9, 10, 11]	[12]	[10]	[10]	[13, 14]	[10]	[10, 15]	[14]

Note 1: Wood energy crops as per bark & wood residue

Note 2: Agricultural crops as per perennial crops

Through the conservation of mass, the biomass chemical composition determines the chemical elements present in the 3 pyrolysis products: non-condensable gas, condensable gas and char. The presence of specific chemical elements in each product fractions is determined by the pyrolysis conditions.

Environmental and purity standards restrict the presence of oxygen, nitrogen, sulphur and inorganics in the pyrolysis products. During pyrolysis, the tendency of producing an aqueous phase generally increases with increasing biomass oxygen fraction (dry weight) since water is produced [16]. The presence of oxygen may also lead to the production of acids, which are detrimental to the oil stability. On the other hand, sulfur and nitrogen are not present in biomass in large amounts as shown in Table 2.2.3, but they will nonetheless be present in the products. In this case, the pyrolysis products may need post-treatment since sulphurous compounds are corrosive, while nitrogen affects reactivity as well as pollutant emissions (fuel-bound NOX, for example). Moreover, these species are also problematic when performing bio-oil upgrade. Finally, inorganics in the biomass and pyrolysis products may represent a risk of slagging and sintering.

Furthermore, the biomass physical properties strongly influence the gas/solid hydrodynamics as well as the heat/mass transfer in the pyrolysis reactor such that it affects the pyrolysis products (respective yield of the three pyrolysis products & their composition). The important physical properties include: the shape of the biomass feedstock, its particle size and moisture fraction. These properties will determine the required biomass physical transformations or pre-treatments.

2.2.3.1 Biomass species

2.2.3.1.1 Bark and wood residues from the pulp and paper sector

Forest mills in the United States of America (USA) produced about 86.7 million dry tons of primary mill residues in 2007 [17], which were composed mainly of bark, sawdust, wood chips and shavings. Of this amount, over 35 million dry tons of wood residues was used as

combustibles and could have been used as a feedstock for biorefineries. Wood pyrolysis has been shown to generate high-value products, such as bio-char (promising activated carbon) and bio-oil. Ensyn and DynaMotive are two companies running commercial-scale pilot plants, which convert wood residue via fast pyrolysis. There are many incentives to develop in situ biorefineries (close to pulp and paper plants) in order to avoid significant issues related to transportation and storage.

2.2.3.1.2 Black liquor

Black liquor pyrolysis has been the subject of several studies, but the main efforts have been invested towards gasification. This has been motivated by the fact that black liquor pyrolysis generates too much solid char [18], which would need to be burned to release the inorganics. The advantage of gasification is that it includes the char combustion process. Thus far, pyrolysis has been mostly considered in the scientific literature as a precursor step to gasification. Consequently, it will not be considered as a potential feedstock for pyrolysis aiming at biorefineries.

2.2.3.1.3 Wood energy crops

The idea of cultivating trees strictly for energy and biorefining purposes has been proposed. Certain fast growing tree species such as cottonwood, aspen and eucalyptus can grow at rates of around 1 m per year or even more. The short-rotation woody crop (SRWC) technique can be used to reach yields of about 10 dry metric tons of woody crops per hectare per year can be achieved. However, the economic viability of SRWC is very fragile due to the high costs of preparation and fertilization of the sites [19].

Depending on the maturity of the woody crops, chemical composition will remain close to that of wood and bark (see section 2.2.2.1.1). The main difference will arise due to the leaves and trimmings, which will accumulate dust and metabolic inorganics up to a few mass percent during the trees' growth.

2.2.3.1.4 Perennial herbaceous crops

Perennial crops are vegetal not edible for humans, which include among others: switchgrass, weeping lovegrass and Napier grass. Herbaceous crops are usually dedicated to alcoholic fermentation because of their high available complex sugar content, but pyrolysis of these vegetal has been shown to produce high oil yields [20]. The oil produced contained water-soluble and water-insoluble fractions. Moreover, significant amount of alkanes and phenolic compounds can be found in these oils [21] suggesting a high potential of perennial crops for specialty chemicals production from pyrolysis.

2.2.3.1.5 Corn and grains

Alcoholic fermentation has been the main focus for these feedstocks with bioethanol as its main product. With the current problematic surrounding worldwide food supply, it is not ethically and politically justifiable to use food as a fuel while certain countries suffer famine. However, food conservation and storage may sometimes be very difficult and some considerable amounts of corn and grains may become unfit for human consumption. Nevertheless, considering the high starch content and appreciable fermentation yields with this feedstock, it has been rarely studied in fields other than bioconversion.

2.2.3.1.6 Oilseeds and plants

Contrarily to corn and grains, oilseeds and their plants show very poor starch content. Many species, such as colza, are dedicated to the production of biodiesel. Although biodiesel production has been demonstrated technically feasible at large scale, it is not economically sustainable without government grants or incentives. Several studies on oilseeds and plants pyrolysis can be found in the scientific literature, which indicates a strong interest for this conversion technology. As an example, castor bean slow pyrolysis yields easily over 65 % oil with as low as 20 % solid residue [22]. Due to the high oil yield, there is interest in mixing these oils with diesel to produce blends for transportation fuels. However, for the same reasons that

were brought in section 2.2.3.1.5, these feedstocks should not be diverted from their primary function, namely food supply.

2.2.3.1.7 Agricultural crops and residues

The fruits and vegetables harvest and transformation processes yield many wastes: trimmings, hulls and shells. In 1995, the US Department of agriculture estimated that over 250 million dry tons of agricultural crops and residue were generated over a year in the country [23]. The chemical composition of agricultural crops and residues is very similar to that of perennial herbaceous plants (see section 2.2.3.1.4). The interest in these feedstocks is reflected in the abundant literature found on agricultural crops and residues pyrolysis [24, 25, 26].

2.2.3.1.8 Animal manures

Animal manures are used as fertilizers: their high urea, phosphorus and organics content enrich soils dedicated to agriculture. Cattles are the main manure producers with production of over 200 million dry tons a year in the US (commercial broilers are showing comparable numbers) [23]. Because manure has a heterogeneous composition, thermal decomposition has gained interest to recover that feedstock. Cattle manure is more difficult to collect than poultry manure [10]. Therefore, the poultry manure is considered as a good candidate for industrial pyrolysis and the scientific literature has been mostly focused on this type of manure.

2.2.3.1.9 Municipal solid waste (MSW)

Municipal solid waste (MSW) management has become a major issue worldwide. Issues related to landfilling include: occupation of large areas, generation of greenhouse gases by digestion of the waste, generation of hazardous and refuse materials, etc. New recovery strategies to generate energy, such as incineration, have also given rise to many problems. In Europe, particularly in Germany, rotary kiln incinerators has been extensively studied and issues related to the high temperature have been reported: leaching of metals, emission of carcinogen compounds, emission

of particulate matter, etc. Pyrolysis has been identified as a promising avenue for MSW management: its lower operating temperature and absence of oxygen decrease the pollutant emissions as well as the cost of post-treating flue gases.

2.2.3.1.10 Municipal biosolids

Waste water treatment is a critical process for our society: waste water contains dissolved organics and inorganics as well as suspended solids and microorganisms that must be eliminated before the water can be released into the environment or purified further to be drinkable. The recovered waste forms sewage sludge, which is difficult to recycle. When dried, contaminants such as heavy metals limit its potential applications. Currently, it is common practice to incinerate sewage sludge with the similar disadvantages to MSW incineration (see section 2.2.3.1.9). However, incineration could be replaced by more efficient technologies, such as pyrolysis.

2.2.3.2 Feedstock pre-treatment for pyrolysis

Physical pre-treatments are key to control feedstock properties, which significantly influence gas/solid hydrodynamics as well as heat/mass transfer in the pyrolysis reactor. Recommended feedstock pre-treatments depend on the initial biomass characteristics, the pyrolysis conditions as well as the reactor type. Pre-treatments also allow the homogenization of the feedstock characteristics with time.

Intrinsic feedstock properties such as specific heat, thermal conductivity and density (dry and true) cannot be easily modified and constitute limitations for thermal processes. On the other hand, feedstock moisture and particle size are the main physical parameters that can be adjusted to optimize the pyrolysis process performance.

Particle fluidizabiliy has been correlated to its average size and density. Geldart classified particles into four groups (Geldart class A, B, C and D) based on their fluidization behaviour at ambient conditions [27]. Figure 2.2.1 illustrates the Geldart classification of powders and indicates the properties of common feedstocks for biorefineries.

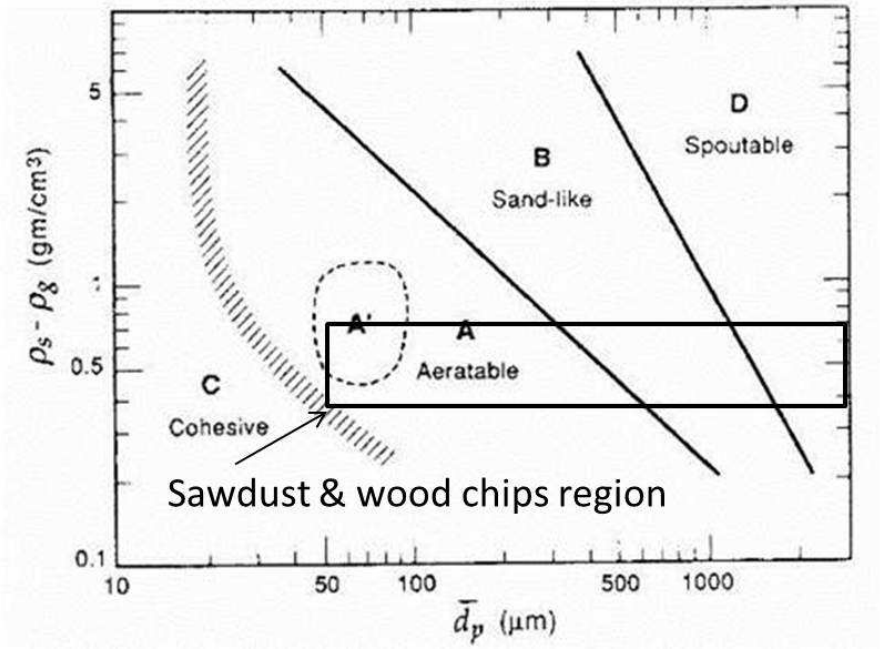

Figure 2.2.1 Geldart classification of particles. Reprinted and modified from ref. [27], Copyright 1973, with permission from Elsevier.

In the Geldart classification, class C (cohesive particles) and D (large particles) can be detrimental to gas/solid mixing as well as heat/mass transfer. For example, these particles cannot be easily and uniformly fluidized in a reactor: class C particles lead to channelling [28]. Furthermore, large particles (class D) are more subject to internal temperature gradients and species diffusion effects, which affect the final pyrolysis product distribution and composition. Species intra-particle diffusion increase the species exposure time to the pyrolysis conditions (additional time for reactions) while temperature gradients lead to uncertainties related to the characterization of the pyrolysis conditions.

Based on typical wood densities (various species) and Figure 2.2.1, sawdust particles (50 500 µm) are classified as Geldart A. On the other hand, coarser bark or wood residue particles are classified as Geldart B or Geldart D.

2.2.3.2.1 Particle size reduction

For particle size reduction, it is preferable to process biomass with low moisture content (after a drying pre-treatment) since its brittleness is increased and higher shear forces are promoted. Taking that into consideration, the most common size reduction techniques are dry shredding and hammermilling. Dry shredding relies on rotating cutters: a geared roll is mounted with sharp designed metal cutters, which are regularly disposed on its surface. Larger wood pieces can this way be converted into wood chips. As smaller pieces will simply bypass the cutters, there is no need to separate the biomass feed before this step. Dry shredding can easily reduce biomass size down to wood chips-like particulate [10].

If a powder-like feedstock (< 500 µm) is required for pyrolysis, further size reduction can be achieved with hammermills [10]. The principle is to grind a material until it reaches a minimal particle size. It is designed to limit particle size by the use of perforated plate outlet whose holes size determines the final average particle diameter. In a small drum, solid metal hammers are mounted on a central shaft. The metal hammers are rotated and the biomass material comes under the action of centrifugal force: the biomass is crushed between the hammers and the drum wall. The drum wall has grooves oriented perpendicular to those of the hammers extremities to maximize shear forces. By gravity, the fine particles percolate at the bottom of the drum where the perforated plate controls their exit in the outlet duct.

2.2.3.2.2 Particle size increase

Some feedstocks are characterized by low densities (such as bark and wood residues) and increasing their particle size may be necessary for some reactor technologies. In fluidized bed reactors, for example, particles with low terminal velocities may be rapidly entrained outside of

the reaction zone resulting only in partial conversion. If the pyrolysis reactor technology requires larger particles, particle agglomeration techniques can be used. Pelletization, also referred to as densification, is a well-established process and it is currently used to transform many MSW into denser particulate RDF (Refuse Derived Fuel) feedstocks to be directly used as fuels [29]. These same processes can also be used for biomass pre-treatment for biorefineries.

The most widely used equipment to produce pellets is the extruder [10]. It consists of one or two (partially overlapped) cylindrical ducts in which screws force deformable solids to flow with very high shear forces. At the end of the extruder, a die controls the pellet average size and a binding agent can be introduced with the solids in order to consolidate the agglomerates. Depending on the objective of the extrusion process, the design can consider multiple outlets to remove water.

Since pulp and paper industry wastes contain significant quantities of water, drying can become very expensive. In this instance, some compacting technologies can mechanically remove water from biomass while forming pellets or briquettes. Some extruders and other hydraulic or pneumatic presses perform compaction as well as remove liquid water. By reaching high pressures using extrusion, Edwards [30] was able to compact a mix of bark and wood residue and lower its moisture content from 56.5 wt% down to 34.8 wt%.

2.2.3.2.3 Drying

Drying constitutes another relevant pre-treatment for bark and wood residues for most pyrolysis reactor technologies. Biomass moisture fraction is generally controlled by the use of rotary drum dryers in the industry [31]. It uses the same principles as conventional clothes dryers: a conditioned air stream with low humidity enters the drum and is charged with moisture evacuated from biomass. Industrial rotary drum dryers can reach volumes as high as 200 m3. Using such drying equipment allows one not only to reach very low moisture fractions, but also attain a given moisture fraction set point that is desired for pyrolysis.

2.2.3.2.4 Sorting

Large pieces of inorganic material (metals and glass, for example) can be present in significant quantities in MSW. Therefore, sorting of MSW is normally required since inert material will not only consume useful volume, while some metal can act as catalyst to produce more pollutants [32].

2.2.3.2.5 Pre-treatment for sewage sludge

In sewage sludge, organic matter is diluted in water and micro-scale inorganic elements can be present. Once the sludge has been chemically and biologically stabilized at the wastewater treatment plant (pH neutralization and microorganisms' denaturation), dewatering is the first step to recover municipal biosolids. Many techniques can be employed for dewatering and centrifugation is commonly used since it can easily yield suspensions of 20 25 wt% biosolids from 0.5-3 wt% diluted sewage sludge with an overall solids recovery of over 90% [10]. Rotary drum filtration can also be used to remove water at lower levels. Depending on the operation, a controlled flow of air can be injected into the rotary drum filter, which can be used as a dryer to obtain moisture fractions below 10 wt% [10]. The wall of a rotary drum filter is meshed so the gas flow will be radial, as clogging of the filter is avoided by constant scrubbing mechanisms. As pure water can be obtained through the wastewater treatment process, the sludge sequesters impurities, which are then very difficult to remove.

2.2.4 PYROLYSIS REACTION KINETICS

During pyrolysis, the feedstock is decomposed under relatively high temperature (300°C – 1000°C) and anaerobic conditions into three products: char, condensable gas (oil & water) and non-condensable gas.

The non-condensable gas (at ambient temperature) is the lightest pyrolysis product and is composed of small hydrocarbons (C1 C4), carbon dioxide, carbon monoxide, hydrogen and other

trace components. For biomass, the high fraction of molecular oxygen promotes the production of carbon monoxide and carbon dioxide. The fraction of trace components depends on the initial composition of the feedstock: sulfur, nitrogen, phosphorus and inorganics.

The second product is a condensable gas (at ambient temperature) whose composition can significantly vary depending on the process and biomass properties. The condensable gas fraction is characterized by two immiscible phases: an aqueous and an oily phase. Since molecular oxygen is present in biomass, aldehydes, ketones, alcohols and acids are formed during pyrolysis and condense with water to form the aqueous phase. The oily phase regroups all hydrocarbons that are immiscible with water. The remaining esters, phenols, thiols, nitriles, amines, amides can be present in both aqueous and oily phases.

The last product is a solid phase that contains a carbon-rich powder (char or bio-char) and inorganics. For biomass pyrolysis, bio-char can have up to 20 wt% in molecular oxygen. Because of the initial fibrous structure of biomass (particularly in ligneous materials), the bio-char is characterized by a high pore volume and specific surface (after treatment and activation). It thus possesses interesting properties to be used as activated carbon [7].

During the pyrolysis of a specific feedstock, the respective yield and chemical composition of the above three products are governed by the pyrolysis reaction kinetics. Furthermore, the yields and chemical composition can be varied by adjusting the pyrolysis conditions in order to promote certain reactions.

2.2.4.1 Kinetics characterization

Pyrolysis reaction kinetics are characterized by hundreds or thousands of parallel reactions and in series (solid and gas phase). Pyrolysis is governed by several chemical mechanisms: resonance, bond breaking, rearranging, dehydrogenation, cyclization, etc. Due to its complexity, the entire

chemical pyrolysis reaction network has not been characterized and pyrolysis kinetics models currently available in the scientific literature are highly simplified.

Since biomass is a solid phase macromolecular system, it is impossible to characterize its reaction kinetics with conventional gas-phase Arrhenius equations containing partial pressures or concentrations. Generally, each reaction step that is considered in the conceptualization of pyrolysis reactions has its own kinetics and parameters to describe its rate: a specific order of reaction and enthalpy of reaction. Pyrolysis kinetics can be expressed in this general modified Arrhenius form [33]:

$$\frac{dm}{dt} = Ae^{-\frac{E}{RT}}f(m)^n \qquad (2.2.1)$$

In equation (2.2.1), the rate of reaction is the function of a pre-exponential factor (A), an Arrhenius term containing an activation energy (E) and a linear function representing the weight of the decomposing sample (f(m)) to the power of the order of reaction (n). The weight function (f(m)) can be written in an absolute (n = 1) or normalized form. In the latter case, the non-dimensional term can be formulated in two ways: (1) normalized with respect to the weight of emitted volatiles or (2) the weight of decomposable material. In the first case (emitted volatiles), the rate of reaction will be referred to as the rate of devolatilization with the weight function f(m) being equal to (1-m). In the second case (decomposable material), the weight function f(m) will be equal to m. When expressed in an absolute form (not normalized), the weight function is also equal to m, but with appropriate weight units. The order of reaction (n) will depend on the reaction model and the biomass material. Generally, authors assume the reactions to be of first or second order. However, since most pyrolysis reaction models are global models, the apparent order of reaction is generally characterized by a value between 0.5 and 3. Few studies have experimentally evaluated pyrolysis kinetics by considering the order of reaction as an unknown [25, 34]. Similarly to the reaction order (n), the activation energy (E) and pre-exponential factor (A) depend on the biomass material as well as the characteristics of the reaction model.

Apart from the assumption related to the kinetic expression, several other factors may bias the measurement of kinetics parameters. In fact, heat and mass transfer are important phenomena to consider during experiments. Biomass is characterized by a very poor thermal conductivity combined with a high specific heat. Therefore, biomass particles may have a significant internal temperature gradient when heated at high rates [35]. When conducting laboratory scale pyrolysis kinetics experiments, static systems (thermogravimetric analysers (TGA)) are often employed where the biomass particles remain immobile. The use of TGA minimizes attrition such that the particles remain intact throughout the experiments and the internal mass transfer is limited. Unfortunately, this may not be representative of industrial pyrolysis systems and the derived reaction kinetics will not be accurate when applied at the industrial scale.

2.2.4.2 Reaction models

Many simplified pyrolysis global reaction models were proposed in the scientific literature. Babu [36] proposed to regroup these conceptualizations of pyrolysis kinetics into three categories: (1) single-step models, (2) independent components models and (3) parallel and series reactions models. Figure 2.2.2 illustrates these models.

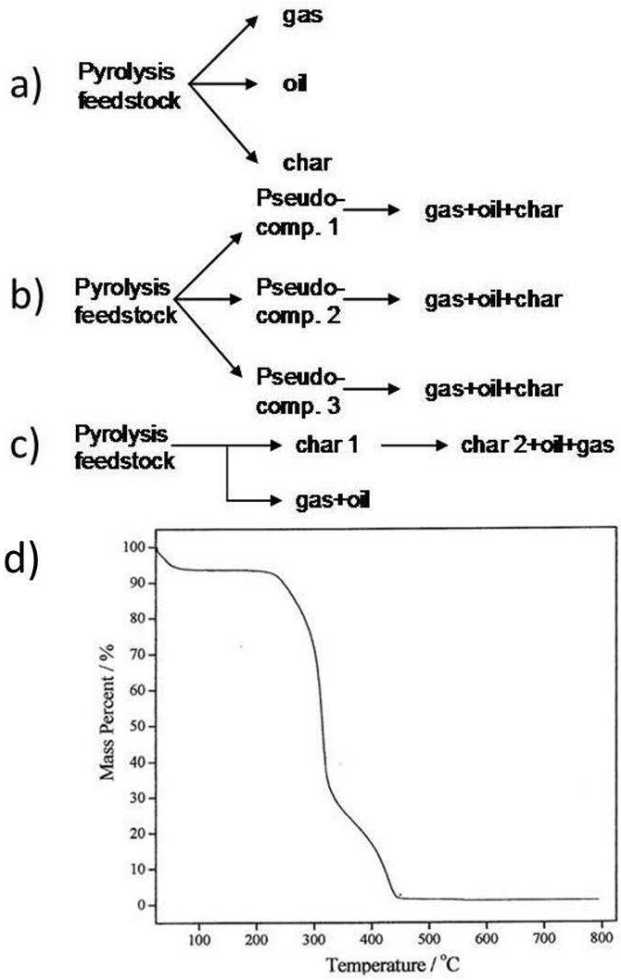

Figure 2.2.2 Pyrolysis conceptualizations with a typical thermogravimetric pyrolysis curve

2.2.4.2.1 Single decomposition step models (1 step models)

The simplest pyrolysis models consider a single decomposition step (Figure 2.2.2a). Biomass decomposition directly yields a stream of bio-char, bio-oil and non-condensable gas. These models have the advantage of simplicity and possess a limited number of parameters. These models can be accurate for a limited range of pyrolysis conditions where the temperature is constant (isothermal system), the temperature is relatively low (< 450°C, thus conventional pyrolysis) and the product composition do not vary significantly.

In reality, biomass decomposition is more complex. In the case of non-isothermal systems at high heating rates, it may appear as if different components are reacting at different temperatures with their specific reaction kinetics. The notion of “pseudo-component” emerges from that behaviour. Even if a system is operated isothermally at high temperature, pyrolysis will happen during the heating step where different products composition will be obtained. Single decomposition step models are thus only suitable in specific pyrolysis situations and are generally inadequate to reproduce industrial fast pyrolysis behaviour.

2.2.4.2.2 Independent components models

Independent components models incorporate the notion of “pseudo-component”. Figure 2.2.2d gives a typical example of pyrolysis with multiple decomposition levels. The combination of “pure” components decomposing in the same system at different temperatures would be equivalent to the reaction pattern in figure 2.2.2b. As the temperature of the biomass particles increases, the stability of the solid macromolecular matrices changes accordingly. This variation is mostly due to the release of low molecular weight compounds as previously explained. The reactivity of the particulate material will thus vary during pyrolysis and this behaviour is similar to having different components decomposing with specific reaction kinetics.

The pyrolysis of wood, for example, can be described by the combination of hemicellulose, cellulose and lignin pyrolysis kinetics, which all show single or two steps decomposition [37]. In this case, the combination of the decomposition steps for each of the three individual components can accurately model the overall pyrolysis behaviour of wood. However, ideal cases like wood are rare and the concept of “pseudo-component” may not be useful for other biomass such as manure and MSW, for example, which are highly heterogeneous. One major disadvantage of this second type of models is its complexity and the large number of reaction parameters involved. With materials having a variable composition from one provider to another, the value of these parameters will change as well as the weighting of each “pseudo-component” species.

2.2.4.2.3 Parallel and series reactions

In these models, a feedstock first reacts to yield volatiles and intermediate solid products (Figure 2.2.2c). The following steps then depend on the feedstock and the model. In most models, the volatiles undergo thermal cracking while the intermediate solid products further decompose into other final and/or intermediate products and so on. For highly heterogeneous materials, where the notion of “pseudo-component” loses its physical meaning, this conceptualization appears more realistic. However, the main disadvantage of this type of model is the high number of parameters and the difficulty to segregate the different reactions experimentally to clearly estimate their kinetics parameters. Considering all the possibilities for the different reactions under various conditions, this family of models will lead to a myriad of different models.

Table 2.2.2 Pyrolysis kinetics parameters for selected materials from literature.

Biomass	Model	A (min-1)	E (kJ/mol)	n	Temperature range of validity	Reference
Poplar	One step decomposition	$2.14x10^{12}$	153.9	1	< 673K	[22]
Wheat straw	Three pseudo-components linear combination	$2.57x10^{12}$	69	2.3	< 873K	[24]
		$3.97x10^{7}$	78	0.65	< 873K	
		$3.17x10^{6}$	80	2.7	< 873K	
Rice husk	Two pseudo-components linear combination	$1.02x10^{2}$	33.1	1.5	< 623K	[26]
		$3.3x10^{1}$	28.3	2	623K - 823K	
Rice husk	Two pseudo-components linear combination	$7.25x10^{3}$	30	0.91	< 640K	[25]
		$5.14x10^{2}$	16.3	0.3	640K - 813K	
Cellulose	Two pseudo-components linear combination	$4.69x10^{5}$	82.7	1	< 623K	[38]
		$1.33x10^{23}$	282	2	623K - 673K	
Cellulose	One step decomposition	$1.6x10^{10}$	244	1	< 623K	[35]
Cellulose	Two pseudo-components linear combination	$7x10^{7}$	126	1	-	[39]
		$4x10^{17}$	234	1	-	
Lignin	Two pseudo-components linear combination	$5.39x10^{4}$	67	1	-	[39]
		$2.1x10^{5}$	70.7	2	-	
Klason lignin	One step decomposition	$1.21x10^{12}$	156.5	1.53	< 1000K	[40]

Table 2.2.2 lists the kinetics parameters of several models available in the scientific literature along with their range of validity. Note that the parameters reported in Table 2.2.2 were all obtained from static thermogravimetric experiments. Furthermore, some of these models assumed an order of reaction, while pyrolysis reactions are in reality characterized by multiple elemental

reactions with their specific reaction order. Moreover, it has been demonstrated that the products yield during biomass pyrolysis is strongly dependent on the temperature, while all the models listed in Table 2.2.2 assume that the product yields follow the non-isothermal or isothermal TGA temperature profile used to evaluate the kinetics. Therefore, none of these models can confidently reproduce the variability of products yields with respect to temperature. Also, there is significant uncertainty as to whether these kinetic expressions will be accurate when extrapolated to industrial pyrolysis conditions. To model industrial scale pyrolysis processes, it is critical to develop reliable and robust pyrolysis models based on experimental data obtained at representative conditions.

2.2.4.3 Effects of pyrolysis conditions on the kinetics

The pyrolysis conditions affect the global kinetics by promoting specific elemental reactions. The main operational parameters for pyrolysis are temperature (and heating rate), the pressure, the co-feeding of different feedstocks and the presence of catalysts.

2.2.4.3.1 Temperature and heating rate

Pyrolysis is governed by many parallel and series reactions characterized by their specific kinetics and the relative importance of each of these reactions will depend on the temperature of the system [41, 42]. Also, a slow heating process implies that the biomass remains at every temperature for a longer time period. As pyrolysis kinetics and heat transfer compete, pyrolysis occurs during the heating of the particles and might even be completed (at thermodynamic equilibrium) before reaching the temperature set-point. At low heating rate, more decomposition happens at low temperature such that more bio-char and less volatile (condensable (bio-oil) and non-condensable gases) are produced.

One of the main mechanisms controlling the interaction between the temperature and the heating rate is the stabilization and reorganization of the macromolecular solids. Thermal decomposition brings lighter molecules to unbind from the solids (biomass or waste in the present case) to form

a volatile phase. In parallel, this creates physicochemical instabilities that lead to a molecular rearrangement. The kinetics associated to these intra-molecular modifications then inhibits the volatile formation kinetics. If the heating rate is slow, stabilization occurs and higher char yield is obtained. On the other hand, heating faster will impede stabilization and volatile production will be promoted. Temperature has a different effect on the pyrolysis products. Char production decreases with increasing temperature and the yield of gas increases (both condensable and non-condensable). The extent of the gas thermal cracking determines the yield of non-condensable gas and average molecular weight of the volatile fraction. Thermal cracking kinetics becomes important with increasing temperature and gas residence time.

2.2.4.3.2 Pressure

Pressure influences the equilibrium reactions and therefore affects the volatile products composition: the condensable (bio-oil) and non-condensable gases. It has also been shown that pressure can promote other gas-solid reactions involving moisture, hydrogen, carbon dioxide and possibly other gaseous species. The mechanisms involved remain unclear, but chemical reactions such as the Boudouard reaction are suspected:

$$C_{(s)} + CO_{2_{(g)}} \rightleftarrows 2CO_{(g)} \qquad (2.2.2)$$

Moisture, which is inevitably present during biomass pyrolysis, has also been shown to influence the volatile yield and composition [43]. These reactions are characterized by fast kinetics only under specific conditions: they generally occur in pressurized gasification and under high temperatures, while pyrolysis is typically performed at milder temperatures.

The solids will not be significantly influenced by pressure if an inert gas is employed [44, 45]. Experimentation is still the best method to characterize the effect of pressure on the pyrolysis products since it is specific to the biomass feedstock used.

2.2.4.3.3 Co-feeding

One of the most evident synergic pyrolysis behaviour has been demonstrated by Brebu [16]. By co-feeding pine cones with waste polyolefin, they showed that it was possible to significantly decrease the overall char yield and increase the amount of volatile produced. For binary blends of pine cones and polyethylene (PE), polypropylene (PP) or polystyrene (PS), the char yield decreased (by over 6 percentage units for polyethylene) compared to the calculated value by linear combination, hence revealing synergic behaviour. When a blend of pine cones and the 3 polymers (PE/PP/PS) was pyrolyzed in the ratio 3:4:2:1, the synergy was even more significant. The reported char yield was lower than the average calculated value by 10 percentage units and the liquid product yield increased by over 11 percentage units. However, while these types of synergies are desired, they have been rarely observed. One typical example is the co-pyrolysis of biomass with coal. Weiland et al. [46] explored the possible synergetic interactions between coal and biomass in pyrolysis. Unfortunately, the interaction was almost nonexistent. Linear combination explained most of the variations with the various blends of coal/biomass.

2.2.4.3.4 Catalysts

Pyrolysis of biomass with catalysts has been widely studied and they are sometimes used to tailor the yields of the pyrolysis products. However, catalysis chemistry is extremely complex and only a very few research groups in the world can explain catalysis mechanistic for specific reactions and in highly controlled conditions. Thus, understanding (in a fundamental mechanistic way) the effects of adding catalysts on the evolution of pyrolysis products distribution and their composition is not currently feasible. The effects of catalysis on pyrolysis reactions are therefore determined empirically and undesired behaviours were often observed: significant drops in liquid yield have been the most common [47].

2.2.5 TYPES OF PYROLYSIS

As previously discussed, the pyrolysis conditions affect the global kinetics by promoting specific elemental reactions. Pyrolysis processes have therefore been classified with respect to the

prevailing conditions during the reaction used to maximize the yield of one of more of these products. Conventional or slow pyrolysis, fast or ultrafast pyrolysis and vacuum pyrolysis are the main three categories of pyrolysis process operation.

2.2.5.1 Conventional or slow pyrolysis

Heat transfer to the biomass particles is generally the main limitation in industrial pyrolysis. Biological and organic polymeric materials have poor thermal conductivity, but high specific heats. Therefore, a limitation is reached in pyrolysis processes when heating a feedstock to high temperatures due to the high temperature dependence of the reaction kinetics (expressed as an Arrhenius law). The limitation arises at the specific temperature where the decomposition rate becomes greater than the heating rate. Acknowledging that pyrolysis is an overall endothermic reaction, increasing temperature from that point is very difficult.

Conventional pyrolysis is also referred to as slow pyrolysis because of the low heating rates (6 60 °C/min [36]). The peak pyrolysis rate will be reached at a relatively low temperature and the limited heat transfer will result in moderate pyrolysis temperatures (300-700°C). These reaction conditions promote bio-char production and minimize volatiles (non-condensable and condensable gases). As the temperature of the pyrolysis process is increased, the weight fraction of volatile increases: this effect is governed by the resonance mechanism. The release of lighter molecules from a macromolecular matrix generates instabilities that are dispersed within this matrix in order to stabilize its structure. As temperature increases, the instability gains in magnitude. In slow pyrolysis, biomass is kept at constant moderate temperatures, such that the macromolecule has time to reach a new stable form with a new composition that will handle higher internal energy without decomposing (thermodynamic equilibrium), hence limiting the release of volatile. This is where conventional (slow) pyrolysis differentiates from fast pyrolysis. Volatile and char yields therefore depend on this resonance kinetics.

2.2.5.2 Fast and ultrafast pyrolysis

Fast and ultrafast pyrolysis are performed under high heating rates (600-12000 °C/min [36]), which are many orders of magnitude higher than those of conventional pyrolysis. Thus, the peak rate of decomposition is reached at higher temperatures compared to slow pyrolysis. Under these conditions, the macromolecular reorganization kinetics is slower than the volatiles release kinetics. Consequently, the bio-char yield is significantly lower compared to slow pyrolysis, while the volatile yield is higher. Since the bio-oil (condensable gases) products are of higher interest for biorefineries, the emerging industrial biomass pyrolysis processes ideally target fast and ultrafast pyrolysis processes. Meanwhile, bio-char obtained at a higher temperature show a greater specific surface, which is another motivation for operating at very high heating rate and temperature. In addition, higher heating and reaction rates allow higher biomass process rates or the use of smaller, more compact systems: both of these aspects increase process profitability.

2.2.5.3 Vacuum pyrolysis

The third category of pyrolysis process is referred to as vacuum pyrolysis: the pyrolysis process is performed under vacuum conditions independently of the heating rate (slow and fast). Under vacuum, the heavier products in the gas phase are entrained out of the reacting environment without having time to crack into smaller molecules. For that reason, vacuum pyrolysis oils contain high molecular weight components and are consequently tarry and more viscous than common pyrolysis oils. Because of their specific molecular composition, vacuum pyrolysis oils are of great interest for specialty chemicals production in biorefineries. It is nevertheless a great challenge to produce industrial scale vacuum environments. The company Pyrovac (Laval, Quebec, Canada) attempted to operate a commercial a large-scale industrial vacuum pyrolysis plant in the 1990’s and failed due to high operating costs.

2.2.6 REACTOR TECHNOLOGIES

The choice of reactor technology is critical to follow the desired kinetic pathway in pyrolysis. The emphasis of this section will be on selected reactor technologies that have been successfully

demonstrated at large scale with a pilot-scale or larger unit. Several reactor concepts have been demonstrated in the scientific literature at small-scales, but they will not be considered.

The mass and energy balances are the main fundamental and semi-empirical tools to design reactors when coupled to reaction kinetics. These balances involve heat and mass transfer equations, which are dependent on the system gas/solid hydrodynamics. Several handbooks are dedicated to reactor design with various hydrodynamics models to represent these equipments. However, the objective of this section is not to review these models in details. Considering that heat transfer is the limiting step in pyrolysis reactors, the emphasis is put on heat transfer parameters evaluation.

2.2.6.1 Bubbling fluidized bed (BFB)

Fluidized beds are widely used in the chemical industry for catalytic cracking and other processes. In fluidized bed reactors, a gas stream (inert gas for pyrolysis) is forced through a bed of powdered material from a distributor plate that supports the bed. At low gas velocities, the bed of particles is non-moving and this is referred to as a fixed bed. As the gas velocity is increased, the drag forces applied on the particles increases until the minimum fluidization velocity is reached: the bed is “supported” by the gas and behaves like a fluid. If the gas velocity is increased further, bubbles are formed at the distributor plate and rise through the bed of solids similarly (but not exactly) to air bubbles in water. Bubbles promote the circulation of solids to ensure a uniform temperature throughout the fluidized bed. A bubbling fluidized bed reactor is designed in a way to avoid the entrainment of particles outside the reactor (also called elutriation). The bed zone is narrower to promote the circulation of particles and the formation of bubbles. The gas exits the bed to enter a freeboard zone and a higher diameter disengagement region where the gas velocity is significantly reduced. In the disengagement region, particles that would be entrained in the bed and freeboard zones fall back into the bed by gravity. There is an appreciable amount of established scientific literature on fluidized beds [48, 49]. Bubbling fluidized bed reactors are used for fast pyrolysis by the company Dynamotive, which is operating a pilot-scale unit to convert biomass into bio-oil. The unit has been reported to process at up to

100 tons of biomass per day [50]. Figure 2.2.3a gives a global view of a possible biomass pyrolysis unit with a bubbling fluidized-bed.

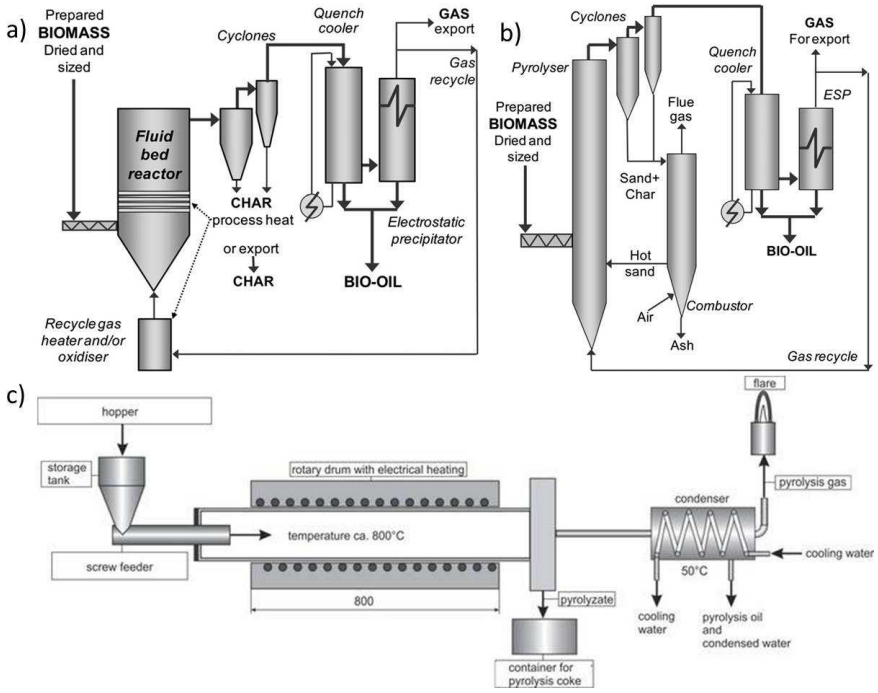

Figure 2.2.3 Pyrolysis units global schemes: a) bubbling fluidized bed [41], b) circulating fluidized bed [41] and c) rotary drum reactor [51]. Reprinted from ref. [41], Copyright 2012, with permission from Elsevier; Reprinted from ref. [51], with permission from Prof. Dr-ing. Roman Weber

2.2.6.1.1 Operability

Biomass particles are generally difficult to fluidize, such that a denser and more homogeneous inert particle media (generally sand) is employed as a fluidization media to improve transport phenomena. Bench and pilot scale continuous operation of a pyrolysis bubbling fluidized bed has been demonstrated by Dynamotive. Char removal from the reactor can be an issue: if char is very fragile, its particle size will decrease within the bed by attrition. When char particle size reaches a critical particle value, it is entrained out of the fluidized bed reactor and it must be separated from the gas and recovered via a cyclone. Therefore, the disengagement region must be carefully

designed to allow char particles to exit the reactor once they are sufficiently small. The main advantages of bubbling fluidized beds for pyrolysis applications include a uniform reaction temperature (minimizes the formation of cold/hot spots in the bed) and capability to operate the reactor continuously (continuous biomass feeding). On the other hand, the main disadvantage of bubbling fluidized beds is that the volatile will be mixed with the inert fluidizing gas. Therefore, the bio-oil can be recovered, but the non-condensable gas is diluted such that it can hardly be used as a primary energy source. Thus, energy must be obtained from the solid char, which is significantly detrimental to the process profitability.

2.2.6.1.2 Hydrodynamics

The fluidization gas acts as a heating media and promotes mass and heat transfer by inducing a movement on the solids particles as well as removing the volatile from the bed. The bubbling fluidized bed can be divided into three phases: (1) the bubble phase (dilute phase – low solids fraction), (2) the emulsion phase (dense phase – high solids fraction) and (3) the cloud phase. The cloud phase is at the interface between the bubble and emulsion phases such that the local solids fraction is between dilute and dense [48]. Several gas-phase (1-phase, multiple-phase, multiple regions, etc.) and solid-phase (counter-current back mixing, etc.) hydrodynamic models are available in the scientific literature [49]. These models can be coupled with pyrolysis kinetics (reviewed in section 2.2.3) to estimate the yield of products. These models have been reviewed in details in several publications [49].

When designing a bubbling fluidized bed pyrolysis system, one could desire to minimize the fluidization gas flow to facilitate post-pyrolysis separation of the products. However, the superficial gas velocity also affects the reaction rates since it influences the heat and mass transfer. When temperature is sufficiently high, the pyrolysis reaction characteristic time becomes shorter than the heating characteristic time, such that heat transfer is the limiting step. In this case, the particles reaction rate (and residence time) is determined by the convection heat transfer to the biomass particles in the fluidized bed and the convection coefficient can be calculated from the following correlation [52]:

$$Nu_{bed} = \frac{h_{bp} d_p}{k_g} = 0.033 Re_p^{1.33} \quad \text{for } 0.1 < Re_p < 100 \qquad (2.2.3)$$

In equation (2.2.3), the overall fluidized bed Nusselt number (Nubed) is a function of the particle Reynolds number (Rep):

$$Re_p = \frac{\rho_g (U - U_p) d_p}{\mu_g} \qquad (2.2.4)$$

The convection coefficient from equation (2.2.3) is averaged over the bed of particles and it is shown to increase with increasing slip velocity (U-Up). As demonstrated by Avidan and Yerushalmi [53], the slip velocity (U-Up) for bubbling fluidized beds is equal to the superficial gas velocity. This is the case because the average particle velocity is zero: solids circulate within the bed (negligible or limited entrainment) and particles flow co-current or counter-current with the gas. Therefore, the fluidization gas velocity should be sufficiently high to maximize reaction rates and the yield in volatiles: there is therefore a trade-off associated with the selection of the fluidization velocity.

Note that equation (2.2.3) has been shown to yield a more accurate estimation of the convection coefficient than the typical correlations involving the Prandtl number [54]. Furthermore, equations (2.2.3) and (2.2.4) should be used by considering the inert (sand) fluidization media, in which case the use of the inert material properties is generally sufficiently accurate (the biomass particles are highly diluted in the inert media). Basic heat transfer estimations with equations (2.2.3) and (2.2.4) suggest that operating a fluidized bed in the bubbling regime widely promotes fast pyrolysis rather than conventional pyrolysis.

To model biomass pyrolysis in a bubbling fluidized bed, less importance is generally given to the bubble characterization since the fluidization gas is inert. The modelling is therefore focused on the dense emulsion phase, which contains the solid biomass particles. If the fluidized bed temperature is uniform and the inert (sand) particles do not leave the bed, the inert particles

temperature can be assumed equal to the gas temperature. In this case, the heat balance strictly involves the biomass particles.

2.2.6.1.3 Feedstock pre-treatment

Dewatering and drying should be considered, since heating the biomass may only vaporize the water while delaying the biomass pyrolysis reactions and increasing the operation costs. Also, studies suggest than steam explosion of biomass could influence the quality of pyrolysis products [55].

Particle size reduction is also important to minimize heat transfer limitations and internal temperature gradients in biomass particles. The Biot number criterion of 0.1 suggests that the maximum wood chips size that should be fed to a bubbling fluidized bed to avoid heat transfer limitations (and product yields issues) is ~2 centimeters (by estimation with typical wood properties). This calculation assumes that the wood chips have a thickness 5 times lower than their diameter (parallelepiped shape). Particle size reduction is therefore recommended for biomass particles that are larger than that value. Heterogeneous feedstocks such as MSW would not be recommended with this technology since pyrolysis operation temperatures do not promote slagging, in opposition to gasification. Undesired particulate would then need to be removed from the bed, which is a difficult operation in bubbling fluidized beds, considering the wide particle size and densities distribution of the inorganics.

2.2.6.2 Circulating fluidized bed (CFB)

A Circulating Fluidized Bed (CFB) works at higher superficial gas velocities than a bubbling fluidized bed to increase the slip velocity and heat transfer to the particles. Due to the high gas velocities, the particles are entrained outside the bed region (called the riser) and cyclones are used downstream to separate the particles from the gas and return them to the bed. During biomass pyrolysis, char and inert (generally sand) particles are present. Depending on the design of the reactor, the char/sand particles mix can be transported to a second reactor where the char is

burned. In this case, the hot sand is returned to the riser and the combustion flue gases can be directly fed to the riser as an inert fluidization and heating medium (see Figure 2.2.3b).

Ensyn is a well-known company that operates a commercial scale CFB biomass pyrolysis system. Their largest pilot plant can process up to 100 bone-dry tons of biomass per day. Sand is co-fed with biomass in the riser, while the residual char and sand are recovered in a separate bubbling fluidized bed combustor where the char is burned. The hot sand is then fed into the riser.

2.2.6.2.1 Operability

The main advantage of circulating fluidized beds over bubbling fluidized beds is that char can be easily separated from the sand and the gas. Similarly to bubbling fluidized beds, the non-condensable gas cannot be considered as a primary heat source for the process: it is diluted into the inert fluidization media. To supply the process with heat, bio-char is instead burned. As this solid pyrolysis product showed an interesting potential [7, 56] for an eventual commercialization, choosing a CFB greatly affects the overall profitability of the pyrolysis process.

2.2.6.2.2 Hydrodynamics

The apparent density in circulating fluidized beds is lower compared to bubbling fluidized beds such that heat transfer calculations are generally performed by assuming single particles convection heating. Since particles are entrained outside the fluidized bed, the relative gas velocity with respect to the particles is their terminal velocity (Ut). Therefore, the particle Reynolds number is calculated using:

$$Re_p = \frac{\rho_g U_t d_p}{\mu_g} \qquad (2.2.5)$$

Two main individual systems must be designed to conduct pyrolysis in a CFB: (1) the riser where pyrolysis occurs and (2) the combustor where char is burned and the flue gases heat the sand media. In the Ensyn technology, the combustor consists of a bubbling fluidized bed. The important design calculations for this component are the mass and energy balances: it must be considered that the biomass and char particles do not circulate at the same rate than sand particles. To design the riser section, very fast heat transfer from the sand to the gas can be assumed such that an average gas temperature can be estimated. This gas temperature is then used to calculate the biomass transient heating over its residence time. The convection coefficient can be estimated with the correlation of Ranz [57]:

$$Nu_p = \frac{h_p d_p}{k_g} = 2 + 0.6 {Re_p}^{0.5} {Pr_g}^{0.33} \qquad (2.2.6)$$

Referring to the calculations made for bubbling fluidized beds, fast pyrolysis is the type of pyrolysis promoted in CFBs; lower gas velocities would not even allow reaching that regime. Similarly to bubbling fluidized bed pyrolysis, the gas flow rate in CFBs must be carefully chosen as well as the biomass and sand circulation rates. Moreover, sand and biomass particle size must be chosen to control the sand/char flow rate ratio. If the gas flow rate in the combustor is too high, the sand temperature may be too low, which would lower the temperature in the riser where pyrolysis occurs. Likewise, a high gas flow rate in the riser would also lower the temperature at which pyrolysis occurs. CFB design considerations have been reviewed in several publications [49].

2.2.6.2.3 Feedstock pre-treatment

It was mentioned previously that the biomass particle size has to be homogenized and controlled in order to obtain a specific sand to char flow rate ratio. In their process, Ensyn uses wood sawdust that has been dried to a low moisture fraction as a pre-treatment. Fine particles are generally required for CFB technologies to promote a homogeneous fluidization. It is critical that this feedstock does not contain particulate metals and inorganics; otherwise it might contaminate

the sand. Highly heterogeneous materials such as MSW, RDF and sewage sludge are thus not recommended with this technology.

2.2.6.4 Entrained-flow reactor

In entrained-flow reactors, free-falling particles are entrained downwards by a gas flow. For gasification, entrained-flow reactors are a promising technology as demonstrated in 2002-2003 by Shell and BTG with woody biomass as feedstock [58]. Preliminary tests for biomass pyrolysis applications have shown very high non-condensable yields [59]. It is believed that the geometry of this type of reactor technology promotes important bio-oil thermal cracking. Since the purpose of pyrolysis for biorefineries is to produce higher molecular weight chemicals, this technology will not be covered.

2.2.6.5 Rotary drum reactor

Rotary kilns have been used for decades to generate energy from wastes. The operation of this type of reactor has been demonstrated in a continuous mode at industrial scale and many problems have been reported. The very high temperatures during incineration promote NOx and SOx production as well as dioxins and furans, which are carcinogens. Moreover, leaching and slagging can affect rotary kiln incinerators operability. Notwithstanding these reports, the interest for using rotary drum reactors for pyrolysis applications is currently growing [15]. Operation of the reactor at lower temperature and without oxygen will likely decrease pollutant emissions as well as minimize risks of leaching and slagging. In most cement plants around the world, rotary kilns can have impressive dimensions (over 100 m long). For pyrolysis applications, some pilot-scale units were built and operated to process waste.

Typically, a rotary drum pyrolysis reactor processes raw materials such as MSW, RDF and waste tires. It consists of a horizontal cylindrical reactor rotating at a certain speed in order to mix the bed of materials and promote transport phenomena. For this application, as oxygen must be purged, heat supply is generally indirect, i.e. gas burners are mounted underneath the rotary drum

and the flue gases are circulated around the drum in a blanket-like chimney. Figure 2.2.3c shows a schematic of a rotary drum pyrolysis system with an electric heater.

2.2.6.4.1 Operability

Rotary kilns are usually operated in full continuous mode, which can complicate its application to pyrolysis. The reactor is purged from oxygen during the process start-up, but no inert gas is fed to the reactor during operation. The major advantage of this mode of operation is that all of the pyrolysis products can be recovered, including the combustible non-condensable gas that is characterized by significantly less dilution compared to the other reactors considered in this chapter. Optimally, the non-condensable gases are used as the primary energy source for the reaction to heat the rotary drum.

Char is also recoverable, but conventional (slow) pyrolysis has the disadvantage of producing less bio-oil. The lower heating rates observed in rotary drum reactors will also complicate its continuous operation: most technologies in this field operate in batch mode. Thus, profitability will be achieved by combining multiple batch pyrolysis units to increase production and benefit volume discounts for the equipment.

2.2.6.4.2 Hydrodynamics

Rotational speed and mixing are probably the most important parameters to consider when designing a rotary kiln pyrolysis system since it governs the heat and mass transfer. Mellmann [60] produced a complete review on rotary drum hydrodynamics, highlighting the flow patterns and regimes as a function of the particulate material friction coefficient, the drum filling level and the Froude number. The Froude number is defined as:

$$Fr = \frac{\omega^2 R}{g} \quad (2.2.7)$$

In equation (2.2.7), ω is the angular rotational speed and R is the drum radius. With increasing Froude number, the motion patterns vary from (1) a slipping motion (sliding, then surging as motion subtypes), (2) a cascading motion (slumping, then rolling, then cascading) and (3) cataracting motion (cataracting, then centrifugating). According to Mellmann [60], reaching the cascading motion regimes is preferable to achieve good mixing and higher homogeneity. If the reactor is properly operated, it can be assumed that the temperature gradient in the bed is negligible. In this case, heat transfer to the particles results from drum wall convection and radiation to the particles. Generally, it is more convenient to estimate the heat transfer coefficient experimentally since it is specific to the studied system. In fact, the heat transfer coefficient can typically vary from 25 W/m²K up to over 200 W/m²K if radiation becomes important. Experiments are needed for that estimation also because baffles are often added on the drum inner wall in order to amplify mixing. As stated previously in this section, rotary drum pyrolyzers can operate at various regimes, depending on their design, to promote very slow pyrolysis up to the fastest conventional pyrolysis heating rates.

2.2.6.4.3 Feedstock pre-treatment

Feedstock does not need much pre-treatment for rotary drums. Moisture control could be required, but the feedstock particle size can be kept relatively high (on the order of centimetres). Also, the purification of MSW into RDF is not necessary for operation. Metals and inorganics removal is related more likely to useful volume: at lower temperature and in the absence of oxygen, undesired catalytic reactions will show significantly lower kinetics than if gasification was performed. For that reason, rotary drum reactors are preferred for MSW and municipal biosolids pyrolysis. Woody biomass is not likely fit to this technology, because the liquids yields are particularly low [61] and that fluidized bed technologies have already been proven successful at industrial scale.

2.2.7 PYROLYSIS PRODUCTS OPTIMIZATION

The sustainability of biorefineries is very sensitive economically and their main objective is to generate the pyrolysis products that maximize the plant profitability.

2.2.7.1 Pyrolysis products for biorefineries

Bio-oil is considered as the most commercially valuable pyrolysis product if it contains specialty chemicals in high percentages. Therefore, maximizing bio-oil production can be an objective during process development. Table 2.2.3 summarizes the main specialty chemicals present in bio-oil obtained from the pyrolysis of selected feedstocks along with reactor type and operating conditions.

Table 2.2.3 Selected feedstocks with their bio-oil main compounds

	Feedstock	**Pine bark**	**Pine wood**	**Pine wood**	**Oak wood**	**Switchgrass**	**Switchgrass**	**Sewage sludge**
	Reference	[62]	[62]	[63]	[62]	[62]	[64]	[65]
	Reactor	Auger	Auger	Auger	Auger	Stirred reactor	Fluidized bed	Fixed bed
	Temperature (K)	723	723	723	723	873	823	723
	Pressure (atm)	1	1	1	1	6.8	1	1
	Moisture (%)	10	10	dried	10	8.4	10	7
	Bio-oil yield (%)	43.5	52	50	53	37	37	13
Specialty chemical	**Estimated price**	Yield based on global bio-oil weight, otherwise specified						
Catechol	80 USD/kg	4.46%	3.79%	<1%	2.25%	-	-	-
Levoglucosan	>100 USD/kg	21.50%	14.20%	6.37%	21.60%	-	-	-
2-Propanone	1,50 USD/L	-	-	-	-	8.78%	2.95%	-
2-Butanone	1,60 USD/L	-	-	-	-	11.49%	-	-
Acetic acid	0,55 USD/L	-	-	-	-	18.91%	6.85%	-
Acetic acid, methyl ester	1,20 USD/L	-	-	-	-	5.47%	-	-
Hydroxyacetaldehyde	1,50 USD/L	-	-	-	-	-	9.14%	-
9-octadecenoic acid	1,50 USD/L	-	-	-	-	-	-	4.01%
Tetradecanoic acid	1,00 USD/L	-	-	-	-	-	-	4.31%
Hexadecanoic acid	1,50 USD/L	-	-	-	-	-	-	15.70%

Fatty acids, phenolic compounds and aldehydes/ketones are among the high value chemicals for crops. On the other hand, woody biomass generates high amounts of levoglucosan, which is a promising biopolymer building block. Also, catechol and its derivatives have a high market value. In addition, hard wood has different pyrolysis behaviour than soft wood through their bio-oil composition (Table 2.2.3: pine wood vs oak wood).

Chemical species containing double bonds and oxygen can be detrimental to the stability of the bio-oil. These chemicals polymerize with time and increase the bio-oil viscosity as well as modifying other properties. Acetic acid is one common pyrolysis products that can cause this phenomenon. Acetic acid is derived from cellulosic biomass and process optimization will generally focus on reducing its production. Moisture fraction has been shown to influence acetic acid production [64]. Another method consists of using metal oxides catalysts [47].

2.2.7.2 Bio-oil applications

The interest for bio-oil resides in its complexity, but this complexity implies an important obstacle: selectivity. Bio-oil composition can be easily modified, but voluntarily promoting the production of one specific chemical species over another is very challenging. There are essentially three markets in which the pyrolysis bio-oil can be categorized: high-value chemicals, biofuels and chemical precursors. If the pyrolysis process is designed to produce a low molecular weight bio-oil, it could be used as a chemical precursor for further recombination to yield heavier and higher value products. On the other hand, high-molecular weight bio-oils are often unstable chemically due to double chemical bonds [66].

Compounds found in the bio-oil include: acids, aldehydes, anhydrosugars, hydrocarbons, saccharides, alcohols, ketones, furans, phenols, etc [3]. The oxygen weight fraction in bio-oil is thus high at approximately 45 % [66]. As a result, bio-oil is likely not suited to be directly used as a fuel. However, co-feeding of polyolefins can help controlling this parameter efficiently [16]. Besides the possibility of producing biofuel through co-pyrolysis of different species, it is also

interesting to observe important variations in specific chemical species in this process. This is only one of the numerous modifications that can be implemented on the pyrolysis process, in order to upgrade the products. Nevertheless, it must be kept in mind that pyrolysis has the great advantage of being a single-step process, so being it must conserve this characteristic through its modification.

2.2.7.3 Bio-char applications

Char is sometimes used as fuel for pyrolysis reactors. However, the market value of bio-char must be considered before taking decisions. Activated carbon sells on the market at around 1 USD per kg, which is comparable to the value of some chemicals found in bio-oil. Bio-oil and bio-char both need post-processing transformation in order to yield their valuable products.

Activated carbon production implies carbonization and chemical activation. Typically, carbonization consists of a very slow pyrolysis process, which yields very high amounts of char. The principal characteristic of activated carbon is a very high specific surface, generally over 500 m^2/g. To be competitive with the actual commercial carbons, this specific surface must be attained and it has recently been demonstrated as feasible [7]. Since 2006, the number of publications on bio-char activity has increased considerably [56].

2.2.7.4 Dealing with foreign elements in pyrolysis products

Biomass and MSW contain oxygen, nitrogen, sulfur, halogens, metals and other elements whose concentrations in the pyrolysis products must be controlled as per existing standards.

Sulfur and nitrogen have been shown to mostly cluster in the bio-oil phase [21]. Sulfur has been successfully avoided in pyrolysis oil from coal in the past [67] by the use of lime (CaO). Similarly, the same experiments showed that the oxygen weight fraction in oil could be as well significantly decreased. The main disadvantage of this technology is that the char will remain

charged with calcium and that the gas phase will mostly receive this excess of sulfur [68]. However, the gas phase can be post-treated efficiently (scrubbing) and considering the high level of inorganics and contaminants in the solid phase, it will not likely be used as bio-char or as activated carbon.

Adding lime in the pyrolysis environment can also significantly inhibit the formation of liquid chlorinated organics in the bio-oil [69]. The co-feeding of lime in MSW pyrolysis could eventually become widespread as this additive is relatively cheap and available.

Post-processing of bio-oil to remove oxygen, nitrogen and sulphur is also possible through hydrodeoxygenation using metal catalysts (and an H2 stream) [70]. For biofuels production, this post-treatment process is desirable, as the oxygen weight fraction can be reduced below 1 %. Furthermore, the effect of this post-treatment on the bio-oil chemical composition has not been investigated such that there is a possibility that it also generates higher value chemicals.

Most metals and metal oxides cluster in the solid phase due to the low temperature associated with pyrolysis, which remain below metal sublimation or melting temperatures. Metals can also be absorbed by activated carbon produced from bio-char [56].

2.2.8 NOMENCLATURE

Abbreviations

A = Pre-exponential factor [=] s-1 for a 1st order reaction

d = Diameter

E = Activation energy [=] Jmol-1

Fr = Froude number

g = Standard gravity [=] m*s-2

h = Heat transfer constant [=] Wm-2K-1

k = Thermal conductivity [=] Wm-1K-1

m = Dimensional & non-dimensional weight

n = Order of reaction, non-dimensional

Nu = Nusselt number

Pr = Prandtl number

R = Universal gas constant OR Radius [=] Jmol-1K-1 OR m

Re = Reynolds number

t = Time

T = Temperature

U = Velocity [=] m*s-1

Symbols

μ = Viscosity [=] Pa*s

ρ = Density [=] kgm-3

ω = Angular velocity [=] s-1

Subscripts

bed = Fluidized bed

bp = Bed of particles (in rotary drums)

g = Gas phase

p = Particle

t = Terminal (velocity)

2.2.9 REFERENCES

[1] Demirbas A (2009) Biorefineries: for Biomass Upgrading Facilities. London: Springer-Verlag.

[2] Kamm B, Gruber P, Kamm M (2010) Biorefineries - Industrial Processes and Products. John Wiley & Sons.

[3] Brown R, Stevens C (2011) Thermochemical processing of biomass: conversion into fuels chemicals and power. Wiley.

[4] Crocker M (2010) Thermochemical Conversion of Biomass to Liquid Fuels and Chemicals. Royal Society of Chemistry.

[5] Waldron K (2010) Bioalcohol production: biochemical conversion of lignocellulosic biomass. Taylor & Francis Group.

[6] Basu P (2010) Biomass Gasification and Pyrolysis: practical design and theory. Elsevier.

[7] Azargohar R, Dalai A (2006) Biochar as a precursor to activated carbon. Applied Biochemistry and Biotechnology, 131(1-3), pp. 762-773.

[8] US Department of Energy (2012) Feedstock types. Consulted on February 1st, 2012, sur http://www1.eere.energy.gov/biomass/feedstocks_types.html

[9] Harkin J, Rowe J (1971) Bark and its possible uses. U.S. Department of Agriculture, Forest Service, Madison, Wisconsin.

[10] Klass D (1998) Biomass for renewable energy, fuels, and chemicals. Academic Press.

[11] Tillman D (1981) Wood combustion: principles, processes and economics. Academic Press.

[12] Gavrilescu D (2008, Sept/Oct) Energy from biomass in pulp and paper mills. Environmental Engineering and Management Journal, 7(5), pp. 537-546.

[13] Onay O, Beis S, Kockar O (2001) Fast pyrolysis of rape seed in a well-swept fixed-bed reactor. Journal of Analytical and Applied Pyrolysis, 58-59, pp. 995-1007.

[14] Rodrigues I, Coelho J, Carvalho M (2012) Isolation and valorisation of vegetable proteins from oilseeds plants: methods, limitations and potential. Journal of Food Engineering, 109, pp. 337-346.

[15] Li A, Li X, Li S, Ren Y, Shang N, Chi Y (1999) Experimental studies on municipal solid waste pyrolysis in a laboratory scale rotary-kiln. Energy, 24, pp. 209-218.

[16] Brebu P, Ucar S, Vasile C, Yanik J (2010) Co-pyrolysis of pine cone with synthetic polymers. Fuel, 89(8), pp. 1911-1918.

[17] USDA Forest Service (2007) Timber Product Output Database. Consulted on January 2012, on Forest Inventory Analysis: http://fia.fs.fed.us

[18] Bhattacharya P, Parthiban V, Kunzru D (1986, April) Pyrolysis of black liquor solids. Industrial Engineering & Chemistry, Process Design & Development, 25(2), pp. 420-426.

[19] Langholtz M, Carter D, Rockwood D, Alavalapati J (2007) The economic feasibility of reclaiming phosphate mined land with short rotation woody crops in Florida. Journal of Forest Economics, 12, pp. 237-249.

[20] Boateng A, Daugaard D, Goldberg N, Hicks K (2007) Bench-scale fluidized-bed pyrolysis of switchgrass for bio-oil production. Industrial Engineering and Chemistry Research, 46, pp. 1891-1897.

[21] Imam T, Capareda S (2012) Characterization of bio-oil, syn-gas and bio-char from switchgrass pyrolysis at various temperatures. Journal of Analytical and Applied Pyrolysis, 93, pp. 170-177.

[22] Singh R, Shadangi K (2011) Liquid fuel from castor seeds by pyrolysis. Fuel, 90, pp. 2538-2544.

[23] National Agricultural Statistics Service (1995) Agricultural statistics. Washington D.C.: U.S. Department of Agriculture.

[24] Mani T, Murugan P, Abedi J, Mahinpey N (2010) Pyrolysis of wheat straw in a thermogravimetric analyzer: Effect of particle size and heating rate on devolatilization and estimation of global kinetics. Chemical Engineering Research and Design, 88, pp. 952-958.

[25] Mansaray K, Ghaly A (1999) Kinetics of the thermal degradation rice husks in nitrogen atmosphere. Energy Sources, 21, pp. 773-784.

[26] Sharma A, Rao R (1999) Kinetics of pyrolysis of rice husk. Bioresource Technology, 67, pp. 53-59.

[27] Geldart D (1973, May) Types of gas fluidization. Powder Technology, 7(5), pp. 285-292.

[28] Bi H, Grace J, Zhu J (1995) Regime transitions affecting gas-solids suspensions and fluidized beds. Chemical Engineering Research and Design, 73(2), pp. 154-161.

[29] Kanury A (1994) Combustion characteristics of biomass fuels. Combustion Science and Technology, 97(4-6), pp. 469-491.

[30] Edwards W (1991) In D KLASS, Energy from biomass and wastes XV (p. 503). Chicago: Institute of gas technology.

[31] Mujumdar A (2007) Handbook of industrial drying. CRC Press.

[32] Joung HT, Seo YC, Kim KH, Seo YC (2006) Effects of oxygen, catalyst and PVC on the formation of PCDDs, PCDFs and dioxin-like PCBs in pyrolysis products of automobile residues. Chemosphere, 65, pp. 1481-1489.

[33] Wendlandt W (1982, April) Thermal analysis. Analytical Chemistry, 54(5), pp. 97R-105R.

[34] Chang YM (1996) On pyrolysis of waste tire: degradation rate and product yields. Resources, Conservation and Recycling, 17, pp. 125-139.

[35] Varhegyi G, Bobaly B, Jakab E, Chen H (2011, January) Thermogravimetric study of biomass pyrolysis kinetics: a distributed activation energy model with prediction tests. Energy & Fuels, 25(1), pp. 24-32.

[36] Babu B (2008, Sept/Oct) Biomass Pyrolysis: a state-of-the-art review. Biofuels, Bioproducts and Biorefining, 2(5), pp. 393-414.

[37] Gasparovic L, Korenova Z, Jelemsky L (2010) Kinetic study of wood chips decomposition by TGA. Chemical Papers, 64(2), pp. 174-181.

[38] Rao R, Sharma A (1998) Pyrolysis rates of biomass materials. Energy, 23(11), pp. 973-978.

[39] Roberts AF (1970) A review of kinetics data for the pyrolysis of wood and related substances.Combustion and Flame, 14(2), pp. 261-272.

[40] Jiang G, Nowakowski DJ, Brigwater AV (2010) A systematic study of the kinetics of lignin pyrolysis. Thermochimica Acta, 498, pp. 61-66.

[41] Bridgwater A (2012, March) Review of fast pyrolysis of biomass and product upgrading. Biomass & bioenergy, 38, pp. 68-94.

[42] Williams P, Besler S, Taylor D (1990, December) The pyrolysis of scrap automotive tyres: the influence of temperature and heating rate on product composition. Fuel, 69(12), pp. 1474-1482.

[43] Demirbas A (2004, June) Effect of initial moisture content on the yields of oily products from pyrolysis of biomass. Journal of Analytical and Applied Pyrolysis, 71(2), pp. 803-815.

[44] Chen G, Sjostrom K, Bjornbom E (1992) Pyrolysis/gasification of wood in a pressurized fluidized bed reactor. Industrial & Engineering Chemistry Research, 31(12), pp. 2764-2768.

[45] Pindoria R, Megaritis A, Messenbock R, Dugwell D, Kandiyoti R (1998) Comparison of the pyrolysis and gasification of biomass: effect of reacting gas atmosphere and pressure on Eucalyptus wood. Fuel, 77(11), pp. 1247-1251.

[46] Weiland N, Means N, Morreale B (2012, April) Product distributions from isothermal co-pyrolysis of coal and biomass. Fuel, 94, pp. 563-570.

[47] Mullen C, Boateng A, Mihalcik D, Goldberg N (2011) Catalytic fast pyrolysis of white oak wood in a bubbling fluidized bed. Energy & Fuels, 25, pp. 5444-5451.

[48] Kunii D, Levenspiel O (1991) Fluidization Engineering (éd. 2nd). Butterworth-Heinemann.

[49] Yang WC (2003) Handbook of fluidization and fluid-particle systems (Chemical Industries). CRC Press.

[50] Dynamotive Energy (2012) Corporate History. Consulted on March 1st, 2012, on Dynamotive, the evolution of energy: http://www.dynamotive.com/about/corporate-history/

[51] Clausthal University of Technology, Institute of Energy Process Engineering and Fuel Technology, Prof. Dr.-ing. Roman Weber, http://www.ievb.tu-clausthal.de.

[52] Kothari A (1967) Master Thesis. Chicago, Illinois: Illinois Institute of Technology.

[53] Avidan A, Yerushalmi J (1985, May) Solids mixing in an expanded top fluid bed. AICHe Journal, 31(5), pp. 835-841.

[54] Watanabe I, Yong C, Hasatani M, Yushen X, Naruse I (1991) Gas to particle heat transfer in fast fluidized beds. Circulating Fluidized Bed Technology III (pp. 283-287). Pergamon Press.

[55] Wang H, Srinivasan R, Yu F, Steele P, Li Q, Mitchell B (2011) Effect of acid, alkali and steam explosion pretreatments on characteristics of bio-oil produced from pinewood. Energy & Fuels, 25, pp. 3758-3764.

[56] Lima I, Boateng A, Klasson K (2010) Physicochemical and adsorptive properties of fast pyrolysis bio-chars and their steam activated counterparts. Journal of Chemical Technology & Biotechnology, 85, pp. 1515-1521.

[57] Ranz W (1952, May) Friction and transfer coefficients for single particles and packed beds. Chemical Engineering Progress, 48(5), pp. 247-253.

[58] Van der Drift A, Boerrigter H, Coda B, Cieplik M, Hemmes K (2004) Entrained flow gasification of biomass. ECN.

[59] Sun S, Tian H, Zhao Y, Sun R, Zhou H (2010) Experimental and numerical study of biomass flash pyrolysis in an entrained-flow reactor. Bioresource Technology, 101, pp. 3678-3784.

[60] Mellmann J (2001) The transverse motion of solids in rotating cylinders - forms of motion and transition behaviour. Powder Technology, 118, pp. 251-270.

[61] Fantozzi F, Colantoni S, Bartocci P, Desideri U (2007) Rotary kiln slow pyrolysis for syngas and char production from biomass and waste - Part II: Introducing product yields in the energy balance. Journal of Engineering for gas turbines and power, 129, pp. 908-913.

[62] Ingram L, Mohan D, Bricka M, Steele P, Strobel D, Crocker D, Mitchell B, Mohammad J, Cantrell K, Pittman Jr CU (2008) Pyrolysis of wood and bark in an auger reactor: Physical properties and chemical analysis of the produced bio-oils. Energy & Fuels, 22, pp. 614-625.

[63] Thangalazhy-Gopakumar S, Adhikari S, Ravindran H, Gupta RB, Fasina O, Tu M, Fernando SD (2010) Physicochemical properties of bio-oil produced at various temperatures from pine wood using an auger reactor. Bioresource Technology, 101, pp. 8389-8395.

[64] He R, Ye X, English B, Satrio J (2009) Influence of pyrolysis condition on switchgrass bio-oil yield and physicochemical properties. Bioresource Technology, 100, pp. 5305-5311.

[65] Sanchez ME, Menendez JA, Dominguez A, Pis JJ, Martinez O, Calvo LF, Bernad PL (2009) Effect of pyrolysis temperature on the composition of the oils obtained from sewage sludge. Biomass and Bioenergy, 22, pp. 922-940.

[66] Mohan D, Pittman Jr C, Steele P (2006) Pyrolysis of wood/biomass for bio-oil: a critical review. Energy & Fuels, 20, pp. 848-889.

[67] Khan M (1987) Production of high quality liquid fuels from coal by mild pyrolysis of coal/lime mixtures. Energy & Fuels, 5(2), pp. 185-231.

[68] Lin L, Khang S, Keener T (1997) Coal desulfurization by mild pyrolysis in a dual-auger coal feeder. Fuel Processing Technology, 53, pp. 15-29.

[69] Cho MH, Jung SH, Kim JS (2010) Pyrolysis of mixed plastic wastes for the recovery of benzene, toluene, and xylene (BTX) aromatics in a fluidized bed and chlorine removal by applying various additives. Energy & Fuels, 24, pp. 1389-1395.

[70] Huber G, Iborra S, Corma A (2006) Synthesis of transportation fuels from biomass: chemistry, catalysts and engineering. Chemistry Review, 106, pp. 4044-4098.

2.3 REVUE CRITIQUE DE LA LITTÉRATURE

Plusieurs facteurs et besoins ont dirigé cette recherche doctorale. Cette section fait état des justifications des trois objectifs spécifiques présentés dans le Chapitre 1.

2.3.1 MODÈLE CINÉTIQUE

Tel que décrit dans la section 2.2, trois familles de modèles ont été répertoriées : les modèles à composante unique, les modèles à composantes ou « pseudo-composantes » multiples et enfin,

les modèles à réactions en série et en parallèle. Un modèle a été sélectionné dans la littérature comme représentant de chacune de ces familles afin de simuler les batches de pyrolyse industrielles obtenues chez un partenaire existant. Le procédé Ecolomondo a démontré son potentiel depuis plusieurs années en réussissant à convertir des tonnes de pneus usagés en gaz, huile et char.

Connaissant en continu la température réelle des pneus durant la pyrolyse, il a été possible de modéliser la production dynamique d'huile et de la comparer à la production monitorée à l'usine. Le graphique suivant montre la performance des trois modèles choisis.

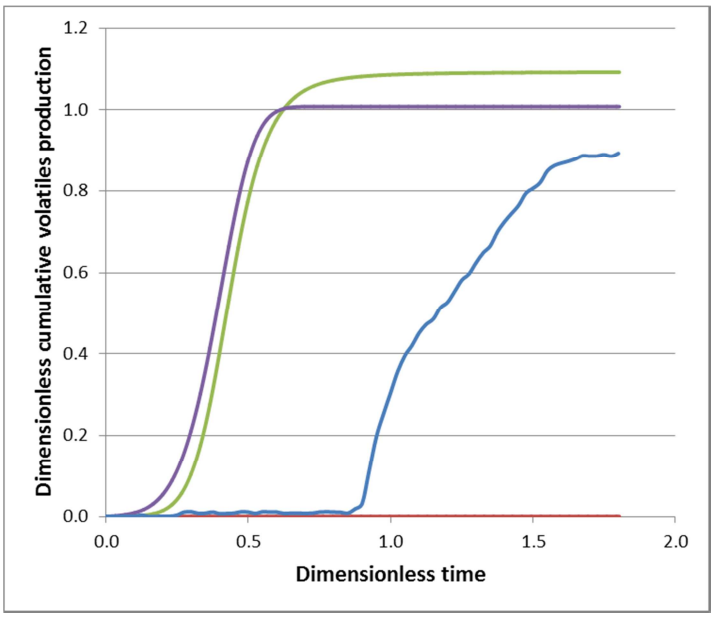

Figure 2.3.1. Simulation de la production d'huile/volatiles; vert = modèle à composante unique (Chang, 1996); violet = modèle à réactions en série/parallèle (Olazar, 2008); rouge = modèle à composantes multiples (Leung, 1999); bleu = production d'huile en usine.

Trois critères peuvent être considérés pour l'analyse de la performance des modèles. Dans un premier temps, un modèle devrait être capable de prédire le moment où la production d'huile débute. Ce facteur dépend grandement de l'ajustement de l'énergie d'activation et du facteur pré-

exponentiel de la loi d'Arrhénius. Dans un deuxième temps, la production dynamique devrait être suivie précisément dans le temps. Dans un système où la température varie, cela dépend non seulement de l'ajustement des constantes cinétiques, mais aussi de l'ordre apparent de la réaction, sachant que l'accélération ou le ralentissement de la cinétique doit être fidèle au taux de production d'huile. Enfin, le rendement cumulatif en huile doit être respecté puisqu'il s'agit du point de validation central du caractère prédictif du modèle.

Au niveau de la prédiction du début de la production d'huile, le modèle à composante unique et à réactions en série/parallèle ont été trop prompts à produire de l'huile, soit trois fois plus rapidement que le temps réel observé. Quant au modèle à composantes multiples, il n'a pas eu de début de production et est demeuré sans production significative tout au long de la simulation.

Ce modèle n'a donc pas non plus réussi à suivre la production dynamique d'huile. Les modèles à composante unique et à réactions en série/parallèle ont été encore une fois trop prompts : leur production dynamique d'huile s'est faite sur une période deux fois plus courte que la production d'usine.

Finalement, la prédiction du rendement d'huile cumulatif a été plus adéquate quoiqu'aucun modèle n'ait pu atteindre une précision suffisante. À nouveau, le modèle à composantes multiples n'a pas eu de cinétique notable, le rendement est demeuré inférieur à 1 % de la masse initiale de pneus. Les deux autres modèles ont prédit trop d'huile, soit un excès d'environ 20 % pour le modèle à composante unique et un excès d'environ 10 % pour le modèle à réactions en série/parallèle.

Les raisons expliquant cette performance insuffisante des modèles tirés de la littérature sont multiples. Tout d'abord, plusieurs modèles sont basés sur la quantité finale de char, W_∞. Or, ce paramètre varie directement avec les conditions de pyrolyse et n'est donc pas une constante, contrairement à ce que les auteurs supposent. Par exemple, dans le cas d'une pyrolyse à basse

température, la quantité de char est de beaucoup supérieure à la valeur utilisée dans la littérature. Le résultat est donc que la convergence se fera malgré tout à la valeur surestimée de char, mais en un temps de résidence plus long.

Aussi, plusieurs modèles ne sont simplement pas capables de prédire la production d'huile puisqu'ils ont été développés pour prédire les volatiles totaux. Comme le ratio gaz/huile n'est pas constant, il n'est alors pas possible d'extraire des rendements pour l'huile seule et ces modèles sont inutilisables.

Une autre raison est l'inexactitude des températures. En effet, plusieurs modèles développés ont vu leurs constantes cinétiques déterminées pour des températures d'opération et non des températures réelles de masse. Puisque la pyrolyse est généralement un processus endothermique, la température d'opération demeure supérieure à la température réelle de la matière décomposée et les constantes sont alors surestimées. Ce sont là les motivations ayant poussé l'élaboration d'un nouveau modèle cinétique pour la pyrolyse des pneus.

2.3.2 BILAN D'ÉNERGIE

Tout d'abord, il est étonnant de constater le nombre limité d'études sur la thermochimie et la thermodynamique en pyrolyse. Encore plus surprenant, malgré la reconnaissance théorique du caractère endothermique de la pyrolyse en général, les courbes obtenues en calorimétrie DSC (Differential Scanning Calorimetry) montrent un pic exothermique, ou de libération de chaleur. Le graphique suivant montre un de ces pics typiquement obtenus.

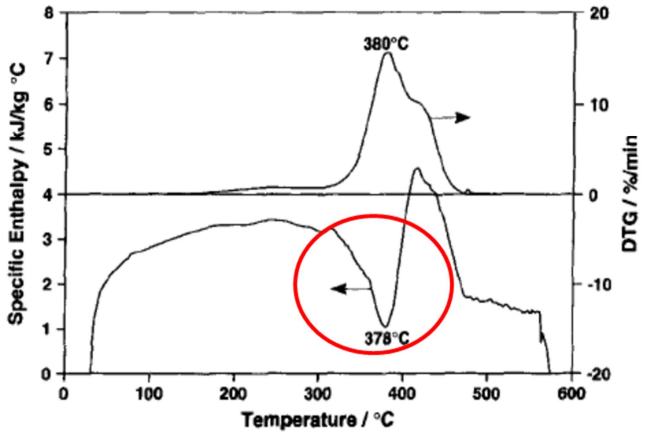

Figure 2.3.2. Observation typique d'un pic exothermique dans une courbe DSC lors d'une expérience en pyrolyse (Chang, 1996).

L'enthalpie de pyrolyse est quant à elle souvent simplifiée en un terme réactionnel et un terme d'évaporation des volatiles, les deux étant des constantes toutes deux proportionnelles à la perte de masse pendant la pyrolyse. Le tableau suivant montre des valeurs retrouvées dans la littérature pour ces deux termes.

Tableau 2.3.1. Enthalpies de pyrolyse tirées de la littérature.

Feedstock	Heat of pyrolysis/Heat of vaporization of liquids (kJ/kg)	Reference
Wood	235	Koufopanos
Wood	190	Klason
Wood	-340	Thomas
Wood	-115 to -280	Roberts
Wood	-254	Beall
SBR	-164/180	Yang
SBR	-500/280	Yang
SBR	-660	Brazier
BR	-760/280	Yang
BR	-880	Brazier
BR	-945	Sircar
NR	-560/170	Yang

Pour obtenir ces termes, il a dû être supposé que la capacité calorifique évolue de façon strictement croissante en fonction de la température, alors que peu d'informations sont disponibles à cet égard.

Pour vérifier la robustesse des données DSC, la loi de Hess et des données industrielles ont été utilisées. La loi de Hess a permis de confirmer que globalement, la pyrolyse est un processus très endothermique pour les pneus, avec des énergies totales impliquées tournant autour des 1 000 kJ/kg. Au niveau des données industrielles, l'évolution de la température pendant la phase de production d'huile n'a montré aucun signe d'emportement, point caractéristique des systèmes réactifs exothermiques. C'est donc sur la base de ces contradictions que l'étude sur l'enthalpie de pyrolyse et l'évolution de la chaleur spécifique pendant la pyrolyse a été justifiée, sachant l'importance d'une estimation précise de la température pour le modèle cinétique.

2.3.3 SÉLECTIVITÉ DU SOUFRE

La présence de soufre dans les pneus est intrinsèque de par la vulcanisation. La normalisation serrée dont font l'objet les combustibles vis-à-vis leur teneur en soufre aurait dû justifier des études approfondies sur le devenir du soufre lors de la pyrolyse des pneus. Pourtant, les huiles de pyrolyse des pneus, souvent considérées pour des applications énergétiques, n'ont pas de littérature abondante à ce sujet. Le tableau qui suit montre certaines données brutes obtenues de la littérature.

Tableau 2.3.2. Données de la littérature sur la sélectivité du soufre dans les produits de pyrolyse.

Temperature (°C)	Pyrolysis weight loss %	Sulfur weight loss %	$s_{SL/TWL}$	Reference	Apparatus	Inorganics in waste tires
350	50	25	0.5	Diez	Static oven, no gas sweep	Zn
450	60	40	0.67			
550	67	48.9	0.73			
400	36	33.3	0.89	Berrueco	Customized TGA, N_2 flow	Zn, Fe
500	47.3	29.6	0.59			
550	47.5	30.8	0.61			
300	4.8[a]	4.8[a]	1.0	Laresgoiti	Autoclave, N_2 flow	Zn, Fe
400	24.8[a]	18.2[a]	0.73			
500	38.0[a]	35.5[a]	0.93			
[a] Based on pyrolysis liquids only						

Un premier auteur a obtenu une sélectivité du soufre dans les volatiles croissante avec la température. Un second auteur a obtenu une tendance contraire, alors que les données d'un troisième auteur n'ont montré aucune tendance nette. Cependant, il est important de noter la présence d'acier structural dans les pneus chez les deux derniers auteurs et les différentes températures étudiées.

Dans ces conditions, des données supplémentaires étaient requises pour permettre une étude plus poussée sur la sélectivité du soufre dans les volatiles, sur les mécanismes contrôlant leur migration vers les volatiles lors de la pyrolyse. Le but visé serait de développer un outil prédictif pour estimer la teneur en soufre des produits de pyrolyse en fonction des conditions d'opération à l'échelle industrielle. Un tel outil faciliterait l'identification et l'optimisation des besoins de traitement des produits pyrolytiques à la phase de design.

CHAPITRE 3 MODÉLISATION DE LA CINÉTIQUE

Cet article a été accepté en 2013 dans le journal Energy & Fuels.

3.1 PRÉSENTATION DE L'ARTICLE

L'objectif de cette publication était de modéliser la cinétique de pyrolyse des pneus pour un procédé industriel existant, afin de prédire les taux de production pour chacun des produits pyrolytiques, nommément le gaz non-condensable, l'huile et le char. Trois modèles différents tirés de la littérature ont été confrontés aux données de production industrielle et n'ont pas permis de représenter adéquatement le début de la production, le temps de résidence requis des pneus et le rendement cumulatif d'huile de pyrolyse.

Le nouveau modèle cinétique développé considère une cinétique de pyrolyse (décomposition) unique, mais combinée à des sélectivités intrinsèques pour chacun des produits de pyrolyse en fonction uniquement de la température. Les simulations réalisées avec des données industrielles réalisées à des conditions différentes (2 batches) ont réussi à prédire avec justesse le début de la production d'huile pyrolytique, la phase de production dynamique d'huile (temps de résidence) ainsi que le rendement cumulatif d'huile. Ces extrapolations ont permis de valider le nouveau modèle cinétique.

3.2 PREDICTIVE KINETICS MODEL FOR AN INDUSTRIAL WASTE TIRE PYROLYSIS PROCESS

Predictive Kinetics Model for an Industrial Waste Tire Pyrolysis Process

*Jean-Remi Lanteigne[1], Jean-Philippe Laviolette[1], Gilles Tremblay[2] and Jamal Chaouki[1]**

1. *Chemical Engineering Department, École Polytechnique de Montréal, C.P. 6079, succ. Centre-Ville, Montréal, Qc, Canada H3C 3A7*

2. Ecolomondo Corp., 3435 boul. Pitfield, St-Laurent, Qc, Canada H4S 1H7

*Corresponding Author (jamal.chaouki@polymtl.ca)

3.2.1 Abstract

A new pyrolysis model was developed to predict the individual products (non-condensable volatiles, condensable volatiles and char) yield for Ecolomondo's industrial waste tire pyrolysis process. This novel predictive kinetics-based model couples products selectivity data obtained from TGA experiments with a global single-step decomposition reaction term to reproduce the non-linear relationship between product selectivity and temperature. A transient energy balance based on a lumped-capacitance method was also used to calculate the tire shreds temperature using the rotary drum wall temperature as an input. The kinetics model was compared with experimental oil production data from the industrial process as well as existing models in the literature. It is shown that the model can successfully predict the oil production of the industrial process and the model accuracy is greater for smooth operating conditions. On the other hand, other pyrolysis models from the literature failed to accurately predict the oil production.

Keywords – Pyrolysis, Waste tires, Model, Predictive, Batch reactor, Rotary drum

3.2.2 Nomenclature

A	Pre-exponential factor (min^{-1})
C_{Pbed}	Tire shred bed specific heat ($J^1kg^{-1}K^{-1}$)
C_{Pchar}	Char heat capacity ($J^1kg^{-1}K^{-1}$)
C_{Psteel}	Steel heat capacity ($J^1kg^{-1}K^{-1}$)
C_{Ptire}	Tire heat capacity ($J^1kg^{-1}K^{-1}$)
E_a	Activation energy (J^1mol^{-1})
Fr	Froude number
g	Gravity constant (m^1s^{-2})
h	Average thermal convection coefficient ($W^1m^{-2}K^{-1}$)

H_{pyr} Heat consumed by pyrolysis (J^1min^{-1})

k Kinetics constant (min^{-1})

m Mass (kg)

m_{bed} Mass of bed (kg)

m_{char} Mass of char (kg)

m_o Initial mass (kg)

$m_{pyrolysis}$ Mass of converted pyrolysables (kg)

m_{steel} Mass of steel (kg)

m_{tire} Mass of tire sample (kg)

$m_{tire\_initial}$ Mass of initial tire sample (kg)

$m_{volatiles}$ Mass of generated volatiles (kg)

m_∞ Mass of residual solids at 100% conversion (kg)

$M_{reactant}$ Dimensionless weight

n Order of reaction

r_{char} Reaction rate (min^{-1})

$r_{devolatilization}$ Rate of devolatilization (min^{-1})

r_{gas} Rate of formation of pyrolysis gas (min^{-1})

r_i Rate of formation of pyrolysis product *i* (min^{-1})

r_{oil} Rate of formation of pyrolysis oil (min^{-1})

$r_{products}$ Rate of formation of pyrolysis products (min^{-1})

$r_{pyrolysis}$ Rate of pyrolysis (min^{-1})

$r_{volatiles}$ Rate of production of volatiles (min^{-1})

R Perfect gas constant ($J^1mol^{-1}K^{-1}$)

S_{char} Instantaneous char selectivity

S_{gas} Instantaneous gas selectivity

S_i Instantaneous product *i* selectivity

S_{oil} Instantaneous oil selectivity

t Time (min)

T Temperature (K or °C)

T_{wall} Wall temperature (K or °C)

T_{bed} Bed temperature (K or °C)

W_{exp} Tire shred bed surface exposed the drum wall (m^2)

Greek letters

ω Rotational speed (s^{-1})

3.2.3 INTRODUCTION

Waste tire management is a major issue and despite an intensification of recovery efforts, a significant part of waste tires is not yet utilized. In the United States, the Rubber Manufacturers Association[1] estimated that approximately 15 % of the 5 million tons of generated waste tires in 2009 remain unmanaged. Moreover, 12.6 % of the managed tires are landfilled and 40.3 % are burned as a tire-derived fuel.

Recent life-cycle analysis has demonstrated that landfilling has the worst environmental impact for waste tire management[2]. On the other hand, the environmental impacts of thermo-chemical treatments, such as pyrolysis and gasification, were shown to be significantly lower than incineration, which is currently the most widely used thermal process[1,3]. The development of reliable industrial pyrolysis and gasification technologies could open new possibilities for the sustainable management and commercial recovery of waste tires. On a smaller scale, pyrolysis

may be techno-economically more interesting compared to gasification since a need of less process equipment and a lower operating temperature result in significantly lower initial capital investments[4]. In addition, the pyrolysis oil produced from conventional waste tires typically contains high fractions of diesel-like fuel[5], which makes it attractive for commercial energy applications. It is estimated that as much as 67.9% of the annually generated waste tires could be reoriented toward pyrolysis processes[1].

Pyrolysis is an anaerobic thermal decomposition process. Waste tire pyrolysis yields three products: (1) a carbon-based powder (solid) named char, (2) an oily liquid rich in hydrocarbons, and (3) a non-condensable gas composed of hydrogen and light hydrocarbons. The respective yield of the three pyrolysis products as well as their chemical composition will depend on the pyrolysis conditions: (1) temperature, (2) residence time, (3) particle size, and (4) pressure. Several pyrolysis processes that promote specific reaction conditions have therefore been proposed and developed. These pyrolysis processes have been categorized into three main types based on the pyrolysis conditions: (1) conventional (slow) pyrolysis, (2) fast (or ultra-fast) pyrolysis and (3) vacuum pyrolysis. Table 1 summarizes the characteristic operating conditions of the three types of pyrolysis.

Table 3.2.1. Types of pyrolysis with their approximate operating parameters.

Type of Pyrolysis	**Parameter**			
	Temperature (°C)	**Residence time (s)**	**Particle size (mm)**	**Pressure (kPa)**
Conventional (slow)	300-450	300-3,600	5-50	100-500
Fast or ultra fast	450-750	0.5-10	<1	100-500
Vacuum	450-750	10-300	5-50	<25

The three types of pyrolysis are characterized by different heating rates. Varying the heating rate will influence the time spent by the feedstock at a specific temperature during the pyrolysis

process and the maximum temperature reached before complete conversion. For conventional and fast pyrolysis, the heating rate will be about < 1°C/s and 5-200°C/s, respectively. Vacuum pyrolysis will be characterized by a slightly faster heating rate compared to conventional pyrolysis, but noticeably slower than fast pyrolysis. The selected heating rate affects the product selectivity and may be limited by the equipment and the solids properties.

The reactor selection is key to promote the desired pyrolysis conditions. Several types of reactors have been studied for pyrolysis, but the main industrial pyrolysis processes use fluidized bed reactors (circulating and bubbling), rotating cone reactors and batch rotary drums. Table 2 lists some of the main pilot and industrial scale pyrolysis processes along with their characteristics.

Table 3.2.2. Large-scale pyrolysis processes list. *CFB: Circulating Fluidized-bed, FB: Bubbling Fluidized-bed, RC: Rotating Cone reactor, BRD: Batch Rotary Drum, IRV: Inclined Retort Vessel

Company	**Feedstock**	**Type of pyrolysis**	**Reactor***	**Temperature**	**Feeding rate**	**Comments**
Ensyn	Dried wood biomass	Ultra Fast	CFB	500-700°C	up to 100 TPD	Industrial scale
Dynamotive	Sawdust-like biomass	Fast	FB	450-500°C	up to 200 TPD	Industrial scale
ROC	Sawdust-like biomass	Fast	FB	450-500°C	up to 200 TPD	Working with Dynamotive technology in Australia
BTG	Dried biomass chips	Fast	RC	450-600°C	up to 200 kg/h	Pilot-scale
Ecolomondo	Waste tire shreds	Conventional	BRD	250-500°C	16 TPD per reactor	Industrial scale Batch process Multi-module plants to minimize the effects of process turndown
Pirore DBA Black and Green	Waste tire shreds	Fast	Unknown	150-400^{o}C	16,500 TPY	Industrial scale Continuous process
Conrad Industries Inc.	Waste tire shreds	Fast	IRV	500-750^{o}C	24 TPD	
Harmonic Energy Inc.	Waste tires	Fast	Kiln	430^{o}C	150 TPD	
Metso Minerals	Waste tire shreds	Fast	Kiln	450^{o}C	91 TPD	

Rotary drums offer significant advantages over the other types of reactors. Firstly, minimal feedstock pre-treatment is required in opposition to fluidized bed processes, which may need significant pre-treatment at additional costs to ensure a good fluidization quality. Secondly, the continuous flow of an inert gas (for example, inert fluidization gas is required in fluidized beds) is not required such that the non-condensable gas is not diluted and can be used (burned) to produce energy. Hence, rotary drum pyrolysis processes can be auto-thermal via non-condensable gas combustion so both oil and char can be marketed. Continuous operation fluidized bed technologies supply their energy demand with char combustion, while non-condensable gas fraction cannot be marketed due to dilution. Nevertheless, batch fluidized beds can recover these gases as an energy source while marketing char.

To design an industrial pyrolysis process, the development of an accurate reaction model is essential to ensure process safety and techno-economic viability. For HAZOP, the prediction of the process behaviour is mandatory to develop efficient emergency procedures. Furthermore, the profitability of a pyrolysis process is highly sensitive on the product yields, which is greatly dependent on the process operation. It is therefore necessary to relate product yields to the operating conditions for process optimization. At the industrial scale, process optimization can require significant time and costs if experimental process tuning is performed: an accurate pyrolysis model will help minimize these costs.

Many pyrolysis models are found in the literature and most of them were developed and validated with thermogravimetric (TGA) data. Babu et al.[6] reviewed most of the pyrolysis models found in the scientific literature. Pyrolysis models were classified into three main categories: (1) single-step reaction, (2) intermediate reactions, and (3) a combination of single-step reactions. Using a global single-step reaction represents the simplest pyrolysis model and it has been shown that many materials cannot be represented by this model as pyrolysis kinetics can significantly change with varying temperatures. Only a few pure materials, like low-density polyethylene, have shown this single-step reaction behaviour. For heterogeneous feedstocks, such as waste tires, biomass, automobile shredder residue, and municipal solid waste, more complex kinetics are required to

model pyrolysis. Most of waste tire pyrolysis studies reported in the literature (based on TGA experiments) showed several stages of decomposition leading to the notion of pseudo-components: these different stages must be accounted for in a model.

The second family of pyrolysis models considers intermediate reactions: the feedstock decomposes into intermediate products, which undergo further reactions. This representation may describe the physical process occurring during pyrolysis, but these models are very hard to tune. In fact, one must precisely know the number of intermediate products to model the secondary reactions and so forth if more than two reactions in series are considered. The uncertainties will then propagate and make the model less robust to changes in operating conditions. This type of model will especially yield uncertainties for heterogeneous materials.

The third family of reaction models consists of a linear combination of single-step pyrolysis reactions. The model can consider a combination of real components (for example, tires contain butadiene and styrene-butadiene rubbers) or it can consider a combination of pseudo-components where every decomposition level observed in TGA experiments counts as one of these pseudo-components. This type of reaction model is robust since the amount of components or pseudo-components are independent from the reaction yield and can be tuned separately. However, it does not physically represent pyrolysis as well as the second family of models.

To estimate the respective yield of pyrolysis products, the three types of models described above use one or several parallel and/or series kinetic steps to calculate their formation rate. These reaction steps are generally expressed as global devolatilization or volatilization rates, which are assumed to follow a modified Arrhenius law[7]:

$$r_{devolatilization} = -\frac{dM_{reactant}}{dt} = k(T) \cdot f(M_{reactant})^n \quad (1)$$

$$k(T) = A \cdot \left(e^{-E_a/RT}\right) \quad (2)$$

As shown in equations (1) and (2), the global devolatilization rate ($r_{devolatilization}$) is a function of temperature (T), a pre-exponential factor (A) and an activation energy (E_a) using the Arrhenius law as well as the mass of the reactant ($M_{reactant}$) to the power n, which corresponds to the order of reaction. Pyrolysis models generally predict the rate of formation of volatiles, but do not differentiate between the condensable and non-condensable fractions. Furthermore, the use of several kinetic steps to predict the pyrolysis of heterogeneous feedstocks involves the evaluation of multiple parameters from experimental data. An increasing number of model parameters most likely leads to greater uncertainties or decreased robustness. Note that in reality, devolatilization most likely involves numerous series and parallel elemental reaction steps. However, micro-kinetics models that can accurately reproduce feedstock devolatilization have yet to be developed. Many authors assume an arbitrary order of reaction (n). Since a myriad of reactions are simplified into only a few global reaction steps, this parameter should ideally be fitted and not fixed. Fixing an arbitrary order of reaction may produce a bias on the activation energy term.

The function $f(M_{reactant})$ in equation (1) is generally normalized to the amount of volatiles that have been released from the sample in a TGA:

$$M_{reactant} = \frac{(m_0 - m)}{(m_0 - m_\infty)} \quad (3)$$

$$f(M_{reactant}) = (1 - M_{reactant}) \quad (4)$$

In equation (3), the terms m_0, m_∞ and m correspond to the initial, final (complete conversion) and instantaneous mass of the pyrolyzed sample, respectively. Furthermore, $M_{reactant}$ represents the

cumulative normalized weight loss of the sample. In equation (4), (1 - $M_{reactant}$) thus corresponds to the instantaneous normalized sample weight.

In the vast majority of models proposed in the scientific literature, the parameters (A, E_a and n) are estimated from thermogravimetric (TGA) experiments[8-15]. Since reaction rates are strongly dependent upon temperature according to equation (2), the estimation of activation energy terms may yield significant errors[16]. The uncertainty may principally arise from the TGA temperature measurements, which correspond to the gas temperature. In fact, the solid sample temperature may be significantly different – during a non-isothermal TGA experiment with a specific temperature ramp-up rate, the solid sample temperature may be lower than the gas temperature due to heat transfer limitations[16]. In this case, the estimated kinetics parameters are biased and the error is transmitted to the other kinetics parameters, depending on their sensitivity. These models may therefore yield significant errors when extrapolated outside the range of conditions at which they were validated.

Furthermore, two other significant uncertainties related to this weight normalization directly affect the models accuracy and robustness. First of all, the complete conversion weight (m_∞) strongly depends on the heating and temperature history. Consequently, a model fitted with the results of a specific non-isothermal TGA experiment may yield significant errors when applied to industrial runs where the heating rate may not be similar. Another source of error may result from the use of the instant normalized sample weight ($1 - M_{reactant}$) in equation (4). This kinetics driving term may not be representative of reality since the parameter m_∞, which represents the total amount of volatiles emitted during decomposition, is strongly dependent on the temperature-time profile.

In the present study, a novel pyrolysis model of waste tire shreds that predicts individual product yields, as well as accounting for their temperature-dependency, was developed for waste tires. The model uses a single global kinetic step to describe the virgin material decomposition and use

the concept of product selectivity to predict individual product yields (char, condensable gas and non-condensable gas) with a minimal number of fitted parameters. Furthermore, to reduce the uncertainties associated with the estimation of model parameters, they were estimated from TGA and industrial data from the Ecolomondo process. Finally, the model was also compared to other pyrolysis models in the scientific literature.

3.2.4 EXPERIMENTAL APPARATUS

Experiments were performed on two main apparatus. A TGA apparatus was first used to evaluate and optimize the model kinetic parameters. Afterwards, industrial data from the Ecolomondo pyrolysis process data were used to estimate heat/mass transfer model parameters and to validate the model under different conditions.

3.2.4.1 TGA apparatus

TGA experiments were performed using a Q5000 apparatus from TA Instruments. Regularly shaped cubic tire samples of 30 mg were used for each experiment. The samples were mounted on a platinum pan with a nitrogen flow of 20 mL/min. The heating rates were selected as per reference[17], i.e. 5°C/min, 20°C/min, 40°C/min and 80°C/min. The experiments were conducted until there was no sample weight loss (less than 0.01 % weight loss during 15 minutes span). During these experiments, the time evolution of the solid mass was measured, which is directly related to the mass of combined volatiles.

3.2.4.2 Industrial Ecolomondo process

Ecolomondo Corporation is an environmental company performing waste tire pyrolysis on an industrial scale rotary drum reactor processes. The plant is located at a distance of about 80 km from Montreal (Quebec, Canada). The Ecolomondo process consists of a pyrolysis process in batch mode using a rotary drum reactor. Prior to the pyrolysis reaction, an industrial shredder is used to reduce waste tires into relatively regular small particles without removing metals.

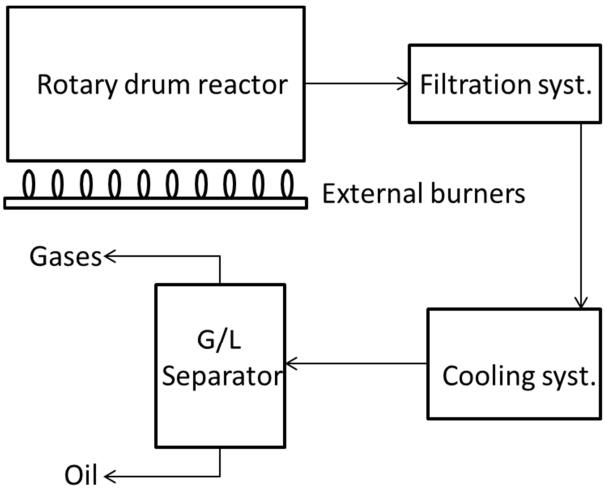

Figure 3.2.1. Simplified representation of the Ecolomondo™ process.

Figure 3.2.1 shows a simplified process flow diagram of the Ecolomondo™ pyrolysis process: waste tire shreds are loaded into the rotary drum reactor, which is sealed and purged of oxygen prior to reaction. At this stage, external gas burners, linearly disposed under the rotary drum, are raised to increase the temperature of the reactor wall and waste tire shreds. The temperature of the reactor wall and the bed of the waste tire shreds as well as the drum internal pressure are continuously monitored using thermocouples and pressure sensors, so that the operator can observe the pyrolysis process in real-time. The state of the art Ecolomondo's TDP process has been designed to be fully automated with minimal operator interaction. The temperature of the reactor wall is measured on the upper side of the rotary drum (opposite the burners, which are located on the bottom).

During the pyrolysis process, the waste tire shreds undergo thermal decomposition that yields gaseous products (condensable and non-condensable gas): these products are continuously evacuated out of the rotary drum reactor to a set of condensers followed by gas-liquid separation drums. The non-condensable gas and condensed gas (oil) are then stored in tanks. During a pyrolysis batch, the weight of produced condensable gas (oil) is continuously monitored.

When the pyrolysis reaction is complete (internal pressure is no longer increasing), the rotary drum temperature and rotational speed are both increased to promote a reduction in char particle size and particle size distribution and the agglomeration of steel residue. The reactor is then cooled by water injection: water is fed inside the rotary drum reactor, vaporized and purged from the reactor. Residual steel and char particles are evacuated (independent vacuum system) to a series of cyclone and bag-house filters where steel is separated from the char particle size and fractionation is performed (2 types of char based on particle size distribution).

The estimated time required for the completion of a batch, including the loading and unloading of the reactor, is less than 6 hours. The rotary drum reactor capacity is 5,500 kg of waste tire shreds.

3.2.5 PYROLYSIS MODEL

The pyrolysis model includes three main components: (1) reactor (rotary drum) solids hydrodynamics, (2) reaction kinetics and (3) energy balance.

3.2.5.1 Rotary drum solids hydrodynamics

In rotary drum pyrolysis, the solids transport phenomena are mainly governed by segregation and attrition. At the beginning of the pyrolysis process, the waste tire shreds are relatively uniform such that segregation is limited. Attrition occurs as the pyrolysis process proceeds when the particle surfaces collapse under the action of repeated collisions induced by the motion of the rotary drum: the particle size distribution widens and the particles segregate within the bed. This phenomenon induces the motion of solids so that heat and mass transfers in the rotary drum reactor are promoted. Moreover, Ecolomondo™'s rotary drum reactor has special means of improving the solids mixing inside the reactor.

This segregation behaviour is supported experimentally by Alizadeh et al.[18], which performed experiments in a small-scale rotary drum. They explicitly demonstrated that the smaller particles tend to segregate to the centre of the bed in a rotary drum, while bigger particles remain along the

outer layer of the bed. This strongly suggests that small particles produced from the attrition of the larger particles at the periphery of the bed will migrate to the center of the bed: this significantly improves the heat and mass transfers.

Mixing in the rotary drum reactor depends on several operating conditions. According to Mellmann[19], the diameter, rotational speed, and filling level of the drum as well as the friction coefficients in the system mainly govern the flowing regime and the quality of mixing. The Froude number characterizes the effects of drum radius (R) and angular rotational speed (ω):

$$Fr = \frac{\omega^2 R}{g} \tag{5}$$

With an increasing Froude number, the rotary drum hydrodynamics have been observed to change from slipping to cascading and, finally, cataracting motion. Of the several types of motions, it has been demonstrated that cascading flow patterns maximize mixing[19]. In the Ecolomondo™ process, the rotary drum reactor is operated with a Froude number between 0.05 and 0.1, which maximizes solids mixing at a cascading regime[19]. It is therefore assumed that the waste tire shred bed is homogeneous.

If the volatiles leave the rotary drum rapidly and the gas residence time is sufficiently low to avoid overpressure and an excess of thermal cracking, equation (1) can be expressed as:

$$\frac{dm_{volatiles}}{dt} = f(r_{pyrolysis}) \tag{6}$$

In equation (6), the term $m_{volatiles}$ corresponds to the mass of gaseous products (condensable and non-condensable) extracted from the rotary drum reactor, while $r_{pyrolysis}$ corresponds to the reaction rate.

3.2.5.2 Reaction kinetics

In the present model, a rate of pyrolysis is used. The rate of pyrolysis term is different from the usual rate of devolatilization, but has the same kinetics formulation:

$$-r_{pyrolysis} = \frac{dm_{pyrolysis}}{dt} = Ae^{-\frac{E_a}{RT}} \cdot \left(\frac{m_{tire}-m_{pyrolysis}}{m_{tire\_initial}}\right)^n \quad (7)$$

In reality, pyrolysis most likely involves hundreds of series and parallel reactions. However, the main difficulty resides in identifying all the individual reactions, evaluating the reaction terms in the model and simplifying the model by keeping only the significant reactions. Based on a black box representation of pyrolysis, the reaction system can be represented as:

Figure 3.2.2. Black box representation of the pyrolysis system.

Since all the reaction terms are not known, a simplified global reaction equation can be formulated:

$$-r_{pyrolysis} = S_{gas}(T)\sum r_{products} + S_{oil}(T)\sum r_{products} + (1-S_{oil}(T)-S_{gas}(T))\sum r_{products} \quad (8)$$

In equation (8), the parameters S_{gas} and S_{oil} correspond to the instantaneous selectivity of non-condensable gases and condensable gases (oil), respectively. These instantaneous selectivity terms ($S_i(T)$) are a function of temperature and are defined as:

$$S_i(T) = \frac{r_i}{\sum r_{products}} = \frac{r_i}{-r_{pyrolysis}} \quad (9)$$

The global pyrolysis reaction rate can thus be formulated as:

$$-r_{pyrolysis} = \frac{r_{char}}{S_{char}} = \frac{r_{oil}}{S_{oil}} = \frac{r_{gas}}{S_{gas}} \quad (10)$$

In the present model, pyrolysis is represented as a single-step process and the rate of formation of the individual pyrolysis products is predicted. Reorganizing equation (10) for all the pyrolysis products yields:

$$r_{char} = -r_{pyrolysis} \cdot S_{char} \quad (11)$$

$$r_{oil} = -r_{pyrolysis} \cdot S_{oil} \quad (12)$$

$$r_{gas} = -r_{pyrolysis} \cdot S_{gas} \quad (13)$$

The selectivity terms as a function of temperature for char, oil and gas can partially be obtained from the results of Williams[17], which performed isothermal waste tire pyrolysis in a larger scale system over a wide range of conditions. In these experiments, Williams[17] reported the final product yields (at the end of the pyrolysis process) as a function of both temperature and heating rate. However, the average temperature at which most of the conversion was achieved was more likely lower than the reported final temperature. The higher the heating rate, the shorter will be this heat up step. And by extension, an infinite heating rate would yield selectivity values that would be temperature dependent only. In fact, it is very difficult to obtain instantaneous

selectivity data experimentally: heating occurs for a significant time period where conversion undergoes before reaching the set point temperature. This is inevitable because of the intrinsic thermal properties of carbonaceous materials, namely a low thermal conductivity combined to a high heat capacity. Therefore, data from Williams was used qualitatively to define the mathematical functions relating the instantaneous selectivity of gas (S_{gas}) and oil (S_{oil}) to pyrolysis temperature (T). The instantaneous char selectivity (S_{char}) was then obtained by difference, as per equation (8).

The order of reaction (n) in equation (7) was assumed as 1.78, based on the results of Chang[20], who calculated the order of reaction for waste tire isothermal pyrolysis. Note that for isothermal pyrolysis experiments, the selectivity terms correspond to constants. Thus, the order of reaction for the rate of devolatilization calculated by Chang[20] at a specific temperature is directly proportional to the rate of pyrolysis considered in equation (7). The final form of the kinetics model is presented as follows:

$$r_{char} = Ae^{-\frac{E_a}{RT}} \cdot \left(\frac{m_{tire} - m_{pyrolysis}}{m_{tire\_initial}}\right)^{1.78} \cdot S_{char} \quad (14)$$

$$r_{oil} = Ae^{-\frac{E_a}{RT}} \cdot \left(\frac{m_{tire} - m_{pyrolysis}}{m_{tire\_initial}}\right)^{1.78} \cdot S_{oil} \quad (15)$$

$$r_{gas} = Ae^{-\frac{E_a}{RT}} \cdot \left(\frac{m_{tire} - m_{pyrolysis}}{m_{tire\_initial}}\right)^{1.78} \cdot S_{gas} \quad (16)$$

3.2.5.3 Energy Balance

Indirect heating exposes the drum region facing the burners to very high temperatures, but the temperature is assumed to be relatively constant over the drum surface because of the rotating motion. For the energy balance, thermal convection between the hot drum wall and the waste tire

bed was assumed as the main heating source and the thermal radiation coefficient was included in the average heat transfer coefficient. The energy balance around the bed of tire shreds was assumed as:

$$m_{bed}(t)C_{p_{bed}}(T)\frac{dT_{bed}}{dt} = \bar{h}W_{exp}(T_{wall} - T_{bed}) - H_{pyr} \quad (17)$$

$$m_{bed}(t)C_{p_{bed}}(T) = m_{steel}C_{p_{steel}}(T) + m_{tire}(t)C_{p_{tire}}(T) + m_{char}(t)C_{p_{char}} \quad (18)$$

As previously discussed in section 3.1, the rotary drum reactor operating conditions maximized the solids mixing such that the waste tire bed was assumed to be well mixed and its temperature to be uniform (no gradient). The parameters of equation (17) were estimated from industrial pyrolysis data.

To estimate the waste tire shred specific heat (C_{Ptire}), the correlation of Yang et al.[21] was used:

$$C_{P_{tire}}(T) = 1230 + 6.55T\ [=]\frac{J}{kg°C} \quad (19)$$

Note that the range of temperatures for which the above correlation is valid was not specified by Yang et al.[21]. In the present model, this can represent a source of error since the correlation predicts that the specific heat doubles between ambient temperature and 190°C (before any decomposition has taken place). Specific heat for char was also obtained from Yang et al.[21] as 1800 J/kg°C. For steel, a temperature-dependent expression was obtained from the literature[22]:

$$C_{P_{steel}}(T) = 425 + 0.773T\ [=]\frac{J}{kg°C} \quad (20)$$

The pyrolysis heat of reaction (H_{pyr}) reported in the scientific literature for various feedstocks vary significantly. For example, Rath et al.[23] showed that values reported for wood vary from highly exothermic to highly endothermic. Their study showed that the presence of a lid over the sample can greatly affect the results. The volatilization heat of reaction is also different from the heat of reaction for decomposition. In the present study, the heat of decomposition was calculated from the available industrial data according to the heat and mass balances as it will be described in the next section.

The novelty of the proposed model lies in its capability to predict individual product (char, oil and non-condensable gas) yields as a function of temperature with a limited number of fitted parameters. Hence, the model predicts decreasing generation rates of volatiles with decreasing heating rates (increasing residence time at lower temperatures). On the other hand, increasing heating rates leads to decreasing char production rates. Finally, the pyrolysis reaction rate increases with increasing temperature according to the Arrhenius law, which makes high temperature pyrolysis difficult to achieve.

3.2.6 RESULTS AND DISCUSSION

3.2.6.1 Estimation of model parameters

The pyrolysis products selectivity as a function of temperature was estimated from TGA experiments.

3.2.6.2 Pyrolysis product selectivity

Isothermal experiments were previously conducted by Williams et al.[17] in a fixed-bed (similar to conventional TGA) with tire samples where they monitored the individual product yield at four different temperatures and four different heating rates. The data of Williams et al.[17] is shown in Figure 3.2.3 and it was initially considered to fit the proposed model (equations (11) to (16)), as selectivity values. However, Williams et al.[17] reported the set-point temperature as the solids temperature, which can yield a significant error as previously discussed in section 3.

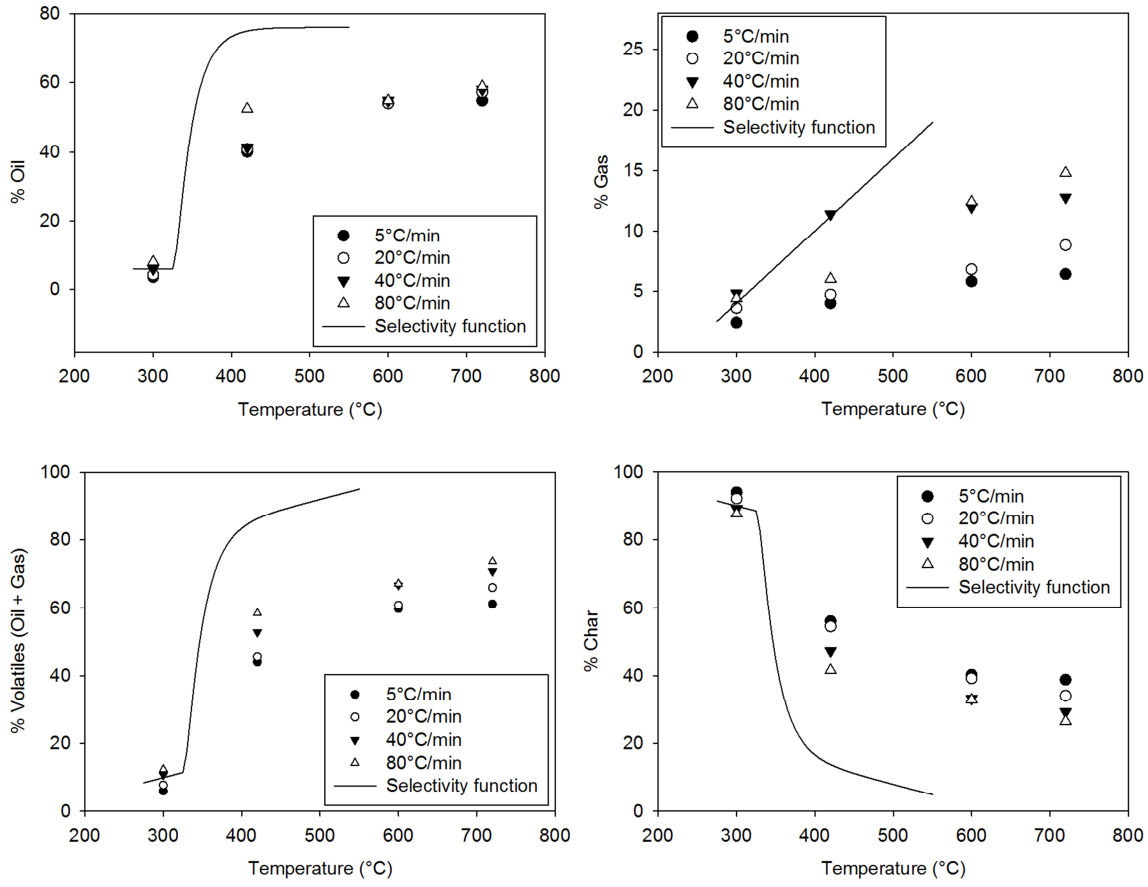

Figure 3.2.3. Product selectivity obtained via isothermal TGA experiments[17] (single points) & calculated selectivity (functions).

To determine the uncertainty generated from this assumption, TGA experiments were conducted at a low heating rate of 5°C/min from ambient temperature to 600°C. In Section 3.2.3, it was emphasized that lower heating rates in TGA runs would be more precise since the measured gas temperature is more representative of the sample temperature. Using the definition of kinetics presented in this work, the rate of production of volatiles can be expressed as:

$$r_{volatiles} = r_{gas} + r_{oil} \tag{21}$$

$$r_{volatiles} = (S_{gas} + S_{oil})(-r_{pyrolysis}) \tag{22}$$

$$-r_{pyrolysis} = \frac{r_{volatiles}}{(S_{gas}+S_{oil})} \tag{23}$$

During a TGA experiment, the integral of the data set obtained from equation (23) should converge to 100 % (not exceeding 100%), as weight loss reaches a solid plateau after a certain time and conversion reaches completion. The last values taken from the TGA run shows a weight loss of the same order of magnitude than the noise from the TGA micro-scale.

Figure 3.2.4 compares the cumulative conversion (integrated curve) of the tire sample from the TGA experiments (current work) and the data of Williams et al.[17]. It is clear that conversion widely exceeds 100 % using data from Williams[17]. Two main factors can explain these results. First, the waste tire shreds conversion has been previously shown to be completed before reaching the temperature set points of 600°C and 720°C at the heating rates used by Williams et al.[17]. This completed pyrolysis temperature, for a constant heating rate experiment, is more likely around 450°C[24,25] (confirmed with TGA experiments in this work). Second, as highlighted in Section 3.2, the heating process of the particles leads to significant sample decomposition before the set point temperature is reached. As a result, the products yields reported by Willams et al.[17] combine both the products emitted before that final temperature and those emitted at the set point

temperature. The real selectivity values (using an infinite heating rate) were thus underestimated (oil and gas) or overestimated (char). Therefore, real selectivity values that are independent on the heating rate must be determined.

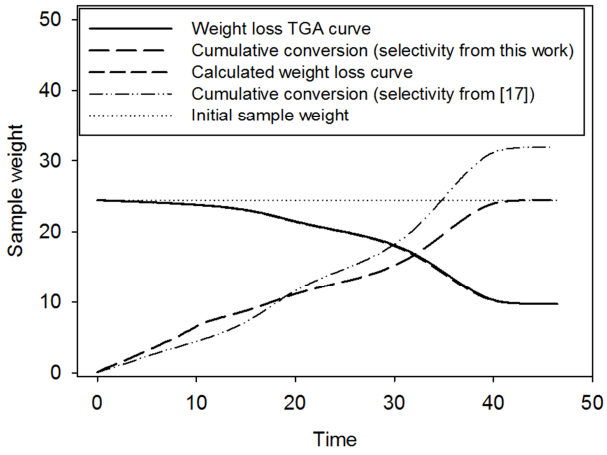

Figure 3.2.4. TGA data used to identify the oil selectivity curves parameters (5°C/min).

The product selectivity data reported by Williams et al.[17] is not accurate, but it is still of interest to qualitatively characterize the shape of the selectivity function ($S_i(T)$). In fact, Figure 3 shows a linear increase of non-condensable gas production with increasing temperature. Considering the isothermal TGA experiments conducted at a heating rate of 80°C/min, the effect of the heating process was minimized and the gas yields were assumed to be close to the real selectivity values since gas production was relatively limited compared to the oil production. Moreover, it can be assumed that the experiments with set-point temperatures of 600°C and 720°C were performed with a set-point temperature of 450°C[24,25]. Finally, the experiment with a set-point temperature of 300°C is assumed to yield results that are closer to the real selectivity values, considering that kinetics remains very slow below that set point temperature. Consequently, instantaneous non-condensable gas selectivity was assumed to follow this linear behaviour with temperature:

$$S_{gas}(T) = 0.0006T(°C) - 0.14\ [=]\ \frac{weight\ gas}{weight\ products} \quad (24)$$

Equation (24) is shown in Figure 3 and is assumed to be valid between 275°C (S_{gas}*=0.025 weight gas/weight products*) and 550°C (S_{gas}*=0.19 weight gas/weight products*). As conventional pyrolysis considers mild heating rates, temperatures higher than 550°C are not expected. For fast pyrolysis, oil cracking at temperatures over 550°C should then be considered. The final selectivity value may seem high, but it must not be forgotten that in conventional pyrolysis, these temperatures are usually met when conversion is close to completion, so the effect on the global gas yield is not significant.

Since conversion likely reached completion at approximately 450°C[24,25], the instantaneous selectivity for oil at high temperature (600°C and 720°C) is expected to be higher than reported by Williams et al.[17]. Observing oil yield data from Williams et al.[17], the morphology of a mathematical function relating instantaneous oil selectivity to temperature is similar to a delayed second-order response plus a constant value, as it reaches a plateau at higher temperatures:

$$T < \theta \qquad S_{oil}(T) = B \quad (25)$$

$$\theta \leq T \leq 550\ ^{o}C \qquad S_{oil}(T) = K\left(1 - \frac{\tau_1 e^{\frac{-(T-\theta)}{\tau_1}} - \tau_2 e^{\frac{-(T-\theta)}{\tau_2}}}{\tau_1 - \tau_2}\right) + B \quad (26)$$

$$\tau_1 = \frac{\tau}{\zeta - \sqrt{\zeta^2 - 1}} \quad (27)$$

$$\tau_2 = \frac{\tau}{\zeta + \sqrt{\zeta^2 - 1}} \quad (28)$$

Equation (26) is assumed to be valid for temperatures (T) between $T = \theta$ and $T = 550°C$. For $T < \theta$ (equation (25)), instantaneous oil selectivity is a constant and is equal to B. Since equation (26) is not fundamentally related to selectivity, the parameters have no physical meaning. However, their contribution to the morphology of the selectivity curve can be identified. The delay (θ) is the temperature from which oil selectivity starts to increase with increasing temperature – θ corresponds to a threshold temperature for oil production. At high temperatures, oil selectivity reaches a plateau ($K + B$). Tau (τ) represents the temperature range in which selectivity changes significantly, in contrast to the real definition of tau, which is the characteristic time range where process response changes significantly, starting from theta (θ). The plateau ($K + B$) is reached at $T \approx 5\ \tau$. Finally, ζ represents the smoothness of the selectivity evolution with temperature.

The coefficients in the oil selectivity equations (25) to (28) were determined with the experimental TGA data: $-r_{pyrolysis}$ was obtained from the TGA data and the calculated S_{gas} (equations (21) to (23)) such that S_{oil} could be calculated as a function of temperature (T). Again, optimal parameters for equations (25) to (28) lead the integral of $-r_{pyrolysis}$ to converge to 100%. The values for the five parameters of the oil selectivity equation that meet this condition were found to be:

- K = 70 %
- B = 6 %
- θ = 325°C
- τ = 10°C
- ζ = 1.3
- τ_1= 21.3°C
- τ_2= 4.7°C

In Figure 3.2.4, it is shown now that with the new selectivity functions for gas and oil (char is obtained by difference) fit the TGA data with very high accuracy. The selectivity values, with temperature (up to 550°C) are presented in Figure 3, along with selectivity for volatiles (oil +

gas). As explained earlier, it is observed that data from Williams et al. (17) underestimated the production of volatiles as it also overestimated the production of char.

3.2.6.3 Kinetics parameters

The kinetics parameters in the pyrolysis rate expression (equation (7)) were calculated from the measured oil production and bed temperature during the typical industrial batch shown in Figure 5 and the product selectivity equations. The following values were obtained for the kinetics of waste tires pyrolysis:

- E_a = 71,000 J/mol
- A = 42,000 min^{-1}

The simulated cumulative oil production profile is then compared with the measured profile in Figure 3.2.5.

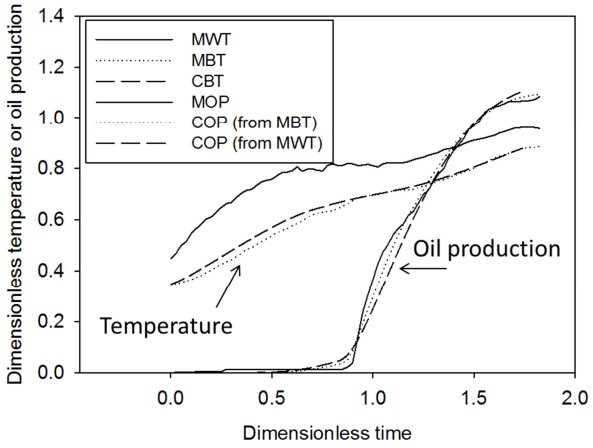

Figure 3.2.5. Oil production and temperature (measured & calculated) during an industrial waste tire pyrolysis batch; C=calculated, M=measured, B=bed, O=oil, W=wall, P=production, T=temperature.

3.2.6.4 Heat transfer parameters

Heat transfer model parameters in the energy balance of equation (17) were estimated from industrial data. Following the initiation of the heating process (t = 0), the bed and wall temperatures increase with time as shown in Figure 5. The absence of significant fluctuations in the temperature measurements (Figure 3.2.5) suggests a uniform tire shreds bed temperature – the bed appears to be well-mixed.

Using the tire specific heat calculated from the correlation of Yang et al.[21] (equation (19)) resulted in a convection term (*h*) that was significantly higher than the values reported by Lin et al.[26] (over 200 W/m²K). In fact, as reported in the literature[26], convection terms for externally heated rotary drums are typically in the range of 25-125 W/m²K. On the other hand, assuming a constant tire specific heat of 1230 J/kg°C (from equation (19)) underestimated the convection coefficient as values below 25 W/m²K were obtained. This suggests that Yang et al.[21] may have experienced bias using a differential scanning calorimeter (DSC). As the order of magnitude of the convection term can be calculated from the literature[26], the specific heat ramp of 6.55 J/kg°C² from equation (19) was instead fitted with the experimental data and the result was closer to the typical char specific heat ramp of 2.09 J/kg°C² from Koufopanos et al.[27].

Concerning the energy consumed by the decomposition reaction (H_{pyr} in equation (17)), it was considered that it behaves endothermically during the whole pyrolysis process. While it combines both specific exothermic and endothermic reactions, it is globally a very endothermic process. However, since the products composition and selectivity evolves with temperature, it is expected that the energy consumed by pyrolysis will more likely vary instead of being constant. The importance of these variations cannot yet be quantified. It would require a full set of data for selectivity and elemental composition of products as well as heating values, in order to implement a full Hess law calculation. As a simplification, an average energy of pyrolysis was fitted, H_{pyr} being

$$H_{pyr} = \widetilde{H}_{pyr.} \cdot (-r_{pyrolysis}) \quad (29)$$

Where $\widetilde{H}_{pyr.}$ is the weight-based energy of pyrolysis. A value of 140,000 J/kg was obtained by fitting. It is very important to notice that in this model, the energy consumed is the heat of pyrolysis and is related to the rate of pyrolysis, in opposition to the heat of devolatilization, which refers to the rate of production of volatiles in most models found in literature. It is thus very difficult to correlate this value to those seen in literature for devolatilization of tires or their components, which vary between 250,000 and 500,000 J/kg[15,17].

3.2.6.5 Model performance

Figure 3.2.5 shows the measured and calculated oil production during a typical industrial waste tire pyrolysis batch: the calculated values closely follow the experimental trend. Figure 5 also shows the measured and calculated wall and bed temperatures: the model is in good agreement with the experimental values.

Selectivity is non-linear with respect to temperature, which renders the model very sensitive to that parameter. Non-typical pyrolysis batches were also produced with lower waste tire bed mass or with different heating processes (varying heating rates) to investigate the robustness of our model. In these tests, oil production and wall temperature were monitored, but not the bed temperature. The wall temperature was implemented in the energy balance, coupled with the mass balance, to calculate the bed temperature as well as the oil production. The two cases studied were: (1) a batch with a typical bed mass, but with a different heating profile and (2) a batch with a smaller initial waste tire bed mass (60% of typical bed mass). The measured and calculated oil production, measured wall temperature and calculated bed temperature are shown in Figure 3.2.6 (batch 1) and Figure 3.2.7 (batch 2).

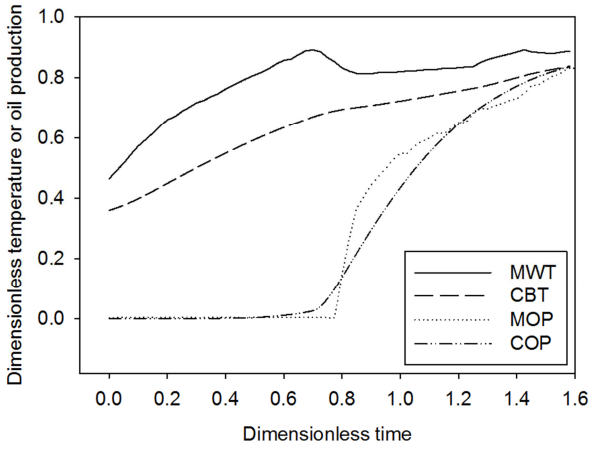

Figure 3.2.6. Measured and calculated oil production and temperature for a different heating profile (batch 1); C=calculated, M=measured, B=bed, O=oil, W=wall, P=production, T=temperature.

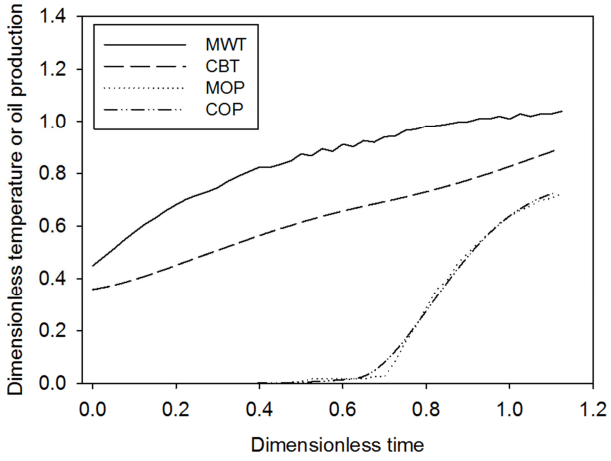

Figure 3.2.7. Measured and calculated oil production and temperature for a smaller bed (batch 2); C=calculated, M=measured, B=bed, O=oil, W=wall, P=production, T=temperature.

For batch 1, the calculated oil production for $t \geq 1.2$ agrees well with the measured values. Nevertheless, oil production between t = 0.70 and t = 1.2 could not be well predicted. This may be related to the fact that the actual bed temperature increased until approximately t = 0.8, where

it started to decrease due to a less intense operation of the burners. As oil production here follows a deformed S-shape with time, there appears to be a change in operating conditions $0.8 \leq t \leq 0.9$, which affected the bed temperature and the kinetics. For batch 2, there is a slight variation between the real oil production threshold and the simulated one. Nevertheless, the dynamics of oil production is well reproduced through the remaining of the batch duration. Overall, the predictive pyrolysis kinetics model simulated successfully the oil production dynamics and final yields for the existing industrial process.

3.2.6.6 Comparison to existing models

The proposed model was compared to three pyrolysis models in the scientific literature. One model from each family of pyrolysis models was chosen: the single-step model of Chang[20], the multi-step pseudo-component model of Leung[28] and the parallel-and-series reaction model of Olazar[29]. Chang[20] performed isothermal experiments in an apparatus similar to a TGA at several set-point temperatures up to 550°C. Leung[28] worked with a conventional TGA at heating rates of 10°C/min, 30°C/min and 60°C/min and temperatures ranging from ambient to 600°C. However, full conversion was always achieved between 450°C and 500°C. Olazar[29] operated a spouted bed at several set-point temperatures between 425°C and 610°C. All three models were developed as intrinsic kinetics models, independent from particle size and pressure. The parameters from each model are summarized in Table 3.

Table 3.2.3. Parameters values for literature models used in this study.

Model	Component	A (min-1)	E (J/mol)	Order of Reaction (n)	Component Ponderation
Chang[20]	Tire-to-volatiles	3.28E+05	61 240	1.78	1
Leung[28]	Pseudo-1-to-volatiles-1	2.00E+04	52 500	1	0.1
	Pseudo-2-to-volatiles-2	6.30E+13	165 000	1	0.48
	Pseudo-3-to-volatiles-3	2.30E+09	136 000	1	0.42
Olazar[29]	Tire-to-Intermediate	4.09E+03	46 090	1	N/A
	Tire-to-gas	2.11E-05	63 080	1	N/A
	Tire-to-liquid	7.80E+02	40 060	1	N/A
	Tire-to-aromatics	3.21E+05	89 260	1	N/A
	Intermediate-to-aromatics	3.00E+01	36 330	1	N/A
	Intermediate-to-tar	1.42E-01	14 120	1	N/A
	Intermediate-to-char	2.87E+01	20 500	1	N/A

The measured bed temperature of Figure 3.2.5 (typical pyrolysis batch) was imposed and the cumulative volatiles (oil and gas combined) production was simulated for all four models. Two out of the three models chosen do not differentiate between non-condensable and condensable (oil) gas fractions such that the cumulative volatiles production was used as basis for comparison. Figure 3.2.8 compares the cumulative volatiles predictions from all four models. As model from Olazar[29] can predict the oil production alone, this was also reported for comparison.

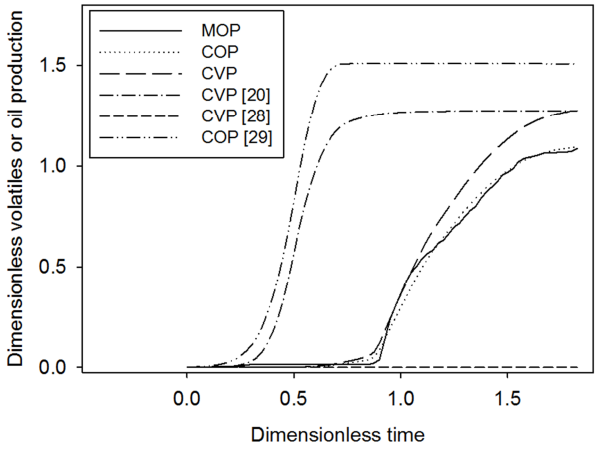

Figure 3.2.8. Calculated volatiles and oil productions with the model from this workin comparison to models by Chang[20], Leung[28] & Olazar[29]; C=calculated, M=measured, O=oil, V=volatiles, P=production.

It is observed that the pseudo-component model of Leung[28] predicted a very low production of volatiles such that they failed to reproduce experimental measurements. This model is characterized by activation energies that are too high. On the other hand, the single-step model of Chang[20] predicted an overall volatiles production of the correct order of magnitude. But, its activation energy is too low since it predicts complete waste tire thermal decomposition before the pyrolysis was initiated in the industrial reactor.

The parallel and series reaction model of Olazar[29] showed similar results as the model of Chang[20] since the activation energies are similarly too low. However, the model of Olazar[29] was able to predict the pyrolysis products selectivity. Unfortunately, it appears that selectivity for liquids and char are dominant at these temperatures. In fact, the gas yield was almost inexistent and the aromatics and tars were produced at a yield of around 1 % (curves mostly overlapped, total volatiles curve not shown). This may highlight the fact that similarly to Williams et al.[17], the set-point temperatures used by Olazar[29] in their experiments were too high: pyrolysis was completed before reaching the set-point temperature and selectivity calculations were biased.

It is interesting to observe that the models of Chang[20] and Olazar[29] yielded similar results while being so different. More in-depth analysis of liquid products may allow a more accurate tuning of the Olazar[29] model. However, Figure 8 reveals that the robustness of this model is low, possibly due to the inclusion of too many reactions. In this work, the robustness of the industrial predictive model lies in the determination of a temperature-dependent selectivity table, as the global set of reactions remains unknown.

Since the market value of pyrolysis oil is much higher than non-condensable gases, models based on total volatiles production cannot be implemented at the industrial scale: their application will most certainly yield large predictive errors. The third family of models presented by Babu[6] is the only category capable of predicting both the kinetics and single product yields of pyrolysis. The model developed in this article is a simplification of the third family of models. Having initial decomposition kinetics, the estimation of selectivity would imply knowing all of the reactions involved in pyrolysis with their respective kinetics. The challenge lies in estimating the products selectivity and the decomposition kinetics parameters as accurately as possible. Ultimately, it strongly appears that thermogravimetry (TGA) alone is not suited for this task since the yield of the different pyrolysis products (char, oil & gas) must be precisely known.

3.2.7 CONCLUSIONS

A predictive pyrolysis model was developed for an existing commercial scale waste tire thermal decomposition process. The reaction was modeled as a global pyrolysis reaction kinetics term. Furthermore, the temperature-dependency of the products selectivity was modeled mathematically with functions derived from TGA data. The energy balance was performed using a lumped-capacitance method which assumed a perfectly mixed bed and a constant convection term that included radiation. The model yields the products (char, oil & gas) generation with time as well as the tire shreds temperature time-profiles.

The model was compared to industrial pyrolysis data from the Ecolomondo™ process. The calculated tire shreds bed temperature and cumulative oil production agreed well with experimental data for the typical process operating conditions. The present model was compared to three other models from the literature: single-step, multi-step pseudo-components and parallel-and-series. It was shown that none of these models could reproduce the industrial pyrolysis kinetics, nor the product yields.

Two main remarks emanated from the present work: TGA alone is not well suited for pyrolysis kinetics calculation and accurate industrial pyrolysis models cannot be based on existing devolatilization rates. These models cannot predict the individual product yields (only combined volatiles), as well as they absolutely need final yield data. The predictive pyrolysis model developed in this work could successfully represent the oil production dynamics and yields for the existing industrial process.

3.2.8 Acknowledgements

The authors would like to extend their sincere thanks to the MITACS Acceleration funding program that, in part, made this project successful. The authors are also thankful to Ecolomondo Corp. For financial assistance and providing industrial data which made this project possible.

3.2.9 References

(1) Rubber Manufacturers Association, U.S. Scrap Tire Management Summary 2005-2009, RMA, October 2011.

(2) Fiksel, J.; Bakshi, B.R.; Baral, A.;Guerra, E.;DeQuervain, B. *Clean Technology Environment Policy*, **2011**, *13*, 19-35.

(3) Saft, R.J. *Journal of Life Cycle Assessment*, **2007**, *12(4)*, 230-238.

(4) Solantausta, Y.; Bridgwater, A.T.; Beckman, D. *Biomass & Bioenergy*, **1995**, *9(1-5)*, 257-269.

(5) Laresgoiti, M.F.; Caballero, B.M.; De Marco, I.; Torres, A.; Cabrero, M.A.; Chomon, M.J. *Journal of Analytical and Applied Pyrolysis*, **2004**, *7*, 917-934.

(6) Babu, B.V. *Biofuels, Bioproducts & Biorefining*, **2008**, *2*, 393-414.

(7) Wendlandt, W. *Analytical Chemistry*, **1982**, *54(5)*, 97R-105R.

(8) Aguado, R.; Olazar, M.; Velez, D.; Arabiourrutia, M.; Bilbao, J. *Journal of Analytical and Applied Pyrolysis*, **2005**, *73*, 290-298.

(9) Aylon, E.; Callen, M.S.; Lopez, J.M.; Mastral, A.M.; Murillo, R.; Navarro, M.V.; Stelmach, S. *Journal of Analytical and Applied Pyrolysis*, **2005**, *74*, 259-264.

(10) Chen, J.H.; Chen, K.S.; Tong, L.Y. *Journal of Hazardous Materials*, **2001**, *B84*, 43-55.

(11) Islam, M.R.; Haniu, H.; Fardoushi, J. *Waste Management*, **2009**, *29*, 668-677.

(12) Larsen, M.B.; Schultz, L.; Glarborg, P.; Skaarup-Jensen, L.; Dam-Johansen, K.; Frandsen, F.; Henriksen, U. *Fuel*, **2006**, *85*, 1335-1345.

(13) Quek, A.; Balasubramanian, R. *Journal of Hazardous Materials*, **2009**, *166*, 126-132.

(14) Senneca, O.; Salatino, P.; Chirone, R. *Fuel*, **1999**, *78*, 1575-1581.

(15) Yang, J.; Tanguy, P.A.; Roy, C. *Chemical Engineering Science*, **1995**, *50(12)*, 1909-1922.

(16) Varhegyi, G.; Bobaly, B.; Jakab, E.; Chen, H. *Energy & Fuels*, **2011**, *25*, 24-32.

(17) Williams, P.T.; Besler, S.; Taylor, D.T. *Fuel*, **1990**, *69*, 1474-1482.

(18) Alizadeh, E.; Dubé, O.; Bertrand, F.; Chaouki, J. *AIChE Journal*, **2013**, published online (DOI 10.1002/aic.13982).

(19) Mellmann, J. *Powder Technology*, **2001**, *118*, 251-270.

(20) Chang, Y.M. *Resource Conservation Recycling*, **1996**, *17*, 125–139

(21) Yang, J.; Roy, C. *AIChe Journal*, **1995**, *41*, 1500-1512.

(22) University of Manchester, Carbon steel thermal properties, URL: http://www.mace.manchester.ac.uk/project/research/structures/strucfire/, 2012.

(23) Rath, J.; Wolfinger, M.G.; Steiner, G.; Krammer, G.; Barontini, F.; Cozzani, V. *Fuel*, **2003**, *82*, 81-91.

(24) Cheung, K.Y.; Lee, K.L.; Lam, K.L.; Lee, C.W.; Hui, C.W. *Fuel Processing Technology*, **2011**, *92*, 856-863.

(25) Unapumnuk, K.; Keener, T.C.; Lu, M.; Khang, S.J. *Journal of the Air & Waste Management Association*, **2006**, *56(5)*, 618-627.

(26) Li, S.Q.; Ma, L.B.; Wan, W.; Yao, Q. *Chemical Engineering Technology*, **2005**, *28(12)*, 1480-1489.

(27) Koufopanos, C.A.; Papayannakos, N.; Maschio, G.; Lucchesi, A. *The Canadian Journal of Chemical Engineering*, **1991**, *69*, 907-915.

(28) Leung, D.Y.C.; Wang, C.L. *Energy & Fuels*, **1999**, *13*, 421-427.

(29) Olazar, M.; Lopez, G.; Arabiourrutia, M.; Elordi, G.; Aguado, R.; Bilbao, J. *Journal of Analytical and Applied Pyrolysis*, **2008**, *81*, 127-132.

CHAPITRE 4 MODÉLISATION DU BILAN D'ÉNERGIE

Cet article a été soumis en 2014 dans le journal Thermochimica Acta.

4.1 PRÉSENTATION DE L'ARTICLE

L'objectif de cet article était de déterminer l'évolution de la chaleur spécifique de la masse décomposée et l'enthalpie de pyrolyse pour les pneus. Les données de laboratoire étant en contradiction avec les données industrielles, il était critique d'éclaircir le comportement thermodynamique de la masse pendant la pyrolyse, dans le but de développer des outils et aider à une meilleure conception des réacteurs de pyrolyse industriels.

Tout d'abord, il a été obtenu que la chaleur spécifique de la masse en pyrolyse diminue pour atteindre un minimum autour de 375°C avant de remonter jusqu'à l'atteinte de l'équilibre thermodynamique (pas de perte de masse). En combinaison avec la perte de masse, cela induit un biais à l'appareil de laboratoire, donnant l'impression d'un comportement exothermique. Il s'agirait plutôt d'une surchauffe involontaire des échantillons induite par le système de contrôle. Les nouvelles chaleurs spécifiques ont permis de déterminer trois termes d'enthalpie de pyrolyse pour les pneus. Le premier est constant et est proportionnel à la perte de masse. Le second dépendrait de la dissociation des ponts soufrés et le troisième serait relié à la formation du char lorsque la conversion est près de la complétion.

4.2 DETERMINATION OF ENTHALPY OF PYROLYSIS FROM DSC AND INDUSTRIAL REACTOR DATA: CASE OF TIRES

Determination of enthalpy of pyrolysis from DSC and industrial reactor data: case of tires

*Jean-Remi Lanteigne, Jean-Philippe Laviolette, and Jamal Chaouki**

Department of Chemical Engineering, École Polytechnique de Montréal,

C.P. 6079, succ. Centre-Ville, Montréal, Qc, Canada H3C 3A7

*Corresponding Author (jamal.chaouki@polymtl.ca)

4.2.1 Abstract

This study came from the contradiction that pyrolysis is globally a net endothermic phenomenon and laboratory scale results showed surprisingly significant exothermic peaks. The heat capacity of the decomposing tires has been determined with more accuracy: instead of assuming char independently from tires during pyrolysis, the heat capacity of thewhole solids was found to depend on temperature and conversion. The value increased until pyrolysis triggered at 250°C. Then, the heat capacity value decreased continuously until 400°C and then started to increase again. This unexpected trend pointed out that the exothermic peak observed with DSC is an artifact generated by the control system of the apparatus. To bypass this limitation, the energy balance was modelled with industrial data and the newly found heat capacity. The enthalpy of pyrolysis was found to have a term dependent of the weight loss derivative, with a constant value of 410 kJ/kg tires. Two other terms for the enthalpy of pyrolysis have been identified, being independent of weight loss. The first one corresponds to the sulfur crosslink breakage at low temperature (65 kJ/kg) and the second one, at the final stage of pyrolysis, accounts for charring reactions approaching the thermodynamic equilibrium (75 kJ/kg). Globally, a new methodology to determine the specific heat of solids with DSC and enthalpy of pyrolysis with larger scale experimental data has been developed.

Keywords – Pyrolysis, Waste tires, Energy balance, DSC

4.2.2 INTRODUCTION

The energy balance is a critical equation when designing chemical processes. For processes operating at cryogenic or at very high temperature, it is a tool used for the choice of technology as well as sizing. It affects the business model, especially when recycling and recovering are considered. Residue and waste recovery is subject to intensive research, which may lead to innovative industrial processes. And one of the keys to successful commercial scale-up of novel waste recovery processes is the determination of the energy balance.

While this equation is relatively easy to build for combustion or conventional chemical reactions, complex systems such as gasification or pyrolysis represent a major challenge. This complexity for gasification comes mainly from the dependence of the mass balance to temperature. Pilot plant data is then better suited to develop the energy balance semi-empirically. For the case of pyrolysis, the challenge arises from several characteristics inherent to the process:

- Compared to gasification/combustion, pyrolysis rate of reaction is very slow;
- During pyrolysis, a plethora of compounds is produced in the three phases and with different thermodynamic properties;
- Composition of pyrolysis products can be very diverse and it depends on the chosen feedstock, temperature, reactor hydrodynamics and conversion;
- Determination of real material temperature during pyrolysis is technically difficult, especially in continuous operation.

More uncertainties also come from the choice of reactor technology. Operating in continuous mode helps simplifying the energy balance equation. On the other hand, it rends very difficult the determination of the real material temperature since most materials decompose endothermically. That is, the continuous reactor is usually operated at a temperature much higher than the actual pyrolysis temperature. In other words, the actual pyrolysis temperature range depends upon the thermodynamic equilibrium and the material composition as material is heated from low temperature up to final decomposition temperature. Nevertheless, because operating temperatures are generally relatively high, decomposition rates are faster and the equation can be simplified.

Reactors operated in batch mode yield a more elaborate energy balance equation. It depends mostly on material heat up energy and on the rate of decomposition of materials, which is usually slower than for continuously operated reactors. This is because of an averagely lower temperature resulting from a batch start at ambient temperature. The unknowns listed above are also pertinent in batch mode, and another difficulty factor can add up to this list if materials with significant

dimensions are fed directly: an intra-material temperature gradient will limit the rate of decomposition and influence the composition of pyrolysis products.

Citing George E.P. Box: “all models are wrong, but some are useful” [1]. To be useful, a pyrolysis model should allow extrapolation to a certain extent, in order to optimize process operation and design. Therefore, it should minimally derive from an elaborate fundamental form to preserve its physical meaning and predictive behaviour. Many energy balances can be found in literature for pyrolysis. Their main flaw, however, remains in the assumptions that were made but not validated, whether in the equation or in the experiments, that led to their final form. The literature review will among others discuss some points that remain unclear in the determination of the pyrolysis energy balance:

- Exothermic vs. endothermic in pyrolysis
- Evolution of heat capacities
- Definition of the heat of pyrolysis ($\Delta H_{pyrolysis}$) term

4.2.2.1 Literature review

4.2.2.1 .1 Pyrolysis mechanisms and thermodynamics

In general, pyrolysis is considered to be an overall endothermic process. Simultaneously, exothermic and endothermic reactions occur, resulting in a net endothermic behaviour. Energetic materials are an exception to this situation. Two kinds of chemical groups are well known for their highly exothermic thermal degradation. Firstly, compounds with high amounts of nitrates produce heat when decomposing. This is mainly due to the high oxygen content, as nitrate acts as an oxidizer. Secondly, azide groups ($R\text{-}N_3$) decompose exothermally to produce nitrogen (N_2) due to their relative instability. Contrary to nitrates, where an oxidizer is intrinsically present in the material to promote partial combustion, azides decompose through pyrolysis without any form of oxidation. A few other organic functional groups are known to behave exothermally in pyrolysis: halogenated nitrogens, fulminates, chlorates, peroxides and ozonides.

Notwithstanding these specific compounds, most organic materials require a net positive heat input to decompose during pyrolysis. Pyrolysis thermodynamics depends upon the dominant mechanisms during decomposition. Therefore, the mechanisms suspected to happen during pyrolysis are presented next. Their occurrence as well as their enthalpic behaviour are highlighted for the purpose of this work. They are listed below by order of increasing temperature:

Table 4.2.1. Types of reactions involved in pyrolysis and their enthalpic behaviour, as viewed by the authors.

Event	Endo/Exo	Comments
Sulfur crosslinks unbinding	Endothermic	Occurs at low temperature (below 300°C)
Free volatiles evaporation (solvents, humidity, etc.)	Endothermic	Occurs at low temperature (below 300°C)
Intensive bond breaking	Endothermic	Occurs from 300°C and up, peak bond breaking rate unknown
Charring	?	Occurs from 300°C and up, peak charring rate unknown
Heavy liquids cracking	Endothermic	Occurs from 300°C and up, peak cracking rate unknown
Pyrolysis volatiles evaporation	Endothermic	Occurs from 300°C and up, represented by weight loss rate
Change in heat capacities (tires to char, dynamic)	?	To be investigated
Gas phase reactions	?	Occurs at any temperature when volatiles are present
Iron/Zinc sulfidation by hydrogen sulfide	Exothermic	Limited by hydrogen sulfide production

In Table 4.2.1, charring corresponds to the formation of char, namely the self-folding crosslinkage of residual solids (mostly carbon). The change in heat capacities is one of the most simplified parameter during pyrolysis. In literature, the model found weighted the heat capacities between tires and final char values [2,3]. However, its dynamic evolution during the core of the decomposition process remains unclear. In dynamically heated systems, a decrease in heat capacity would make the material easier to heat up during the process, giving the impression of an exothermic process, while the opposite would result in an apparent endothermic behaviour. To that can be added the effects of total weight decrease, which combined to heat capacity changes, will affect the energy balance non-linearly.

Many of these phenomena happen simultaneously, such that the resulting thermodynamic behaviour will depend upon their relative rate. For example, if the rate of charring is greater than the rate of pyrolysis volatiles evaporation and that they are occurring together, the net behaviour

would depend upon the exothermicity or endothermicity of charring, if it is assumed that their respective specific enthalpy is similar.

4.2.2.1.2 The energy balance for pyrolysis

Generally speaking, for any pyrolysis batch run, the global energy balance is written:

$$\frac{dE_{batch}}{dt} = \dot{Q}_{input} - \frac{dm_{out}}{dt}\widehat{H}_{out} \text{ (E1)}$$

Where the rate of energy change in the batch ($\frac{dE_{batch}}{dt}$) is equal to the energy input rate ($\dot{Q}_{input}$) minus the energy leaving the batch ($\frac{dm_{out}}{dt}\widehat{H}_{out}$) in terms of mass ($\frac{dm_{out}}{dt}$), that is, a term proportional to the rate of production of volatiles. Developing the left-hand term, the energy change corresponds to the change in internal energy. It is, by neglecting the volume change term (PV_{batch}):

$$E_{batch} = U_{batch} = H_{batch} = m_{batch}\widehat{H}_{batch} \text{ (E2)}$$

Substituting equation (E2) in equation (E1), and by expanding the left-hand term in equation (E1), the balance becomes:

$$\frac{dm_{batch}\widehat{H}_{batch}}{dt} = \widehat{H}_{batch}\frac{dm_{batch}}{dt} + m_{batch}\frac{d\widehat{H}_{batch}}{dt} = \dot{Q}_{input} - \frac{dm_{out}}{dt}\widehat{H}_{out} \text{ (E3)}$$

In a conventional reaction system, the mass derivative in the left-hand side of equation (E3) would resume in a reaction consumption term and whether there are or not inlets/outlets, as it represents the deviation from the sensible heat term (second term in the left-hand side of equation (E3)). In the present case, it is assumed that the former contains exclusively the outlet term from the right-hand side of equation (E3) and a term for the energy of pyrolysis:

$$\widehat{H}_{batch}\frac{dm_{batch}}{dt} = \dot{H}_{pyrolysis} - \frac{dm_{out}}{dt}\widehat{H}_{out} \text{ (E4)}$$

By combining equations (E3) and (E4) and reorganizing, the energy balance for pyrolysis is obtained in its general form:

$$m_{batch}\frac{d\widehat{H}_{batch}}{dt} = m_{batch}Cp_{batch}\frac{dT}{dt} = \dot{Q}_{input} - \dot{H}_{pyrolysis} \text{ (E5)}$$

In equation (E5), m_{batch} depends upon conversion, and therefore, time. The heat capacity in the system depends upon temperature, which itself depends upon time. The heat input term, $\dot{Q}_{input}$, may be represented by external thermal convection or thermal radiation, for example. The heat of pyrolysis term, $\dot{H}_{pyrolysis}$, may vary and literature explored mostly what it could contain. But as well, this energy balance could also apply to any reaction where an initial solid reacts to yield volatile and evolving residual solids.

For Yang et al. [2,3], the sensible heating (left-hand side of equation (E5)) is composed of temperature dependent heat capacities ($C_p(T)$). They assumed that tires heat capacity was independent of pyrolysis char heat capacity, since their model assumes a shrinking core (assuming char formation triggers on the surface of particles). The heat of pyrolysis is formed of an energy term for the evaporation of heavy liquids produced during decomposition ($\dot{H}_{evaporation}$) and a term for the net energy involved in pyrolysis ($\dot{H}_{net\_pyrolysis}$):

$$m_{batch}Cp_{batch}\frac{dT}{dt} = \dot{Q}_{input} - \dot{H}_{evaporation} - \dot{H}_{net\_pyrolysis} \text{ (E6)}$$

For many authors, the evaporation term is not considered, such that the energy of pyrolysis also includes the potential heat of vaporization of products. But as stressed in section 1.1.1, many thermochemical phenomena may be developed and lead to an elaborated form of the energy balance. Values of heat of pyrolysis, for wood and rubbers, from highly endothermic up to highly exothermic, can be found in literature:

Table 4.2.2. Literature values for heat of pyrolysis for wood and tires.

Feedstock	Heat of pyrolysis/Heat of vaporization of liquids (kJ/kg)	Reference
Wood	235	[4]
Wood	190	[5]
Wood	-340	[6]
Wood	-446	[7]
Wood	-254	[8]
SBR	-164/180	[3]
SBR	-500/280	[9]
SBR	-660	[11]
BR	-760/280	[9]
BR	-880	[11]
BR	-945	[10]
NR	-560/170	[3]

A particularity of these values is that they were mostly obtained with SDTA or DTA apparatuses. This technology combines thermogravimetry analysis (TGA) with differential scanning calorimetry (DSC). In all cases, the main limitation was a curvaceous baseline and wider transition peaks. As initially, DSC was not designed to consider weight loss, one should be careful with results obtained for samples involving weight loss. For both wood and tires, SDTA curves from literature often showed potential exothermic peaks:

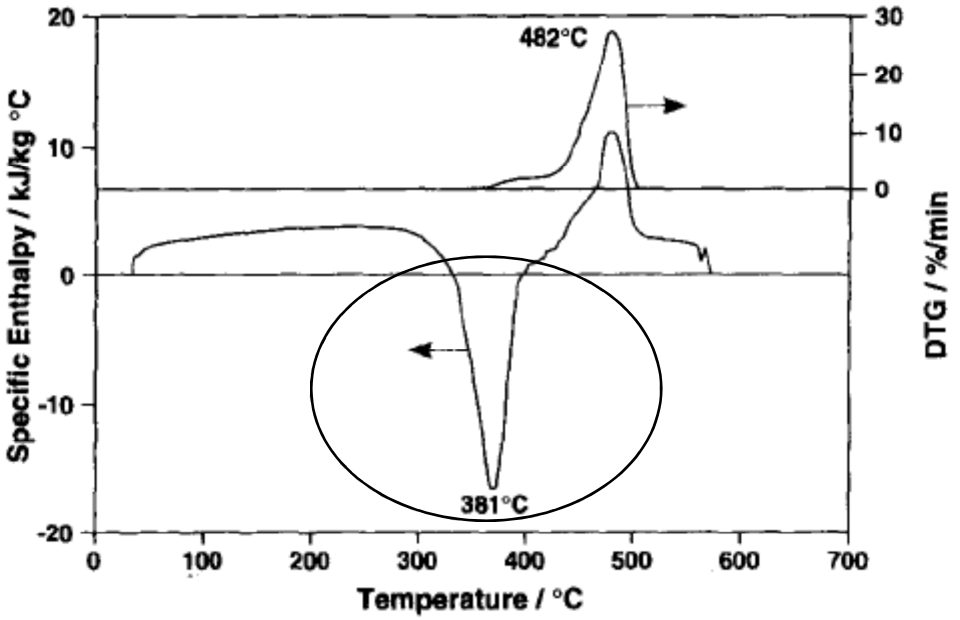

Figure 4.2.1. Exothermic peak (circled) obtained by Yang et al. during pyrolysis experiments [3].

Nevertheless, if observing a pure exothermic behaviour, it would imply that when running a large batch pyrolysis run with tires or wood, material and reactor temperature would increase significantly, even if this is further slowed down with endothermic reactions. This can be verified with industrial data for batch pyrolysis of waste tires [12]:

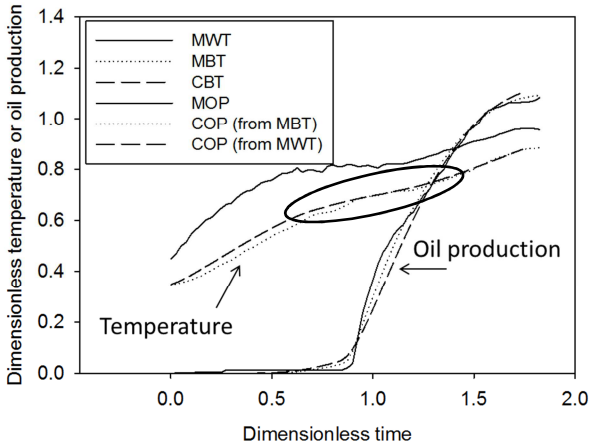

Figure 4.2.2. Industrial production of oil and reactor wall and tire shred temperatures. M = measured; C = calculated; W = wall; B = bed; O = oil; T = temperature; P = production.

As it is observed, with constant heat up input (at the reactor external burners), measured material temperature only increases when the mass starts to decrease significantly, i.e. when conversion is advanced. This is reported by the measured oil production. A deceleration of temperature increase is observed, as a result of the decrease of heating driving force ($T_{wall} - T_{tire}$) and total tire shreds bed mass [12]. From these important results, no absolute exothermic behaviour should be expected in DSC data, knowing a proven exothermic reaction would instead result in temperature upsurge.

Figure 4.2.3 shows results obtained by Yang et al. for natural rubber and styrene-butadiene rubber.

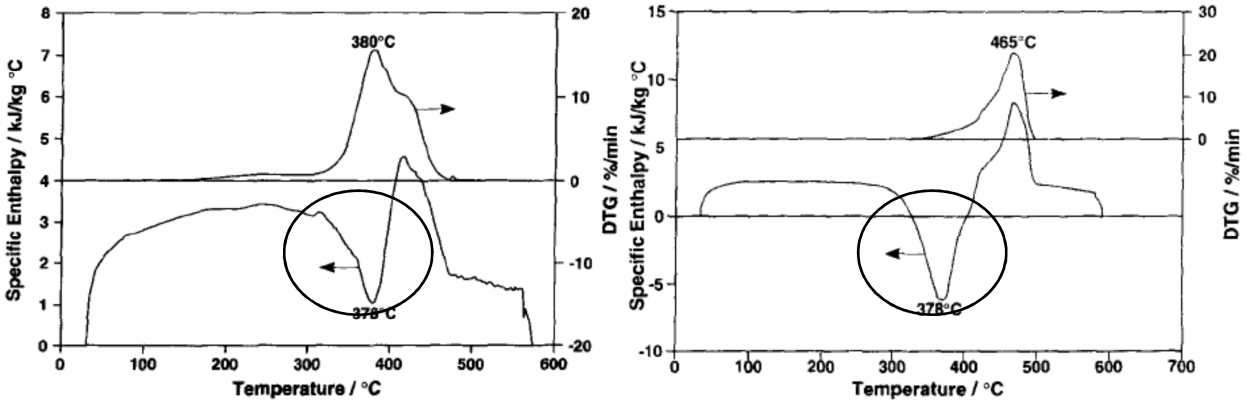

Figure 4.2.3. Pyrolysis experiments with natural rubber (NR, left) and styrene-butadiene rubber (SBR, right) from Yang et al. [3].

The same heat flux profile is obtained for both materials, but the magnitude shows that the first peak maximizes endothermically for NR and exothermically for SBR. As well, weight loss derivative (DTG) peak is attained during the exothermic part for NR while it only starts to increase in the same case for SBR. It suggests that weight loss during the core of the pyrolysis process may possibly explain the exothermic peaks.

4.2.2.1.3 DSC for pyrolysis

Historically, DSC has been developed to observe thermal transitions in solid/liquid materials. Heat flux DSC has rapidly become the most popular type of DSC, but the main weakness observed in DSC was bias associated with the thermal baseline. Thermal equation in heat flux DSC initially considered heat flux through the sample, driven by temperature difference between sample and reference, to be the only heat flux in the system (first right-hand term in equation (E7)).

$$\dot{q} = -\frac{\Delta T}{R_r} + \Delta T_0 \left(\frac{1}{R_s} - \frac{1}{R_r}\right)^{\cdot} + (C_r - C_s)\frac{dT_s}{dt} - C_r \frac{d\Delta T}{dt} \quad \text{(E7)}$$

However, curvaceous baselines showed without a doubt that losses or other heat fluxes occurred. In the 2000s, TA Instruments™ developed a new technology to address this important issue: the Tzero™ technology. Three more heat fluxes have been identified to yield a four-term heat equation (T4) [13].

In addition, effects of pan heat resistance have also been addressed, such that the baseline is now mostly flat and more thermal phenomena can be studied. Schematically, all of these heat fluxes can be identified:

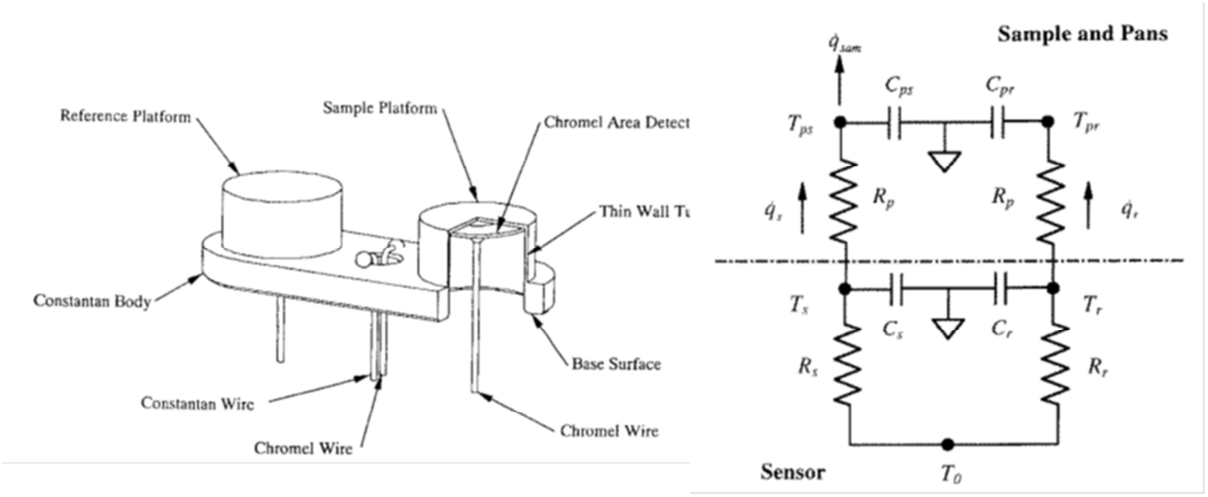

Figure 4.2.4. View of the DSC sensor without samples (left) and of the equivalent system of thermal resistances and capacitances with sample (right) [13].

$$\dot{q}_s = \dot{q}_{sam} + m_{ps} c_{pan} \frac{dT_{ps}}{dt} = \frac{T_s - T_{ps}}{R_p} \qquad (8)$$

$$\dot{q}_r = m_{pr} c_{pan} \frac{dT_{pr}}{dt} = \frac{T_r - T_{pr}}{R_p} \qquad (9)$$

As shown on Figure 4.2.2, the endothermic heat flow is represented in equation T4P (combined equations (E7)-(E9)) by having the sample temperature below the reference temperature. In the case of a significant weight loss, the sample temperature eventually gets closer to the reference temperature and passes it, then being an exothermic behaviour.

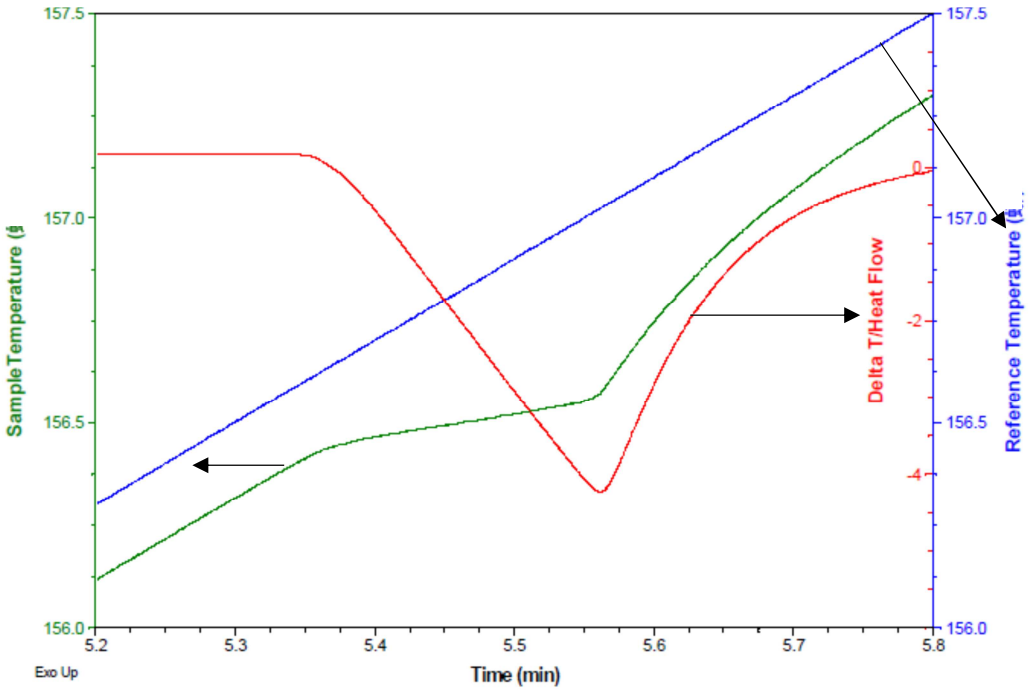

Figure 4.2.5. Typical view of the heat up of a sample with an endothermic transition.

Depending on whether sample side or reference side temperature is placed first in the energy balance (equation T4P), the DSC heat flux will be negative or positive. In the present work, reference temperature will always be placed first to yield a positive value for heat flux when heating up samples.

Ultimately, a precise heat flux measured over a full range of temperature can be obtained and decomposed into the thermodynamic and thermochemical components, among which the sensible heating (heat capacity) and the heat of reaction (pyrolysis, etc.), as per equation (E5).

$$\dot{q}_{sam} = \dot{q}_{sensible\_heat} + \dot{H}_{pyrolysis} \text{ (E10)}$$

However, results found in literature were obtained without the Tzero™ technology, thus affecting the accuracy of the results when measuring transitions/reactions [13], as shown in the next figure:

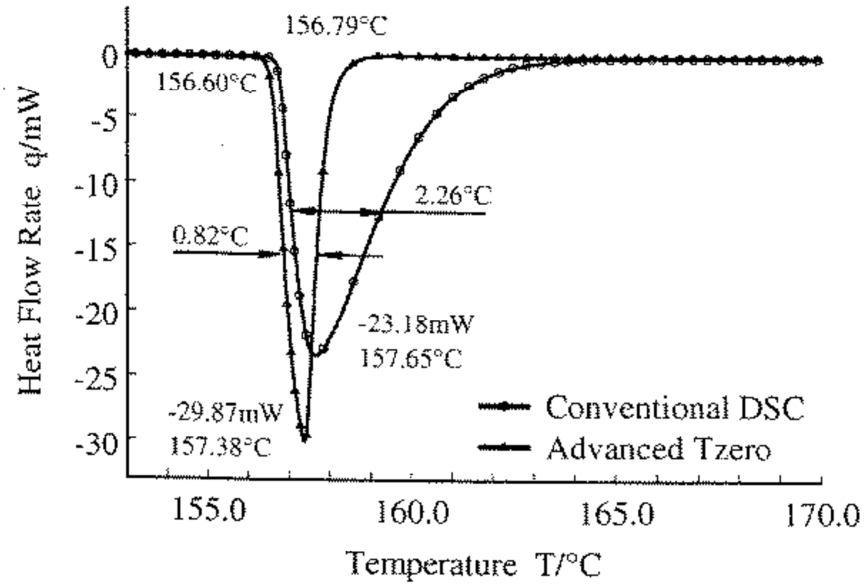

Fig. 6. Indium melt Tzero™ vs. conventional DSC.

Figure 4.2.6. Typical view of a thermal transition measured with a conventional DSC and with the Tzero (TM) technology [13].

4.2.2.1.4 Application of the Hess law to pyrolysis

The application of the Hess law on a global pyrolysis experiment translates in subtracting the energies of formation of the feedstock (tires, wood, etc.) from the energies of formation of the overall cumulated products at a reference temperature. The energy input/output of the feedstock/products are also accounted for to complete the thermochemical balance. This way, a global amount of energy needed to complete pyrolysis can be extracted. Some assumptions must be made whether the enthalpy of formation of condensable volatiles is taken for the liquid or the gas phase. In the present case, it is supposed that the volatiles are eventually emitted hot in the

gas phase, so the latter is considered. Next is presented the schematic view of these transformations as well as its translation in a global equation.

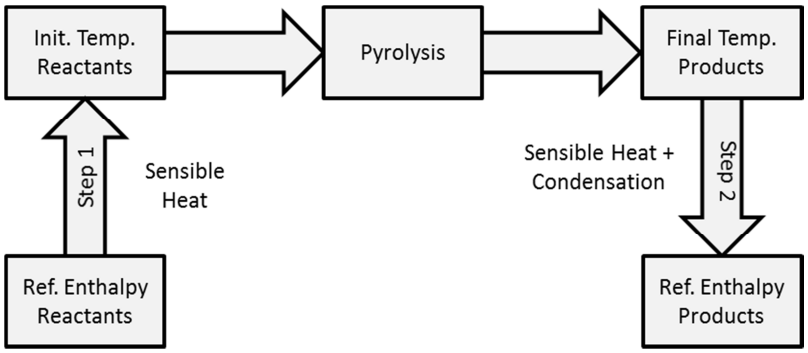

Figure 4.2.7. View of the equivalent steps considered for the global enthalpy change calculation.

$$\Delta H_{global}^{pyrolysis} = \sum H_{formation-products}^{0} - H_{formation-tire}^{0} + \Delta H_{sensible\_heat}^{Step\ 1} + \Delta H_{sensible\_heat-condensation}^{Step\ 2} \quad \text{(E11)}$$

However, pyrolysis is not a homogeneous process and assuming a global enthalpy of pyrolysis is not rigorous. Products emitted throughout decomposition change and evolve, such that Hess law should rather be calculated at several times to obtain true energy of pyrolysis values. This would require knowing the heat of formation of evolving solids at every stage of conversion as well as the full composition of volatiles produced and all the temperatures in the system.

Because it is technically very challenging to obtain this information, heat of pyrolysis as a function of conversion and temperature cannot yet be obtained with the Hess law, but only as a global enthalpy change. Nonetheless, this energetic summation corresponds to the same calculation done by the integral of a DSC heat flow curve in the same conditions for a pyrolysis experiment. It can thus be used as a reference to compare with DSC experiments.

4.2.2.1.5 Objectives

As seen in the literature review, there remain a lot of unanswered questions concerning the energy balance in pyrolysis. It would mostly be explained by the complexity of the processes involved and by technological limitations. Because of the latter, this work will not seek to establish a definitive energy balance for pyrolysis. The purpose of this research will rather be to revisit this important subject that has been flooded with assumptions and simplifications. The objectives will be to:

- Improve the understanding of thermodynamic behaviour of tires during pyrolysis;
- Investigate the interactions between the energy balance and the mass balance during pyrolysis;
- Investigate the reliability of DSC to characterize pyrolysis thermodynamics.

Improving the understanding of pyrolysis thermodynamics will help optimizing process control for industrial pyrolysis processes. Investigating the interactions between the balances will yield reliable tools to optimize the operation of industrial pyrolysis processes. At last, characterizing the reliability of DSC will allow a better criticizing of experimental data in the future and produce better experimental set ups.

4.2.3 EXPERIMENTAL APPARATUS

4.2.3.1 TGA apparatus

TGA experiments were performed using an SDTA851^{e} apparatus from Mettler Toledo^{TM}. Regularly shaped cubic tire samples of 8 mg were used for each experiment. The samples were encapsulated in non-hermetic DSC pans and mounted on the balance pan with a nitrogen flow of 20 mL/min, such that nitrogen could flow freely around the samples. To prevent the pans from deforming during volatiles release, a hole was gently punched on the lids with a needle.

The heating rate was fixed at 10°C/min, as per DSC samples. Five temperatures were considered for this work: 300°C, 350°C, 400°C, 450°C and 500°C. As for all temperatures below 500°C, pyrolysis was not completed during the dynamic heating part, all experiments were kept isothermal (at their respective temperature set point) in order to let the decomposition process to resume. The experiments were run until there was no sample weight loss (less than 0.01 % weight loss during 15 minutes span). During these experiments, the time evolution of the solid mass was measured, which is directly related to the mass of combined volatiles. All experiments were done in triplicate.

4.2.3.2 DSC apparatus

DSC experiments were led using a Q2000 DSC apparatus from TA Instruments™. DSC experiments were led in the same conditions as per TGA. Cubic waste tire samples with an average weight of 8 mg were encapsulated in non-hermetic DSC pans and mounted properly in the DSC apparatus. A hole was gently punched on the lids with a needle to prevent the pans from deforming during volatiles release.

The heating rate was fixed at 10°C/min. Five temperatures were considered, namely 300°C, 350°C, 400°C, 450°C and 500°C. Nitrogen was swept over the samples at a flow rate of 20 mL/min. As for TGA experiments, when the set point temperature was reached, the experiments were continued isothermally until weight stabilization (less than 0.01 % weight loss during 15 minutes span), as per TGA experiments.

After weight stabilization, samples were cooled down at a rate of -10°C/min until the initial temperature of 50°C is reached. Pyrolyzed samples were reheated up to their respective set point temperature at 10°C/min to obtain the thermal behaviour of the resulting char.

4.2.4 RESULTS

4.2.4.1 DSC and TGA data

DSC curves alone give only partial information for pyrolysis. Indeed, the loss of weight from the sample must be taken into account to obtain a full view of the thermodynamic behaviour. DSC curve is presented overlapped with the DTG curve.

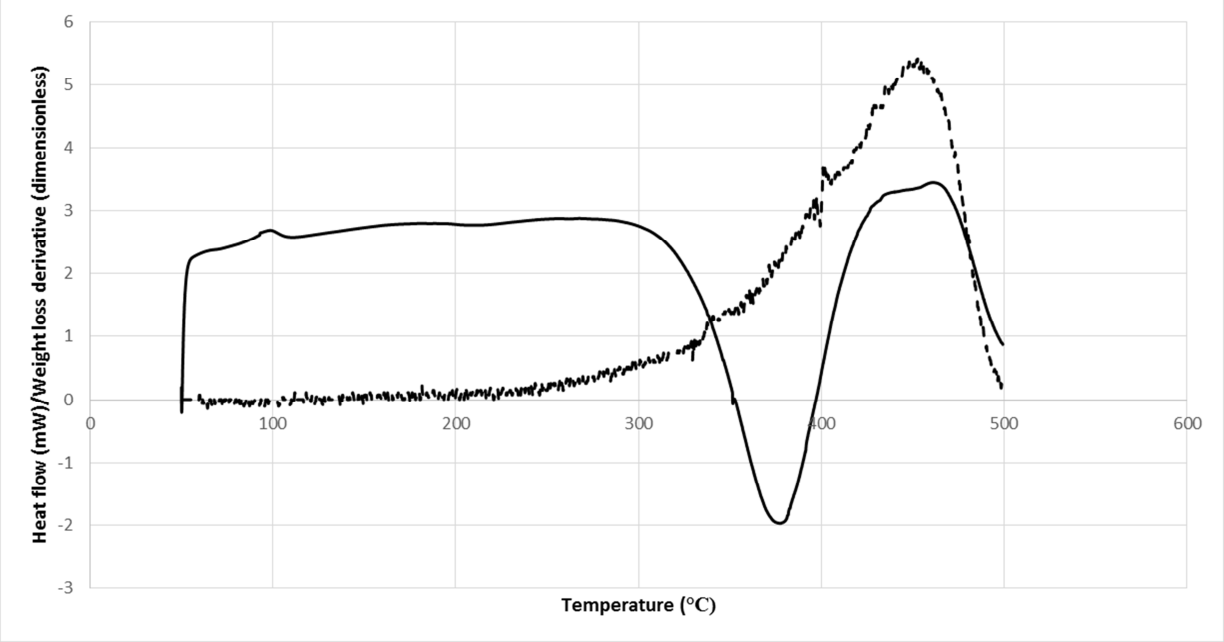

Figure 4.2.8. DSC curve (plain curve) and TGA derivative curve (dashed curve) obtained in this work.

In Figure 4.2.8, the transition from endothermic to exothermic and back to endothermic is observed between 300°C and 450°C, which is also the case for Yang et al. However, since the latter used a different apparatus to measure heat flows, the accuracy of the peaks cannot be compared. Because of the improvement of technology, data obtained in this work are assumed to have produced more precise peaks. If the TGA curve is compared with the DSC curve, one

important observation is that the transition from endothermic to exothermic around 350°C happens precisely when the weight loss derivative accelerates. As well, when the weight loss derivative decelerates, the transition from exothermic to endothermic occurs.

When the weight loss derivative reaches a maximum value, the heat flow through the sample also does. Both curves decrease together at the end of the run, i.e. when the weight loss rate decreases, heat flow decreases.

The heat capacity evolution during pyrolysis of waste tires can be investigated. By assuming that below 250°C, heat capacity will remain that of waste tires, and that pyrolysis has not yet triggered, the heat capacity of tires is obtained (first term in the right-hand side of equation (E10)). In order to calculate it, heat flow was considered purely for sensible heat in the energy balance, and temperature change was constant at 10°C/min.

$$\dot{q}_{sam} = \dot{q}_{sensible\_heat} = m_{batch} Cp_{batch} \frac{dT}{dt} = m_{batch} Cp_{batch} 10℃/min \qquad (12)$$

The heat capacity of char at different stages of the pyrolysis reaction was also evaluated with the TGA by using a heating sequence involving a first heat up ramp followed by the isothermal decomposition up to a specific temperature. Once pyrolysis was completed (no more weight loss), the sample was cooled down at 10°C/min to 50°C and the cooled char was re-heated up to the initial set point temperature. Heat capacities were taken for char samples at their set point temperatures, where thermodynamic equilibrium was reached.

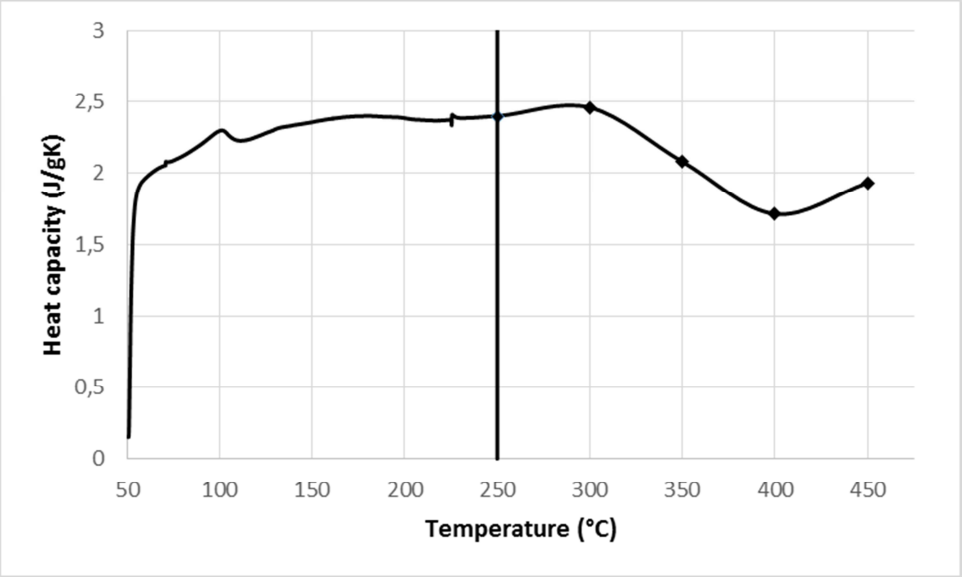

Figure 4.2.9. Heat capacity for tire and the evolving char as a function of temperature.

At first glance, it is observed that 300°C char has a slightly higher heat capacity than waste tires. At 350°C and 400°C, there is a significant decrease of the heat capacity value of the chars, while at 450°C, the heat capacity increases again, though still lower than the waste tires heat capacity. At 500°C, heat capacity could not be obtained, since heat flow curve went exothermic when set point temperature was reached. It is suspected that high porosity and break up of resulting char sample biased the heat flow during the run.

4.2.4.2 Hess law calculation

To demonstrate the overall endothermic behaviour of tires pyrolysis, data from Diez were taken to implement the Hess law [14]. It is one of the most complete sets of data that can be found for waste tires pyrolysis, as elemental or molecular compositions, products yields and lower calorific values (LCV) are given for all the products. First, a correction of the oxygen content of condensable volatiles was applied because the oxygen balance suggested that more oxygen could be found in condensables than in original tires. This would essentially be explained by the forced flow of volatiles through a buffer of water at the outlet of the experimental reactor. This is

suspected to have hydrated the condensables partially to produce alcohols, while they flowed hot through water.

Table 4.2.3. Oxygen distribution among products and pyrolysis yields (Diez et al.).

	Oxygen (%wt)			Yield (%wt)			Oxygen (per kg tire)		
	350°C	450°C	550°C	350°C	450°C	550°C	350°C	450°C	550°C
Tire	0.9	0.9	0.9	N/A	N/A	N/A	0.009	0.009	0.009
Char	0.06	0.02	0.01	50	40	33	0.0003	0.00008	0.000033
Oil	11.9	10	3.5	30	33	38	0.0357	0.033	0.0133
Gas	3.67	3.79	4.24	20	27	29	0.00734	0.010233	0.012296

From Table 4.2.3, the oxygen in char and in non-condensable gases (CO and CO_2) corresponds to the amount of oxygen found in original tire. Therefore, it can be assumed that traces of oxygen would instead be found in oil, which is more likely to other results found in literature [15]-[17]. For the calculations, oxygen in oil was fixed at the same weight percentage that of oxygen in char, which makes CO and CO_2 the main oxygenated compounds in the system.

To obtain the enthalpies of formations for tires, char and condensables, the Hess law was performed on these products, knowing their respective gross calorific value (LCV) and their elemental composition (corrected for oil obtained by Diez et al.). For non-condensables, having their molecular composition known, the energies of formations were taken from thermodynamics tabulated data. The following table presents the enthalpies of formation for the tires and the pyrolysis products as well as the overall enthalpies of pyrolysis at three temperatures (350°C, 450°C and 550°C). These enthalpies of formation are calculated at 25°C.

The enthalpy of formation at a reference temperature of 25°C is obtained by equation (E11), without the last two terms in the right-hand side. It is isolated from the resulting equations below:

$$LCV\ Tires = \sum H^0_{formation-flue\_gas-tire} - H^0_{formation-tire} \quad \text{(E13)}$$

$$LCV\ Char = \sum H^0_{formation-flue\_gas-char} - H^0_{formation-char} \quad \text{(E14)}$$

$$LCV\ Oil = \sum H^0_{formation-flue\_gas-oil} - H^0_{formation-oil} \quad \text{(E15)}$$

Table 4.2.4. Standard enthalpies of formation calculated for the pyrolysis products at different operating temperatures.

	LCV (kJ/kg)			Enthalpy of Formation (kJ/kg)		
	350°C	450°C	550°C	350°C	450°C	550°C
Tire	-35 930	-35 930	-35 930	-2 410	-2 410	-2 410
Char	-28 700	-28 460	-28 500	-3 580	-4 010	-3 990
Oil[a,b]	-39 480	-39 790	-40 040	-460	-1 030	-770
Gas	-55 890	-57 060	-59 050	-490	-460	-380
a. Corrected value for oxygen (water)						
b. Enthalpies of formation in liquid phase						

The Hess law calculation (Enthalpy of formation of products minus Enthalpy of formation of reactants) thus yields standard enthalpy changes for pyrolysis at 25°C. It corresponds to equation (E11) without the last two terms in the right-hand side.

Table 4.2.5. Standard enthalpy change for pyrolysis calculated for different operating temperatures.

	Standard enthalpy change (kJ/kg)
	Hess law (Diez)
350°C	390
450°C	360
550°C	700

To obtain the global enthalpy change during pyrolysis as presented in equation (E11), heat capacities had to be obtained gas, oil and char. For the latter, integration of DSC curves for the reheating experiment up to the set point temperature of pyrolysis was performed.

For non-condensable gases, since the composition was known, direct calculation of enthalpy change between standard temperature and final set point temperature could be done. For oil (condensable gases), enthalpy was calculated in liquid phase up to an average temperature of 175°C, with a heat capacity of 2.12 kJ/kg°C (average between gasoline and kerosene). This hypothesis is reasonable since pyrolysis condensables obtained from tires have shown very similar composition compared to transportation fuels [18]. Then a heat of evaporation was considered with a specific value of 275 kJ/kg (average between gasoline and kerosene). Finally, the heat capacity of the gaseous condensable volatiles was calculated, and the value was again averaged between gasoline and kerosene for the temperature change between 175°C and average set point temperature.

As an indicator to compare with DSC data, global enthalpy changes were calculated with products yields obtained in this work, as Diez et al. product compositions were very similar to those obtained from tires in this work [12].

Table 4.2.6. Pyrolysis products yields obtained with TGA for samples in DSC cups.

	Yield (wt%)	
	350°C	450°C
char	52	33
oil	41	54
gas	7	13

Equation (E11) was thus used assuming the enthalpies of formation obtained in Table 4 and the same heat capacities and heat of evaporation of volatiles used to obtain the global enthalpy change for pyrolysis with data from [14].

DSC curves obtained in this work were integrated to compare with the values obtained with the Hess law. All the experiments and calculations consider heat up from 50°C to set point temperature until weight loss has resumed.

Table 4.2.7. Global enthalpy change for pyrolysis at different operating temperatures.

	Enthalpy change (kJ/kg)			
	Hess law (Diez)	Hess law(this work)	DSC integrated curve	DSC (at reach of SP Temp)
350°C	930	1190	290	600
400°C	N/A	N/A	375	510
450°C	1120	1330	710	660
500°C	N/A	N/A	640	640

In Table 4.2.7, four values were compared. The first column represents the global enthalpy changes for data from [14]. The second column shows global enthalpy change during pyrolysis for yields from this work adapted with energies of formation of products obtained with data from Diez et al. (Table 4). The third column shows the integral values for the whole DSC curves, that includes the isothermal part of the runs. The fourth and final column shows the integral values only for the dynamic heating part of the DSC curves, i.e. at reach of set point temperature. For 350°C and 400°C, the isothermal part was respectively of 360 minutes and 120 minutes, while at 450°C, the isothermal part lasted 15 minutes.

4.2.5 DISCUSSION

4.2.5.1 Global enthalpy change during pyrolysis

As shown in Table 7, values from both Diez and this work are more endothermic than those obtained at reach of set point temperature with DSC (column 3). However, values at 350°C and 400°C cannot be compared for one main reason: pyrolysis has not sufficiently resumed in DSC at the set point temperature. That is, a significant amount of volatiles have not been released, which will affect the integrated curve over the whole pyrolysis experiment. In fact, the global enthalpy change drops down over 50 % of its value at reach of set point temperature from 600 kJ/kg to 290 kJ/kg.

At 450°C, values can be compared since at reach of set point temperature, pyrolysis has mostly resumed and weight loss rate is very low. The fact that the integrated global enthalpy change value increases from 660 kJ/kg up to 710 kJ/kg shows that the char product structure has thermodynamically stabilized and that the remaining product release is a residual endothermic term. The global enthalpy change from this work is significantly greater than the integrated DSC curve at 450°C.

4.2.5.2 Heat capacity below 250°C

Contrarily to other references from literature, the increase of heat capacity with temperature occurs mostly between 50°C and 100°C. Waste tires heat capacity remains almost constant between 100°C and 250°C, there is only a slight increase according to temperature. At 300°C, since a significant weight loss has occurred, the energy balance can no longer be simplified to heat capacity alone (equation (E12)). Yang et al. [3] rather assumed a constant increase rate for heat capacity of tires:

$$Cp_{tire} = 1.230\ \frac{J}{kgK} + 0.00655\ \frac{J}{kgK^2} \quad \text{(E16)}$$

There is a net advantage of using DSC at low temperature, i.e. below 250°C: accuracy. With very low weight loss, heat capacity could be obtained as an array dependent of temperature (Figure 9)

rather than a mathematical function (equation (E16)). This DSC technology also proves its accuracy in another way; at 100°C, a very slight endothermic peak shows the evaporation of moisture in tires. However, the weight loss is not significant compared to sample weight. It was therefore not taken into account in the energy balance.

4.2.5.3 Heat capacity over 250°C

The evolution of heat capacity and sample weight during pyrolysis experiments in DSC triggers an important bias in heat flow measurements. As shown in Figures 8 & 9, both weight and heat capacity decreases from 300°C up to 400°C. Since DSC operates in dynamic heating conditions, it appears that at every time step, the heat amount supplied to the sample is overestimated. That is, a fraction of the energy is in excess, because both sample heat capacity and weight decreases continuously. The consequence, as seen in the T4P equation, is an increased sample temperature (Ts) and an apparent heating rate over 10°C/min. Therefore, the system sees this as an exothermic behaviour and gradually decreases the energy input to the system with a progressive excess of energy in the sample.

The energy input to the system is calibrated with the blank run, such that the relative heat flow shown in the DSC curves hides that there is an absolute heat input which is determined by the DSC control system and controller default settings.

Because for temperatures over 400°C, the heat capacity start increasing and weight loss rate starts diminishing, the apparent exothermic behaviour vanishes to reveal a net endothermic behaviour. Nevertheless, this exothermic behaviour really starts to vanish around 375°C, wich corresponds to the deceleration of weight loss rate. This supports the idea that exothermic behaviour is induced by both DSC effects and thermodynamic properties variations.

In comparison, Yang et al. assumed that tire heat capacity was independent from char heat capacity. As well, they assumed that a heat of evaporation was dominant and proportional to the weight loss derivative. The residual energy was finally assumed to fit completely for the heat of pyrolysis. Moreover, potential biases generated by the apparatus itself have not been considered, resulting overall in a heat of pyrolysis term absorbing deviations from these hypotheses.

4.2.5.3 Energy balance simulation

Instead of trying to define directly the energy balance terms for pyrolysis, the strategy is first to integrate the new heat capacity evolution from Figure 9 to a proven system. In a previous work, a predictive kinetics model have been developed and validated with industrial data. An energy balance had then been rather fitted to plant data, because the effort was initially to characterize the kinetics of pyrolysis.

Globally, a convective heat transfer term was considered between the hot drum wall and the bed of tire shreds as the heat input in the system. With heat capacity data from literature [3], a constant heat of pyrolysis was fixed and assumed fully dependent on the weight loss derivative that was obtained through the kinetics model. The energy balance then used was as per equation (E5), assuming a single constant heat of pyrolysis term. Since steel was present in the system, the left-hand term had to be decomposed, as shown below:

$$m_{batch}(t)Cp_{batch}(T) = m_{steel}Cp_{steel}(T) + m_{tire}(t)Cp_{tire}(T) + m_{char}(t)C_{p_{char}} \quad \text{(E17)}$$

As it is seen in equation (E12), tire heat capacity was assumed independent from that of char, as it has been simplified in other works as cited previously.

In light of these new results, in equation (E5), knowing the measured wall and bed temperatures as well as the newly obtained solids (as a whole) heat capacity evolution with temperature from

DSC experiments, the convection heat transfer coefficient have been calculated with more precision below 250°C. The heat of pyrolysis term has been left as a variable unknown term, expecting it not to be constant.

Figure 4.2.10 shows the heat flow calculated for convection heat transfer to the bed of tire shreds. It is presented along the heat capacity curve.

$$\dot{q}_{sam} = \dot{q}_{convection} = \bar{h} W_{exp} (T_{wall} - T_{bed}) \text{ (E18)}$$

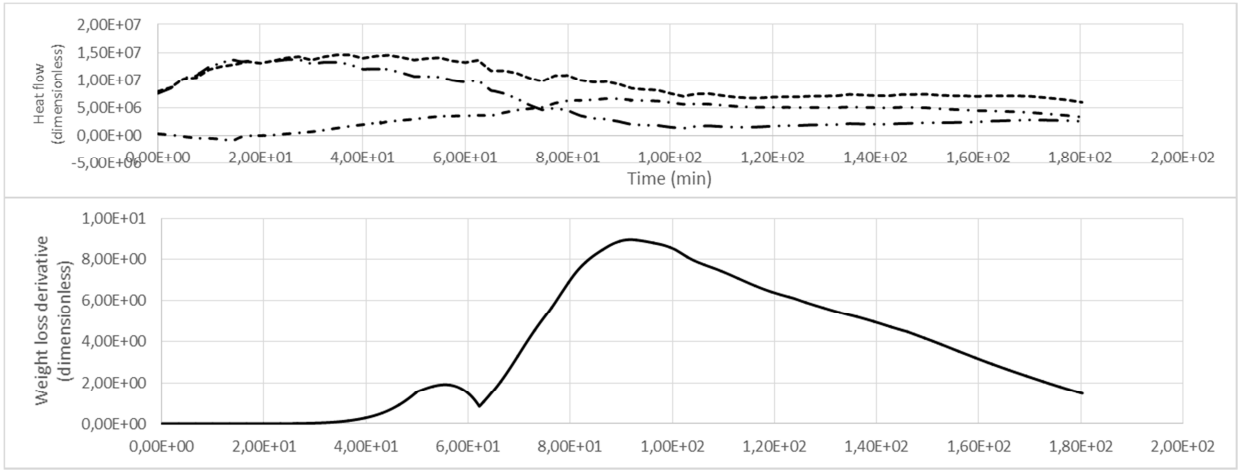

Figure 4.2.10. Heat flow to the tire shreds simulated with equation (E17). In the upper graph: convection heat input = dashed curve; sensible heat = dash-dot-dotted curve; pyrolysis heat = dash-dotted curve.

The sensible heat flow ($\dot{q}_{sensible\_heat}$) follows well the heat input from convection ($\dot{q}_{convection}$) up to 250°C, then it relatively becomes less important and other phenomena takes place that also consumes energy. This also starts up while weight loss triggers. Sensible heat alone is calculated independently as per equation (E12) using data from Figure 9 and known heat up ramp (measured sample temperature).

To observe more specifically the pyrolysis heat flow ($\dot{H}_{pyrolysis}$) for the whole run, the sensible heat flow curve has been subtracted from the convection heat flow curve. The result is shown in Figure 4.2.10.

As it have been suspected by many authors, this heat flow should be greatly dependent on the derivative weight loss, because among others of pyrolysis liquids evaporation. Therefore, this resulting heat flow have been divided by the weight loss derivative to see if any constant tendency could emerge.

In Figure 4.2.10, it is shown that during the most intensive volatile release part of pyrolysis, i.e. between the 80th minute and the 130th minute, the sensible heat flow is very stable and constant, which strongly indicates a dependency on the weight loss derivative, namely the rate of production of volatiles during pyrolysis. The value of this specific global heat of reaction is 765 kJ/kg of volatiles. It is believed that a part of this parameter is explained by the heat of evaporation of volatiles, and the remaining fraction of it should be related to the thermal cracking, reforming and expulsion of gaseous volatiles from tire shreds.

Energy within the weight loss derivative term can be extended to the whole run, such that now three energy terms are known: energy input to the tires, energy consumed by heat capacity and energy consumed by weight loss derivative term. By subtracting the two latter from the energy input, a residual energy term is obtained. This residue is significant compared to the overall energy input only before the trigger of pyrolysis and in the final minutes of pyrolysis most of the volatiles have been released.

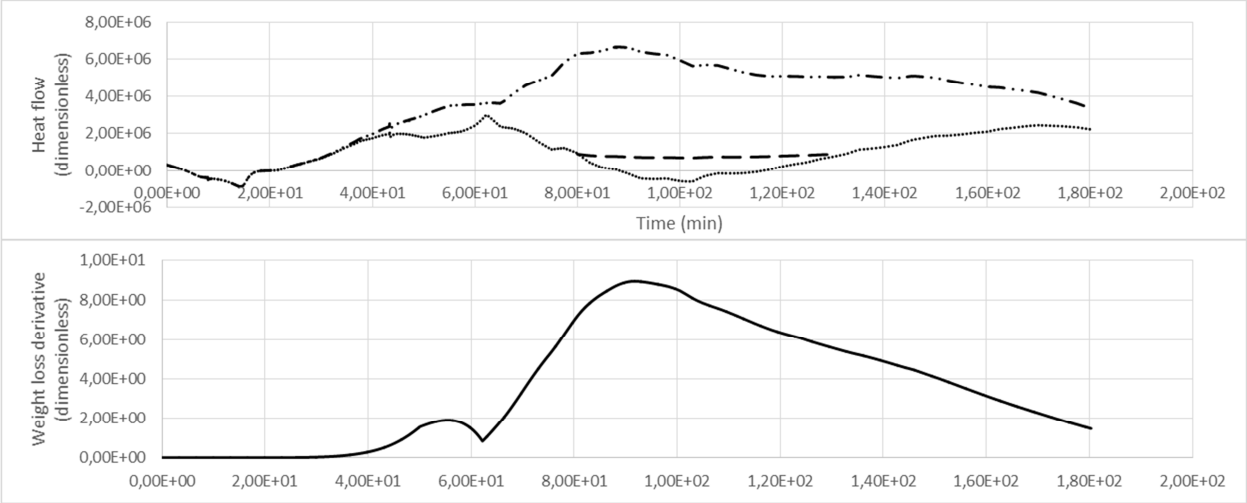

Figure 4.2.11. Heat flows associated with pyrolysis. In the upper graph: pyrolysis heat = dash-dot-dotted curve; residual heat = dotted curve; constant specific heat of pyrolysis proportional to weight loss derivative = dashed curve.

The first residual energy is expected to represent the sulfur crosslink breakage, as highlighted in Table 1; it mostly occurs before the main weight loss triggers. It is thus not related to the weight loss derivative of the system, but rather dependent on the density of crosslinkage in tires. This term is presented as

$$\dot{H}_{crosslink} = H_{crosslink}^{2} \frac{dm_{crosslink}}{dt} \quad \text{(E19)}$$

When the weight loss derivative decreases and where it is expected that pyrolysis resumes, the residual heat flow becomes as important as the sensible heat flow. As this residual heat flow is assumed not to be dependent on the weight loss derivative, it is suspected to be a function of charring reactions in the solids. As per Table 1, this term was expected to participate in the energy balance, but at that time, it was not known whether these reactions were globally endothermic or exothermic. From the pyrolysis simulation, it seems to behave endothermically. These reactions would then depend on active sites within the solid matrix and is thus

representable by a mass term (m_{active_sites}). The energy balance for pyrolysis would then have the following form:

$$\dot{q}_{sam} = \dot{q}_{convection} = \bar{h} W_{exp} (T_{wall} - T_{bed}) =$$
$$m_{batch}(t) Cp_{batch}(T) \frac{dT}{dt} + H^1_{pyrolysis\_dmdt} \frac{dm_{out}}{dt} + H^2_{crosslink} \frac{dm_{crosslink}}{dt} + H^3_{charring} \frac{dm_{active-sites}}{dt}$$
(E20)

By integrating the energy input to the system (equation (E18)) from which the energy given to steel is subtracted (first term in the right-hand side of equation (E17)), a specific global enthalpy change of **1,340** kJ/kg is obtained for tires. It is a deviation of about 1% compared to the value of 1,330 kJ/kg obtained theoretically for 450°C in Table 7 in this work and a deviation of 16% compared to the value of 1,120 kJ/kg obtained with the data from [14].

The exothermic peak obtained in this work with DSC (Figure 8) has a negative impact on the energy balance of 250 kJ/kg. It corresponds to the region defined by a triangle in Figure 4.2.12.

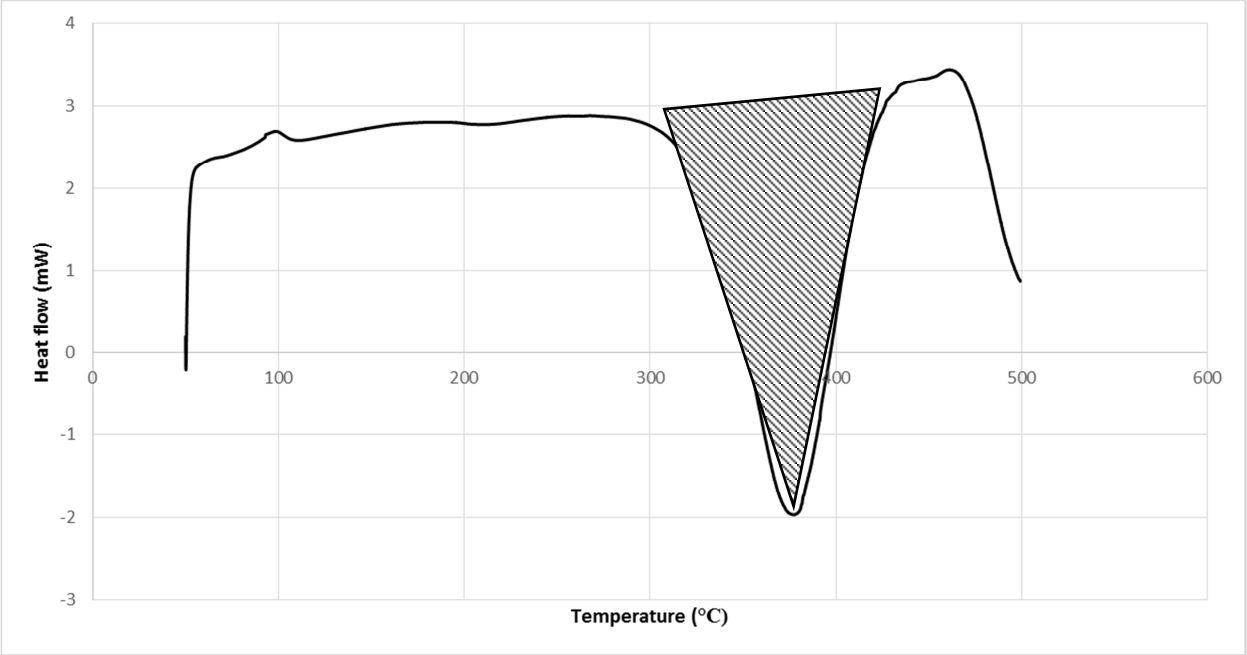

Figure 4.2.12. Area of the DSC curve corresponding to the exothermic peak.

Assuming this value to be the excess energy produced by DSC and that the resulting curve would have followed the endothermic peak obtained at 450°C, it can be added to the integral value of 710 kJ/kg presented in Table 7. The result is **960** kJ/kg, which is still 28% below to the overall heat transferred to the tires in the industrial model.

This strongly demonstrates that the behaviour of waste tires is rather strictly endothermic during pyrolysis and that exothermic peaks obtained during DSC experiments are an artifact produced by the control system of the apparatus. Because the industrial set up do not tend to follow a temperature heat up ramp, which could have led to bias, the heat flow calculated from industrial data and by the Hess law are closer to the real thermochemical and thermodynamic behaviour of pyrolysis.

From equation (E20), the distribution of the input energy within the different terms can be compared between the theoretical value from the Hess law, the simulated value with the

industrial model and the curve obtained with DSC. However, this comparison is mostly resumed between sensible heat and global pyrolysis reactions.

Table 4.2.8. Fraction of the global enthalpy change consumed by sensible heat.

Energy consumed by heat capacity (%)	
	450°C
Hess law (data from Diez et al.)	72
Hess law (data from this work)	60
DSC curve (integral whole curve)	83
DSC curve (integral at set point T)	113
Industrial model (energy balance)	60

The value of 83% for the DSC curve show that the hypothesis made to correct the integral was not sufficient. In fact, there should also be pyrolysis reactions involved and the result for DSC curve integral should be greater than the estimation of 960 kJ/kg, to get closer to the value of 60% of the overall energy input consumed by sensible heat obtained with the industrial model, and closer to 60% and 72% obtained with the Hess law.

Finally, the energy balance simulation that led to equation (E20) also allowed breaking down the energy terms for pyrolysis. First, the energy for heat capacity is approximately 790 kJ/kg tires and the energy for pyrolysis reactions is 550 kJ/kg tires. From this 550 kJ/kg tires, 410 kJ/kg is dependent of the weight loss derivative, 65 kJ/kg is related to sulfur crosslink breakage and 75 kJ/kg is related to charring. These specific enthalpy values correspond respectively in equation (E20) to the second, third and fourth right-hand side terms.

4.2.6 CONCLUSIONS

The enthalpy of pyrolysis has been investigated in this article with DSC and industrial batch reactor data. Initially, there was a contradiction between the fact that pyrolysis is mostly an

endothermic phenomenon and DSC produced heat flow data showing exothermic peaks during decomposition.

First, the DSC data showed indeed that even with new technologies, the exothermic peak appears, but only with more precision. However, industrial data showed without a doubt that if an exothermic behaviour would exist, a temperature upsurge in the reactor would occur. Contrarily to that, a deceleration of the temperature increase confirmed that DSC produces an artifact during pyrolysis.

For the case of tires, at low temperature, i.e. below 250°C, the heat capacity have been found with more accuracy, while over 250°C, the heat capacity was found to decrease significantly up to 400°C before starting increasing until the reach of thermodynamic equilibrium. As a conclusion from these results, it is believed that the combination of sample weight loss and heat capacity decrease induce a bias in the control system of the DSC, generating the impression of an exothermic behaviour.

To consolidate these results, the energy balance was modelled with the industrial batch reactor data, where temperatures and weight loss were measured. The simulation allowed isolating the enthalpy of pyrolysis, which was found to be formed of three significant terms. The first one is dependent of the weight loss derivative, with a specific enthalpy of 410 kJ/kg tires. The second and third ones are independent of weight loss derivative. One is observable at lower temperature (around 250°C) and accounts for sulfur crosslinks breakage while the other accounts for charring reactions approaching the thermodynamic equilibrium.

In conclusion, this work helped pointing out that DSC is not suited to observed thermal transitions when weight loss and heat capacity decrease occurs simultaneously. Nevertheless, the new DSC technology allowed finding the heat capacity of the evolving pyrolysis samples with more accuracy. With these new data, the enthalpy of pyrolysis could be investigated on a

completely new angle, with the help of industrial batch reactor data. This work opens the door to further investigations, whether to optimize industrial size systems or to characterize the pyrolysis energy balance with other feedstock showing unclear or more complex thermal transitions. This methodology could also apply to any system where initial solids react to yield volatile products and an evolving residual solid.

4.2.7 Acknowledgements

The authors would like to extend their sincere thanks to the NSERC funding program that, in part, made this project successful.

4.2.8 References

[1] Box, G. E. P.; Draper, N. R. Empirical Model Building and Response Surfaces, John Wiley & Sons, New York (1987).

[2] Yang, J.; Tanguy, P.A.; Roy, C. Heat transfer, mass transfer and kinetics study of the vacuum pyrolysis of a large used tire particle. Chemical Engineering Science 50(12) (1995) 1909-1922.

[3] Yang, J.; Roy, C. A new method for DTA measurement of enthalpy change during the pyrolysis of rubbers. Thermochimica Acta 288 (1996) 155-168.

[4] Koufopanos, C.A.; Papayannakos, N.; Maschio, G.; Lucchesi, A. Modelling of the pyrolysis of biomass particles. Studies on kinetics, thermal and heat transfer effects. Canadian Journal of Chemical Engineering 69 (1991) 907-915.

[5] Klason, P. Versuch einer Theorie der Trockendestillation von Hols. Journal fur Praktische Chemie 90 (1914) 413.

[6] Thomas, P.H.; Bowes, P.C. Some aspects of self-heating and ignition of solid cellulosic materials. British Journal of Applied Physics 12 (1961) 222.

[7] Roberts, A.F.; Clough, G. Thermal Decomposition of Wood in an Inert Atmosphere. Ninth Symposium (International) Combustion, New York (1963) 158.

[8] Beall, F.C. Differential calometric analysis of wood and wood components. Wood Science and Technology 5 (1971) 159-175.

[9] Yang, J.; Kaliaguine, S.; Roy, C. Improved quantitative determination of elastomers in tire rubber by kinetic simulation of DTG curves. Rubber Chemistry and Technology 66 (1993) 213.

[10] Sircar, A.K.; Lamond, T.G. Carbon black transfer in blends of cis-poly(butadiene) with other elastomers. Journal of Applied Polymer Science 17 (1973) 2569.

[11] Brazier, D.W.; Schwartz, N.V. Effect of heatimg rate on the thermal degradation of polybutadiene. Journal of Applied Polymer Science 22 (1978) 113.

[12] Lanteigne, J.-R.; Laviolette, J.-P.; Tremblay, G.; Chaouki, J. Predictive kinetics model for an industrial waste tire pyrolysis process. Energy & Fuels 27 (2013) 1040-1049.

[13] Danley, R.L. New heat flux DSC measurement technique. Thermochimica Acta 395 (2003) 201-208.

[14] Diez, C.; Martinez, O.; Calvo, L.F.; Cara, J.; Moran, A. Pyrolysis of tyres. Influence of the final temperature of the process on emissions and the calorific value of the products recovered. Waste Management 24 (2004) 463-469.

[15] Williams, P.T.; Besler, S.; Taylor, D.T. Pyrolysis of scrap automotive tyres. The influence of temperature and heating rate on product composition. Fuel 69 (1990) 1474-1482.

[16] Laresgoiti, M.F.; Caballero, B.M.; De Marco, I.; Torres, A.; Cabrero, M.A.; Chomon, M.J. Characterization of the liquid products obtained in tyre pyrolysis. Journal of Analytical and Applied Pyrolysis 71 (2004) 245-253.

[17] Berrueco, C.; Esperanza, E.; Mastral, F.J.; Ceamanos, J.; Garcia-Bacaicoa, P. Pyrolysis of waste tyres in an atmospheric static-bed batch reactor: Analysis of the gases obtained. Journal of Analytical and Applied Pyrolysis 74 (2005) 257-269.

[18] Lopez, F.A.; Centeno, T.A.; Alguacil, F.A.; Lobato, B.; Urien, A. The GRAUTHERMIC-Tyres process for the recycling of granulated scrap tyres. Journal of Analytical and Applied Pyrolysis 103 (2013) 207-215.

CHAPITRE 5 LE COMPORTEMENT DU SOUFRE LORS DE LA PYROLYSE DES PNEUS

Cet article a été soumis en 2014 dans le journal Energy & Fuels.

5.1 PRÉSENTATION DE L'ARTICLE

Le but de cet article était de déterminer les mécanismes dominants pour la distribution du soufre dans les différents produits lors de la pyrolyse des pneus et de développer un indicateur permettant de prédire ce comportement en fonction des conditions d'opération. Ce nouveau paramètre, la sélectivité du transfert du soufre vers les volatiles, est une sélectivité intrinsèque dépendant uniquement de la température. Elle tient compte de l'impact du transfert de matière et de l'influence du zinc et du fer.

Suite à l'analyse des résultats obtenus et des données disponibles dans la littérature, les valeurs limites de la sélectivité du soufre vers les volatiles ont été déterminées. En l'absence de métaux et lorsque la cinétique est limitante (température élevée), la sélectivité tend vers la valeur de 1, c'est-à-dire qu'en pourcentage massique, la quantité de soufre retrouvée dans les volatiles est proportionnellement égale à la quantité de volatiles produite. À basse température (< 300°C) et en l'absence de métaux, la sélectivité sera supérieure à 1, soit que proportionnellement, la fraction massique de soufre retrouvée dans les volatiles est supérieure à la quantité de volatiles produite. Enfin, en présence de métaux et à une température modérément élevée (> 350°C), la sélectivité devient inférieure à 1, soit que proportionnellement, le pourcentage massique de soufre retrouvé dans les volatiles est inférieur à la quantité de volatiles produits et donc, que le soufre a tendance à demeurer séquestré dans le char.

5.2 ON THE BEHAVIOUR OF SULFUR DURING THE PYROLYSIS OF TIRES

On the behaviour of sulfur during the pyrolysis of tires

*Jean-Remi Lanteigne, Jean-Philippe Laviolette, and Jamal Chaouki**

Department of Chemical Engineering, École Polytechnique de Montréal,

C.P. 6079, succ. Centre-Ville, Montréal, Qc, Canada H3C 3A7

*Corresponding Author (jamal.chaouki@polymtl.ca)

5.2.1 Abstract

The mechanisms of transfer of sulfur to the volatiles phase and char phase during the pyrolysis of tires have been investigated by complementing the available literature data with TGA experiments. For isothermal experiments, the global selectivity expression could be simplified into an intrinsic form of sulfur loss selectivity, which is solely a function of temperature. Two other phenomena have been found to influence the intrinsic sulfur loss selectivity: solid matrix desulfurization and metals sulfidation. In the case where tires would contain no metals and pyrolysis was performed such as decomposition kinetics is limiting, the intrinsic sulfur loss selectivity would converge to the value of 1. Below 350°C, mass transfer limitation will promote solid matrix desulfurization, producing sulfur loss selectivity greater than 1. Over 350°C, if zinc and/or steel are present in tires, sulfidation will cluster sulfur in the solid phase and sulfur loss selectivity will become lower than 1. A developed form of intrinsic sulfur loss selectivity could be obtained to account for these phenomena.

Keywords – Pyrolysis, Waste tires, Sulfur, Selectivity, Mechanisms

5.2.2 INTRODUCTION

Sulfur is essential to life. Paradoxically, it can also be toxic, such that standards have been developed in order to minimize undesired effects on human health and the environment [1,2]. Industrial recovery of waste is greatly influenced by these standards, including waste tires recovery since sulfur is one of their important constituents.

Waste tires pyrolysis generates products in three phases: non-condensable combustible gas, condensable gas (oil) and carbonaceous powder (char). The choice of reactor technology and operating conditions are critical in determining the distribution of intrinsic sulfur within these three products, as emerging from literature [3]-[7]. It can therefore have a major influence on pyrolysis process profitability and viability, as sulfur distribution determines the needs in purification efforts according to the products' specific intended applications.

Few researches have been conducted on the subject of post-processing purification of oil and char from tire pyrolysis [8]-[10]. Research aiming at understanding the mechanisms leading to sulfur distribution during pyrolysis of waste tires is scarcer [11]. In a context of tightening environmental regulations, a better comprehension of sulfur distribution in the products could lead to wiser upstream design decisions. In the end, this could yield pyrolysis processes with higher efficiency and lower cost, which would require less decontamination and purification treatments downstream.

The behaviour of sulfur during pyrolysis of tires is dependent upon several key factors that are also affecting pyrolysis at large. The following are considered in this work:

1. Pyrolysis temperature;
2. Heat and mass transfer limitations;
3. Volatiles composition during pyrolysis.
4. Waste tire chemical composition (inorganics);

5.2.2.1 Definition of global selectivity

By definition, pyrolysis implies a transient heating step and usually, sulfur is analyzed in the cumulated final products. Sulfur distribution must then be considered as the integral of sulfur selectivity over a whole experiment. That is, when thermodynamic equilibrium is reached. From a batch system, global selectivity would be for sulfur loss:

$$S_{SL/TWL} = \frac{\int_{t0}^{t} r_{SL} dt}{\int_{t0}^{t} r_{TWL} dt} \quad (1)$$

That is, the global rate of sulfur transfer to volatiles (r_{SL}), integrated over total batch duration (t_0 to t), over the global rate of release of volatiles (r_{TWL}), also integrated over total batch duration. The rate of total weight loss is assumed to be dependent upon temperature and global pyrolysables, as per developed in a previous work [12]:

$$r_{TWL} = \left(s_{gas} + s_{oil}\right)\left(-r_{pyrolysis}\right) = \left(s_{gas} + s_{oil}\right) A e^{-\frac{E_a}{RT}} \cdot \left(\frac{m_{tire} - m_{pyrolysis}}{m_{tire\_initial}}\right)^n \quad (2)$$

Where intrinsic selectivities for gas and oil are respectively s_{gas} and s_{oil} and are assumed to be fully dependent of temperature. The rate of production of volatiles (r_{TWL}) is proportional to the rate of pyrolysis ($-r_{pyrolysis}$) which is the global rate of decomposition. The kinetics equation for the rate of pyrolysis is a function of the pre-exponential constant (A), an energy of activation (E_a), as per the Arrhenius law, and the mass of available pyrolysables (m_{tire} is the mass of pyrolysables through time; $m_{pyrolysis}$ is the amount of pyrolysables decomposed through time; $m_{tire\_initial}$ is the initial weight of pyrolysables) at the n-th order.

5.2.2.2 Definition of intrinsic selectivity

The pyrolysis temperature is the driving force of pyrolysis and by extension, it is the main parameter influencing the formation of sulfur compounds. The effect of temperature alone on tire pyrolysis is however difficult to characterize, because other factors, such as heat and mass transfer, may bias the study of kinetics. The presence of metals may as well influence the sulfur loss rate at the molecular scale.

To account for the influence of temperature as the main parameter, the rate of sulfur loss must be developed. As the rate of total weight loss is assumed to be dependent upon temperature and global pyrolysables, it is assumed that sulfur weight loss will follow a proportional trend:

$$r_{SL} = s_{SL/TWL}(T) r_{TWL} \quad (3)$$

Where the intrinsic selectivity for sulfur loss ($s_{SL/TWL}(T)$) is solely a function of temperature, similarly to ther gas and oil intrinsic selectivity in equation (2).

The batch selectivity (equation (1)) can reach limit values if the reaction rates, over certain time span, remain stable. For example, in a TGA experiment where the heating rate is fast enough to shorten the residence time of the sample during the dynamic heating step, it can be assumed that selectivity is calculated for the final set point temperature. The selectivity term becomes constant and the expression can be simplified to the intrinsic form of selectivity:

$$S_{SL/TWL} = \frac{\int_{t0}^{t} r_{SL} dt}{\int_{t0}^{t} r_{TWL} dt} = \frac{s_{SL/TWL}(T) \int_{t0}^{t} r_{TWL} dt}{\int_{t0}^{t} r_{TWL} dt} = s_{SL/TWL}(T) \quad (4)$$

The intrinsic selectivity would then be, in the limit case, a function of temperature, i.e. when the intrinsic selectivity alone can explain the sulfur distribution. The units of the intrinsic selectivity are defined as percentage sulfur loss (*SL*) per percentage pyrolysis volatiles losses (*TWL*).

In this situation where decomposition kinetics would be limiting during pyrolysis, and since pyrolysis is a probabilistic process, one would obtain a sulfur weight loss (found in volatiles) proportionally equal to the pyrolysis weight loss:

$$s_{SL/TWL}(T) = 1\ \%SL/\%TWL \quad (5)$$

In other words, for an experiment where the heating time is short enough such that it can be neglected, the sulfur loss yield in percentage over the total volatile loss yield in percentage would be equal to 1 for the remaining isothermal part.

This can be assumed because sulfur is present as an organic functional group in tires, in very small amount, and is not part of the core of resin chains. Crosslinks are indeed weak points in tires, but their unbinding alone during pyrolysis will not release significant amounts of volatiles. Sulfur would then be statistically present in the same relative proportion in the volatiles than in the remaining solids compared to the initial state. Therefore, in such conditions, the global selectivity for sulfur weight loss will be approximately equal to the intrinsic selectivity, with the limit value of 1:

$$S_{SL/TWL} = s_{SL/TWL} = \frac{Sulfur\ weight\ loss\ percentage}{Total\ weight\ loss\ percentage} = 1 \quad (6)$$

Some data can be found in literature regarding sulfur distribution within pyrolysis products. They are presented in Table 5.2.1.

Table 5.2.1. Literature data on sulfur distribution within the products of waste tire pyrolysis

Temperature (°C)	**Pyrolysis weight loss %**	**Sulfur weight loss %**	**$s_{SL/TWL}$**	**Reference**	**Apparatus**	**Inorganics in waste tires**
350	50	25	0.5	[13]	Static oven, no gas sweep	Zn
350	30[a]	21.7[a]	0.72	Idem	Idem	Zn
450	60	40	0.67	Idem	Idem	Zn
450	33[a]	25.7[a]	0.78	Idem	Idem	Zn

550	67	48.9	0.73	Idem	Idem	Zn
550	38[a]	33.8[a]	0.89	Idem	Idem	
400	36	33.3	0.89	[14]	Customized TGA, N_2 flow	Zn, Fe
400	30[a]	22[a]	0.73	Idem	Idem	Zn, Fe
500	47.3	29.6	0.59	Idem	Idem	Zn, Fe
500	39.9[a]	25.2[a]	0.625	Idem	Idem	Zn, Fe
550	47.5	30.8	0.61	Idem	Idem	Zn, Fe
300	4.8[a]	4.8[a]	1.0	[15]	Autoclave, N_2 flow	Zn, Fe
400	24.8[a]	18.2[a]	0.73	Idem	Idem	Zn, Fe
500	38.0[a]	35.5[a]	0.93	Idem	Idem	Zn, Fe

[a] Based on pyrolysis liquids only

An apparent trend emerging from this data is that absolute sulfur weight loss percentage to the volatiles generally increases with increasing pyrolysis temperature, which can be expected knowing pyrolysis weight loss percentage increases with temperature.

Referring to data from Table 5.2.1, the sulfur weight loss selectivity decreases with increasing temperature for Berrueco et al. [13], while it is the total opposite for Diez et al. [14]. Furthermore, no tendency can be extracted from data obtained by Laresgoiti et al. [15]. For all cases except the 300°C experiment from Laresgoiti et al., the selectivities were lower than 1, but very close to 1. Note that the waste tire samples used by Berrueco et al. and Laresgoiti et al. contained zinc and steel while those used by Diez et al. only contained zinc.

All analyses in literature discussed sulfur either by elemental composition or by overall sulfur losses from initial state. However, since these values cannot be related to a reference state, namely an expected value, it limits the analysis.

These contradictory results justify further investigation, as many factors other than temperature could explain these variations. As well, more experimental results are needed to discuss the tendencies of the sulfur weight loss selectivity and conclude on the influence of factors other than temperature on sulfur loss.

5.2.2.3 Influence of heat and mass transfer

A study by Barbooti et al. [16] demonstrated that particle size and inert gas flow rate have a major influence on pyrolysis products yields. These two independent parameters affect the heating rate of waste tire samples (heat transfer) and the intra-particle residence time of volatiles (mass transfer). They are thought to be also of importance in determining sulfur distribution between pyrolysis products. Experimental data from Barbooti et al., obtained with a static furnace swept with N_2 with controlled temperature, are shown in Table 5.2.2.

Table 5.2.2. Data points on sulfur distribution within pyrolysis products from [16].

Set Point Temperature (Celsius)	Nitrogen flow rate (m^3/h)	Particle size (mm)	Char yield (wt%)	Oil yield (wt%)	Gas yield (wt%)
420	25	6	39	50.5	10.5
420	25	16	51	36	13
420	45	6	35.7	57	7.3
420	45	16	34.7	51.9	13.4

The nitrogen flow rate had a significant effect on the pyrolysis products selectivity: increasing nitrogen flow rates resulted in higher convective heating rates and average tire sample temperature during pyrolysis. That is, with nitrogen flow rates from 25 m^3/h to 45 m^3/h, char yield went from 39 wt% to 35.7 wt% for 6 mm particles and from 51 wt% to 34.7 wt% char for 16 mm particles. The nitrogen flow rate also had an influence on the pyrolysis gas and oil yields.

Increasing the nitrogen flow rate increased the average pyrolysis temperature. This increased the volatiles average molecular weight while decreasing the non-condensable gas production. With nitrogen flow rates from 25 m^3/h to 45 m^3/h, the gas yield went from 10.5 wt% to 7.3 wt% and from 13 wt% to 13.4 wt% for 6 mm and 16 mm particles, respectively. For 16 mm particles, this change in yield occurred despite a 16 wt% (absolute) increase in volatiles production. This is further supported by the results obtained by Williams et al. [7]. At a set-point temperature of 300°C, they measured an almost equal distribution between oil and gas as well as a low average molecular weight of the oil for atmospheric pressure pyrolysis of waste tires. The average molecular weight of condensables increased with temperature from 190 g/mol at 420°C and 20°C/min to 230 g/mol at 720°C and 20°C/min. These observations suggest significant intra-particle cracking of the volatiles produced during pyrolysis at low temperatures, resulting from low volatiles mobility.

Table 5.2.2 also highlights the effect of particle size: increasing particle size increases the non-condensable gas yield due to a greater intra-particle residence time of volatiles, which promotes thermal cracking. The non-condensable gas yield increased from 10.5 wt% (6 mm) to 13 wt% (16 mm) gas at a nitrogen flow rate of 25 m^3/h. This effect is even more obvious at a higher nitrogen flow rate of 45 m^3/h where gas yield increased from 7.3 wt% to 13.4 wt%. However, increasing particle size also promotes the formation of intra-particle temperature gradients especially at low nitrogen flow rate. At a nitrogen flow rate of 25 m^3/h, the char yield increased by about 10 wt% (absolute) due to lower averaged pyrolysis temperature. Char yield remained however unchanged at a nitrogen flow rate of 45 m^3/h due to greater thermal convection.

5.2.2.4 Influence of volatiles composition

The composition and partial pressure of volatiles during pyrolysis is among others a function of waste tire composition (inorganics), pyrolysis temperature, heat and mass transfer and intra-particle residence time. Volatile species can react with sulfur-bearing compounds to form hydrogen sulfide. Murena [11] conducted experiments where pyrolysis of waste tires was done under a hydrogen donor atmosphere at various pressures and temperatures. The hydrogen donor

(tetralin with formula $C_{10}H_{12}$) was suspected to react with radicalized liquid products to yield hydrogen sulfide (H_2S) and desulfurized pyrolysis liquids, while converting tetralin into naphthalene ($C_{10}H_8$).

$$2\ \text{R-S} + C_{10}H_{12}\ (\text{tetralin}) \rightarrow 2\ \text{R} + 2\ H_2S + C_{10}H_8\ (\text{naphthalene}) \qquad (7)$$

The conclusions of that work suggest that if sulfurized volatiles remain in contact with hydrogen (H_2) or cycloalkenes for sufficient time at high temperature, hydrogen sulfide could be produced at significant levels. As both reactants can be limiting in this type of reaction, their relative concentration is an important factor determining whether sulfur can be transferred from solids to volatiles and from condensable to non-condensable gases during pyrolysis of tires. Hydrogen or cycloalkenes could directly react with radicalized solid sulfur compounds to produce H_2S and desulfurized resin chains. The formation of H_2S would thus be dependent of temperature, concentration of reactants (sulfur compounds and hydrogen donor) and contact time (hydrodynamics).

Many scientific papers [13]-[15] showed that the production of hydrogen (H_2) and aromatics (including cycloalkenes) increases with increasing pyrolysis temperature. Based on the mechanisms proposed by Murena, this suggests that the kinetics of hydrogen sulfide production should be faster at higher temperature. In other words, migration of sulfur to volatiles would be enhanced intrinsically with increasing temperature. However, it should be kept in mind that the kinetics of volatiles production also gets faster with increasing pyrolysis temperature, such that sulfur concentration in condensables will not necessarily decrease. For these reactions to occur the chemical bonds (S-S, C-S, C-C and C-H) should be broken and the required bond dissociation energy (BDE) differs significantly depending on the type of bond as previously discussed.

For example, the C-H and C-C bonds are characterized by a dissociation energy between 360 kJ/mol and 460 kJ/mol depending on the molecular structure [17]. In contrast, C-S and S-S bond

dissociation energies are significantly lower with values estimated between 230 and 280 kJ/mol [17]. This strongly suggests that pyrolysis of tires is initiated by S-S and C-S bond breakage [18], which leads to the production of sulfur radicals, the precursors of desulfurization reactions.

5.2.2.5 Influence of waste tire chemical composition (inorganics)

The organic composition of waste tires of the same type (e.g. cars, trucks, heavy equipment, etc) is very similar between samples [19]. The present study used one specific type of tires such that its organic composition was not considered as a key parameter [20]. On the other hand, the composition of inorganics may vary between tire samples: it is an independent parameter that may influence the outcome of sulfur compounds. Among the tire components, two metals are of interest for sulfur capture: zinc and iron.

5.2.2.5.1 Zinc

Zinc is present homogeneously in tires in the form of zinc oxide or zinc stearate. It essentially acts as a plasticizer during the tire production process to facilitate vulcanization. Zinc can capture sulfur as suggested by Darmstadt et al. [21], which demonstrated that with increasing temperature, zinc oxide converts into zinc sulfide (ZnS). In fact, their results show that at a vacuum pyrolysis temperature of 420°C and higher, conversion of ZnO into ZnS is significant. ZnO reactivity with H_2S is no stranger to this behaviour, because this particular reaction is spontaneous and highly exothermic in this range of temperatures [22]. Consequently, it is assumed that the presence of ZnO in waste tires will partially retain sulfur in the solid phase during pyrolysis.

$$ZnO_{(s)} + H_2S_{(g)} \leftrightarrow ZnS_{(s)} + H_2O_{(g)} \quad (8)$$

Zinc sulfide rate of formation is a function of hydrogen sulfide partial pressure, temperature, and ZnO concentration (limited to ZnO availability). The rate of reaction should follow this behaviour:

$$r_{ZnS} = f(k(T,S_{ZnO}),P_{H2S}) \quad (9)$$

Partial pressure of hydrogen sulfide is dependent upon the pyrolysis behaviour, such that significant H_2S production will follow the volatiles production rate in a certain way.The apparent kinetics constant depends upon temperature, because of the intrinsic activation energy of the zinc sulfidation reaction (equation (8)). However, it is also influenced by the density of active sites for this reaction, which depends on factors such as homogeneity of distribution and char porosity during the decomposition process.

5.2.2.5.2 Iron

Iron is also a constituent of tires in the form of steel. Steel is not homogeneously dispersed in tires and is employed as a structural reinforcement. Dravnieks et al. [23] demonstrated that steel can react with hydrogen sulfide to form iron sulfide (FeS) even at very low hydrogen sulfide partial pressures.

$$Fe_{(s)} + H_2S_{(g)} \leftrightarrow FeS_{(s)} + H_{2(g)} \quad (10)$$

More recently, Lauretta et al. [24] studied the kinetics of iron sulfidation with Fe foils exposed to various H_2S partial pressures and temperatures. A pertinent work involving raw tire pyrolysis has been conducted by Berrueco et al. [14]. They performed waste tires decomposition without removing structural steel from the samples. An elemental mass balance was done for sulfur, but without further analysis or discussion. At 550°C, the tire pyrolysis yielded 47.5 %wt of volatiles,

which contained 30.8 %wt of the initial sulfur present in the tire samples. In comparison, Diez et al. [13] performed pyrolysis experiments with tire resin (without steel) at the same temperature: the reaction yielded 67 %wt volatiles having 48.9 %wt of the initial sulfur in the tire samples. The fact that Berrueco et al. obtained almost 20 %wt units less sulfur transferred to volatiles suggests that sulfidation of iron is a potential side reaction during pyrolysis of waste tires.

5.2.2.6 Work objectives

While previous studies presented much experimental data, none attempted to generalize the observed behaviours to sulfur migration mechanisms or tires pyrolysis mechanisms. Nonetheless, this train of thought could be an influent factor in the development of phenomenological industrial pyrolysis processes. Therefore, the purpose of this article is to first investigate experimentally the behaviour of sulfur during the pyrolysis of waste tires. More specifically, the experiments will cover temperature and heating rate for a constant nitrogen flow rate and particle size. The second objective is to explore the importance of various parameters in the thermal decomposition mechanisms with the sulfur loss selectivity as a new tool.

5.2.3 EXPERIMENTAL APPARATUS

A TGA apparatus was employed to perform all pyrolysis experiments with waste tires and several technologies were used to analyze the samples. They are all presented in this section.

5.2.3.1 TGA apparatus

TGA experiments were performed using an SDTA851^{e} apparatus from Mettler Toledo. Regularly shaped cubic tire samples of 30 mg were used for each experiment. The samples were mounted directly on the balance pan with a nitrogen flow of 20 mL/min, such that nitrogen could flow freely around the samples.

Pyrolysis experiments were performed using three heating rates (1°C/min, 10°C/min and 100°C/min) and five set-point temperatures (300°C, 350°C, 400°C, 450°C and 500°C). During all

experiments with set-point temperatures below 500°C, pyrolysis was not completed during the dynamic heating part. All samples were maintained at their respective temperature set point in order to let the decomposition process resume to completion and until the sample weight loss reached a constant value (less than 0.01 % weight loss during 15 minutes). During these experiments, the time evolution of the solid mass was measured, which is directly related to the mass of combined volatiles. All experiments were done in triplicate.

5.2.3.2 Elemental analysis

The CHNS elemental composition was obtained with an EAS1108 apparatus from Fisons Instruments S.P.A. For virgin tires analysis, fine tire powder samples were used. The cubic char samples (pyrolyzed samples) were also powdered prior to elemental analysis. The analyses were conducted with 5 mg samples in duplicate, such that every TGA operating condition was analyzed with six elemental analyses.

The organic part of tires could be characterized via elemental analysis, but neutron actional analysis (NAA) was also employed to determine the inorganics contents. Char and oil samples from an industrial pyrolysis batch were also analyzed to observe the tendency for inorganics distribution within pyrolysis products. NAA was performed at École Polytechnique de Montréal with the SLOWPOKE nuclear reactor. Uncertainty for measurements in the range of ppm (mass) is on the order of ± 5 %.

5.2.4 RESULTS AND DISCUSSION

In the present study, the analysis of TGA data is performed on the char and volatiles, the latter combining both the condensables (oil) and non-condensables (gas). The TGA apparatus used small waste tire samples such that the volatiles produced were difficult to recover for further analysis. Therefore, all results for the volatiles are obtained by difference with their char counterpart.

5.2.4.1 Characterization of virgin tires and pyrolysis products

5.2.4.1.1 Elemental mass balance

The inorganic compounds in the virgin waste tire samples are listed in Table 5.2.3, which also presents the inorganics found in char and oil from an industrial batch.

Table 5.2.3. Elemental composition for the inorganics contained in virgin tire resin and char and oil from an industrial pyrolysis batch (measured via NAA).

Element Species	Tire resin (ppm)	Char (industrial) (ppm)	Oil (industrial) (ppm)	Element species	Tire resin (ppm)	Char (industrial) (ppm)	Oil (industrial) (ppm)
Na	114	112	11	Br	0.95	17	6.7
Mg	195	147	17.2	Rb	0.62	10	<0.5
Al	655	254	7	Zr	20	240	<10
Si	1505	2627	<170	Mo	0.087	7	0.5
Cl	152	178	75	Cd	0.69	9	1
K	432	130	0.5	In	<0.001	0.134	<0.001
Ca	1839	1616	47	Sn	<3	39	0.75
Sc	0.025	0.3	<0.003	Sb	0.47	4	0.050
Ti	396	373	8.5	I	0.50	1.2	0.83
V	1.15	9.62	0.007	Cs	<0.1	1	<0.1
Cr	0.59	25	<0.3	Ba	5	8	<3
Mn	3.72	12	0.18	La	1.97	3.5	<0.5
Fe	**100**	**14576**	**<20**	Hf	0.05	0.3	<0.02
Co	0.48	41	0.48	W	0.092	0.5	<0.01

Ni	<6	75	<6	Au	0.0006	0.01	0.001
Cu	6.56	90	<0.3	Hg	<0.02	0.3	0.1
Zn	**4735**	**6778**	**1.5**	Th	0.025	0.49	<0.02
As	0.11	2	2	U	0.04	0.5	<0.01
Se	<0.3	0.63	0.7				

Since there was steel in the industrial batch, the char sample contains much more iron and a little more zinc. At the opposite, the oil sample shows only traces of inorganics. For the tire resin, the amount of iron is negligible, as it is almost 50 times lower than that of zinc. Therefore, it is supposed that tire resin does not contain iron.

The elemental analysis was performed on the recovered char samples for all TGA experiments. The results are presented in Table 4, which includes the average elemental composition for the waste tires obtained in this work. The oil sample was essentially free of inorganics, so it was assumed that all of the inorganics remained in the char fraction.

Table 5.2.4. Elemental composition of the waste tire and char obtained from TGA pyrolysis. [†Inorganics were obtained in char assuming none was transferred to the volatiles phase. *By difference.]

Temperature (°C)	**Heating rate (°C/min)**	**C (wt%)**	**H (wt%)***	**N (wt%)**	**S (wt%)**	**Inorganics† (wt%)**	**O* (wt%)**
Virgin tires	N/A	86.04	7.19	0.34	1.95	1.01	3.47
300	1	87.96	5.91	0.21	1.74	1.29	2.89
	10	87.20	5.83	0.22	1.75	1.35	3.65
	100	88.31	6.12	0.17	1.26	1.30	2.84
350	1	87.31	3.46	0.23	2.49	1.95	4.57
	10	87.11	4.37	0.18	2.28	1.83	4.24
	100	87.41	3.65	0.16	2.05	1.95	4.79

400	1	88.86	0.78	0.11	1.76	2.58	5.92
	10	88.03	1.09	0.12	2.12	2.75	5.89
	100	87.58	0.45	0.13	2.22	2.78	6.85
450	1	87.89	0.07	0.11	2.19	3.03	6.72
	10	88.42	0.27	0.15	2.31	2.98	5.88
	100	89.14	0.00	0.12	1.94	2.87	5.94
500	1	88.32	0.07	0.12	1.85	2.89	6.76
	10	89.96	0.00	0.17	1.76	2.79	5.33
	100	88.47	0.00	0.17	2.06	2.92	6.39

From Table 5.2.4, it is seen that the carbon, nitrogen and sulfur contents remained relatively constant in the char and at levels similar to the virgin waste tire samples. On the other hand, the hydrogen weight fraction decreased with increasing pyrolysis temperature and it reached a value below the detection limit at 500^{o}C. The inorganics mass fraction increased in the char with increasing pyrolysis temperature: it increased by a factor of 3 as the pyrolysis temperature was increased from 300^{o}C to 500^{o}C. This increase in inorganics mass fraction in the char resulted from the devolatilization of organic compounds, while it is assumed that all of the inorganics remained in the solids phase at these relatively low temperatures.

From the elemental composition of the virgin tires and char samples, the elemental composition of the global volatiles could be calculated from a mass balance and it is shown in Table 5.

Table 5.2.5. Calculated volatiles elemental composition [*Obtained by difference]

Temperature (°C)	**Heating rate (°C/min)**	**Weight loss (%)**	**C (wt%)**	**H (wt%)**	**N (wt%)**	**S (wt%)**	**O* (wt%)**
300	1	22	79.10	11.82	0.81	2.71	5.57
	10	25	82.52	11.31	0.68	2.54	2.95
	100	22	77.98	10.97	0.92	4.37	5.75

350	1	48	84.67	11.23	0.45	1.35	2.30
	10	45	84.71	10.69	0.53	1.53	2.54
	100	48	84.56	11.02	0.53	1.83	2.06
400	1	61	84.22	11.33	0.48	2.07	1.90
	10	63	84.88	10.75	0.46	1.84	2.07
	100	63	85.16	11.06	0.45	1.79	1.54
450	1	67	85.11	10.77	0.45	1.82	1.85
	10	66	84.82	10.76	0.43	1.76	2.24
	100	65	84.35	11.11	0.45	1.95	2.14
500	1	65	84.81	11.04	0.45	2.00	1.70
	10	64	83.81	11.29	0.43	2.05	2.42
	100	65	84.75	11.02	0.42	1.88	1.93

In opposition to char whose hydrogen mass fraction decreased significantly with increasing pyrolysis temperature, the carbon and hydrogen weight fractions in the volatiles remained constant. However, variations are observed for sulfur and a more in-depth data analysis is presented in section 5.2.4.2.

5.2.4.1.2 Sulfur distribution

Since pyrolysis char yields and chemical composition were measured, it is possible to characterize the migration of sulfur to the volatiles during the decomposition process. Table 6 shows the calculated sulfur distribution within the pyrolysis products.

Table 5.2.6. Total weight loss and sulfur weight loss during the TGA pyrolysis experiments.

Temperature (°C)	**Heating rate (°C/min)**	**Sulfur loss* (wt%)**	**Pyrolysis weight loss (wt%)**
300	1	30	21.6
	10	31.6	24.7
	100	49.3	22

350	1	34	48
	10	34.9	44.6
	100	45.6	48
400	1	64.6	60.7
	10	59.8	63.1
	100	58.5	63.5
450	1	62.4	66.5
	10	59.9	65.9
	100	65.5	64.7
500	1	66.7	64.9
	10	67	63.7
	100	62.9	65.2

*Sulfur loss calculated from initial sulfur content in Table 4

As previously explained, the sulfur weight loss selectivity is expected to be 1 (when decomposition kinetics is highly dominant). Figure 5.2.1 shows these selectivities for the raw data obtained with the TGA, referred to as “original TGA”.

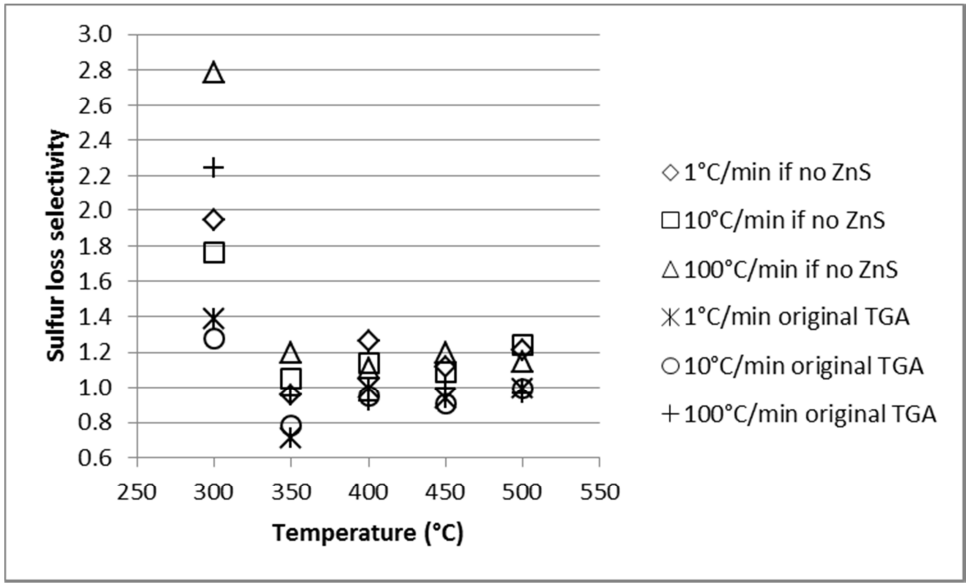

Figure 5.2.1. Sulfur loss selectivities obtained in this work.

On Figure 5.2.1, a selectivity of 1 means that sulfur is proportionally well distributed between the char and volatiles phases. When the value is higher than 1, more sulfur can be found in volatiles by proportion. On the other hand, a value below 1 means that sulfur is mostly found in char by proportion. At 400°C and up, the selectivities are closely below 1 while at 300°C and 350°C, the deviation from 1 is significant.

Two types of observations are also presented as they bring further clues towards the distribution of sulfur among the pyrolysis products: (1) apparent hardness of char samples and (2) swelling of char samples. These observations provide information regarding the volatiles mobility within tire particles during pyrolysis or in other words, mass transfer.

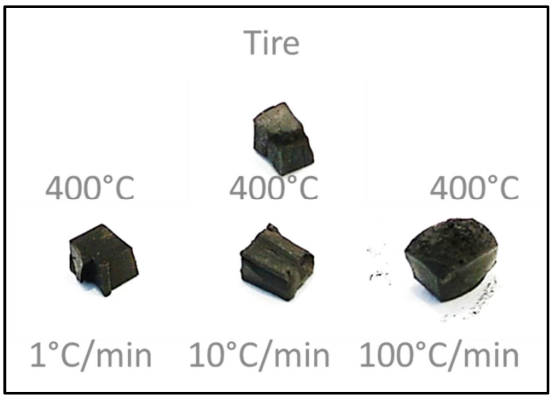

Figure 5.2.2. Waste tire samples before (tire) and after (char) pyrolysis at 400°C and three heating rates (1°C/min, 10°C/min and 100°C/min).

Figure 5.2.2 shows images of waste tire and char samples obtained via TGA pyrolysis with three different heating rates (1^{o}C/min, 10^{o}C/min and 100^{o}C/min) at 400^{o}C. It is observed that at a heating rate of 100°C/min, the sample had swollen to reveal a particular behaviour compared to the lower heating rates. The swelling behaviour was also observed at 300°C, 350°C, 450°C and 500°C, at the same heating rate of 100°C/min and at 450°C and 500°C, 10°C/min, which sometimes caused the sample to fall down the TGA pan during runs.

The second observation is related to the apparent hardness of the samples. While virgin waste tire samples showed good elasticity, char samples obtained after pyrolysis at a final temperature of 300°C were so hard that crushing them into powder for elemental analysis was a challenge. With increasing pyrolysis temperature, this hardness decreased significantly: at 450°C and 500°C, it was not possible to remove the pyrolyzed sample from the TGA pan without breaking it.

Table 5.2.7. Qualitative observations during and after the TGA pyrolysis experiments.

Temperature (°C)	Heating rate (°C/min)	Char hardness	Swelling
300	1	High	No
	10	High	No
	100	High	Yes
350	1	Moderate	No
	10	Moderate	No
	100	Moderate	Yes
400	1	Low	No
	10	Low	No
	100	Low	Yes
450	1	Very low	No
	10	Very low	Yes
	100	Very low	Yes
500	1	Very low	No
	10	Very low	Yes
	100	Very low	Yes

The observations summarized in Table 7 indicate that high heating rates produced a significant swelling of the char samples while high temperature decreased the hardness of the char sample.

Swelling of the sample is an indication of constraints to the volatiles mobility (limiting mass transfer) inside the sample. However, the fact that swelling occurred may also suggest that this constraint was overcome by the volatiles during the pyrolysis process: this likely occurred in samples characterized by low char hardness (high porosity) and would have resulted in high volatiles mobility.

Finally, one TGA experiment was stopped once the temperature reached about 280°C (10°C/min). The furnace was directly opened and the hot sample removed had a fluffy texture, similar to a marshmallow. When squeezed, the sample did not come back to its original shape as it had lost its elasticity. This strongly indicates that crosslink breakage is the initial step during pyrolysis of waste tires.

5.2.4.2 Sulfur behaviour

5.2.4.2.1 Effects of temperature on sulfur distribution

First of all, runs at 100°C/min must be discussed. With heating rates of 1°C/min and 10°C/min in TGA, the temperature control was observed to be fairly accurate. However, at a higher heating rate of 100°C/min, limitations in the temperature control system produced an overshoot in sample temperature. For different TGA final temperatures (300^{o}C, 350^{o}C, 400^{o}C, 450^{o}C and 500^{o}C) and heating rates (1°C/min and 100°C/min): the temperature set point is largely exceeded at 100^{o}C/min.

At 100°C/min, the temperature overshoot was between 20°C to 40°C, and was accompanied with significant weight loss, in particular for temperature set points of 350°C, 400°C and 450°C. This indicates that these samples were in fact exposed to a higher set-point temperature: decomposition kinetics was then fast enough to generate significant bias to the experimental conditions expected initially.

Referring to the sulfur loss selectivity, the global rate of sulfur loss is then not representative for the expected set point to define the intrinsic selectivity. In Figure 1, the fact that 100°C/min experiments at 400°C, 450°C and 500°C have the same selectivity values than at 1°C/min and 10°C/min is explained by the weight loss peak reached in TGA runs around 450°C. Even if there is an overshoot, the weight loss rate is less affected by temperature.

As another highlight, the sulfur loss selectivity can be considered as a reference parameter for sulfur distribution within pyrolysis products. At 400°C, 450°C and 500°C, without iron, with low amounts of Zn, with heat and mass transfer not limiting, the values strongly converged to 1, meaning that the sulfur weight loss percentage should be equal to the pyrolysis weight loss percentage when decomposition kinetics is dominant and there are no metals in the system.

Nevertheless, selectivity values at 300°C and 350°C were significantly different from the reference value of 1. That is, other factors than the reference temperature dependent intrinsic selectivity may impact of sulfur distribution. The following sections will focus on defining them.

5.2.4.2.2 Influence of heat and mass transfer on sulfur distribution

Data from the present work were compared with data from Diez et al. in Figure 3. One important difference between the two sets of experimental data is the particle size of the waste tire samples: the average particle size in the present work was approximately 10 times greater than that of Diez et al., where they used sieved powdered tires ($\leq$ 420 µm). Assuming that cubic waste tire particles were used for both investigations, the total particle surface area in the present work was about 20 times lower than that of Diez et al. No inert gas was forced through their samples in opposition to the present work where nitrogen was continuously flowed over the samples in TGA. They have some points in common: no iron, three temperature points and the possibility to compare the sulfur loss selectivities.

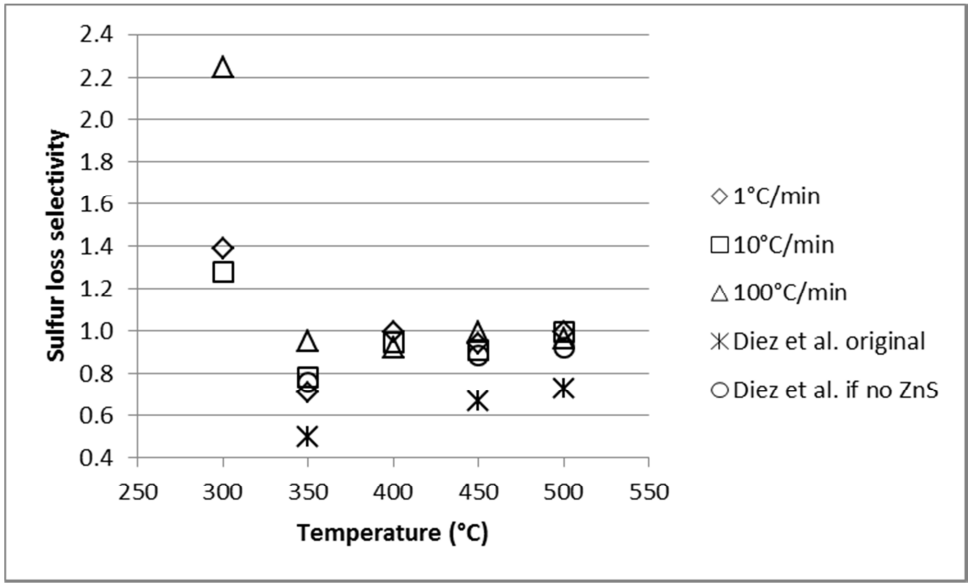

Figure 5.2.3. Sulfur loss selectivities for two series of data without steel (original from this work and from [19].

At first glance, the data of Diez et al. show significantly lower sulfur transfer to the volatiles phase (oil + gas). The same stoichiometric balance than performed for Figure 5.2.1 was done to account for zinc sulfidation, assuming a complete conversion into ZnS. By considering the potential effect of Zn sulfidation, most sulfur still remains in the char phase: this is in opposition with the observations from the present work.

ZnO is expected to have mostly converted into ZnS because of the particular experimental set up used by Diez et al. Since no nitrogen was swept through the samples, their experimental conditions must have resulted in increased H_2S partial pressure with longer contact time with Zn, according to equation (9).

The higher non-condensable gas fraction of the volatiles obtained by Diez et al. is considerably higher than what can be observed in most works [4,6,12,14,15,16,19,20]. However, they grinded tires and screened the waste tire samples such that the particle size used was 420 µm and smaller. Significant mechanical energy (grinding) was injected in this system to create new surfaces, but also a great number of new free end-chain molecular segments. This could explain the high

amount of almost sulfur-free non-condensable gas obtained by Diez et al. (less contact time for the reaction in equation (5)) as well as why most sulfur was retained in the char phase, or in other words, why more short hydrocarbons were released from the solids. Globally, decomposition kinetics and transport phenomena were affected by this very choice. The effect of total sample surface is even more important at 350°C, where, as reported in Section 5.2.4.1.3, solids porosity might have limited mass transfer and volatiles emission throughout particles.

While heat transfer was proven to influence the production of condensables and non-condensables during pyrolysis, results in Table 1 showed there is not much of a distinction in sulfur weight loss selectivities between 1°C/min and 10°C/min for all temperatures. It was previously explained that because of TGA controls settings, all runs at 100°C/min yielded a temperature overshoot.

Nevertheless, since it was not possible to compare sulfur distribution within condensables and non-condensables, further investigation is needed, in particular at very fast heating rates.

5.2.4.2.3 Influence of volatiles composition on sulfur distribution

As discussed in section 1.4, it is expected that the productions of hydrogen (H_2) and cycloalkenes (aromatics) as hydrogen donors would influence the transfer of sulfur from tires or char to volatiles, in particular as H_2S. This is aside the direct production of sulfur-bearing condensables.

For Diez et al., sulfur migration in condensables increased with temperature despite an intensification of hydrogen production. That is, selectivities calculated for condensables alone increased from 0.72 to 0.78 to 0.89, as the temperature was increased to 350°C, 450°C and 550°C respectively. There was also a net increase in H_2S production, from 3.3 wt% of sulfur at 350°C to 14.3 wt% at 450°C, meaning high desulfurization kinetics. This could be due to faster

desulfurization kinetics (equation (5)), since the rate of production of volatiles greatly increases from 350°C to 450°C and that temperature also increases.

In contrast, the condensable fraction obtained by Berrueco et al. contained less sulfur with increasing temperature. They produced selectivities of 0.73 for condensables at 400°C and 0.63 at 500°C, while sulfur percentage in solids (including steel) went from 66.7 wt% from the initial amount in tires to 70.4 wt%, even if char yield decreased of 12 wt% units. Hydrogen production was over 5 times lower at 400°C than at 500°C (respectively 2.6 % vol. and 14.2 % vol.), but also, sulfur in non-condensables (as hydrogen sulfide) diminished from 11.3 wt% to 4.4 wt%. As mentioned in section 5.2.4.2.2, it indicates that desulfurization of condensables was promoted; that was not the case for experiments led by Diez et al. It suggests that variations in the H_2 and H_2S partial pressures in the volatiles and the presence of steel are responsible for this behaviour.

Coming back on results observed at 300°C in Figure 1, it is believed that the excess of sulfur released in the volatiles is mostly produced in the form of H_2S in the non-consensable fraction. As stressed in the previous sections, the lower porosity of solids at 300°C promotes a longer residence time for gases. In these conditions, hydrogen partial pressure would react with sulfur molecularly bonded with the organic matrix to produce hydrogen sulfide.

The simplest form of the rate of desulfurization would be formed of a temperature dependent kinetics constant and a term for hydrogen partial pressure:

$$r_{DESULF} = k_{DESULF}(T)P_{H2} \quad (11)$$

Where P_{H2} is the hydrogen partial pressure. This kinetics would not be basically fast; it would be more that it is significant compared to the decomposition kinetics below 350°C. At higher temperatures, desulfurization kinetics will be negligible compared to decomposition kinetics.

5.2.4.2.4 Effects of inorganics on sulfur distribution

The waste tire samples used in the present study contained significant amounts of zinc as shown in Table 5.2.3, but no iron. Some data with tires containing iron in the form of steel could be found in literature to bring a basis for comparison.

5.2.4.2.4.1 Zinc oxide

It is first assumed that the Zn contained in the waste tire samples is stoichiometrically fully converted to ZnS during the pyrolysis experiments whose results are reported in Figure 5.2.1. Using this assumption, the fraction of sulfur captured as ZnS for the results of Figure 5.2.1 can be estimated from a mass balance: if it were not in char as ZnS, it would be in volatiles as H_2S according to equation (8). Consequently, the corresponding sulfur loss selectivities can be calculated and these values were reported in Figure 5.2.1, referred to as “if no ZnS”.

As observed in Figure 5.2.1, there is already a net tendency for sulfur to migrate to the volatiles phase at a final pyrolysis temperature of 300°C, such that the impact of zinc is not distinguishable. For samples at a final pyrolysis temperatures of 350°C, 400°C, 450°C and 500°C, the selectivity increases from values below 1 (proportionally more sulfur in char as ZnS) to values above 1 (proportionally more sulfur in volatiles as H_2S). This strongly suggests that partial or complete conversion of ZnO to ZnS occurs within tire samples at these pyrolysis temperatures.

A kinetics model would have been a helpful tool to characterize ZnO conversion into ZnS. Many models were found in literature, but all of them were developed for surface reactions. For the needs of this work, an intrinsic kinetics model would instead be required, since zinc is diffused in tire resin at the molecular scale. That is, a kinetics equation considering molecular ZnO, with an intrinsic kinetics constant and activation energy and a known order of reaction.

However, Efthimiadis and Sotirchos [25] showed that ZnO sulfidation at very low H_2S concentration (0.5 %) had fast kinetics at 400°C and higher. At 350°C, kinetics would be significantly fast, if interpolating between 300°C and 400°C. But since volatiles emission in TGA was observed for over 6 hours at 350°C, this is suspected to allow complete conversion of ZnO into ZnS. Results obtained by Efthimiadis and Sotirchos are presented in Figure 5.2.4.

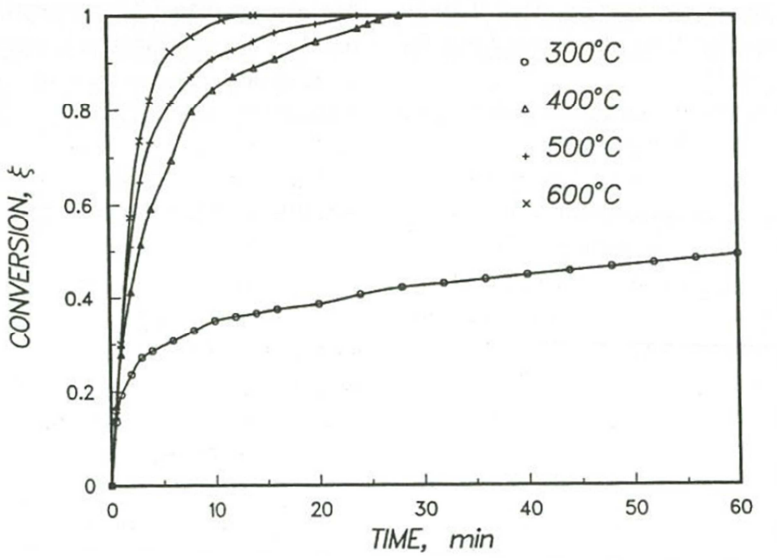

Figure 5.2.4. ZnO conversion into ZnS through time from [25]; H_2S concentration = 0.5 %.

The sulfur loss selectivity will be diminished by the effect of zinc sulfidation. At molecular scale, since zinc is homogeneously dispersed in tires, the simplest form of reaction rate would be:

$$r_{ZnS} = k_{ZnS}(T)P_{H2S} \quad (12)$$

Where $k_{ZnS}(T)$ is the intrinsic kinetics constant and P_{H2S} is the hydrogen sulfide partial pressure. As observed for all temperatures and heating rates over 350°C in Figure 5.2.1, the rate of zinc sulfidation might have been significant compared to the rate of decomposition of tires such that all sulfur loss selectivities measured were below the reference value of 1.

5.2.4.2.4.2 Steel structure (Iron)

As the experiments in this work used tire samples that did not contain iron significantly, data from Berrueco et al. were used. Their tire samples contained steel. Because Zn content was not given in Berrueco et al., both samples were assumed to contain the same mass fraction of Zn than of this work (0.47 %wt). The selectivities were calculated from their published data (one data point at 400°C and one data point at 500°C): the values are shown in Figure 5.2.5. The heating rate used by the authors was 15°C/min, which is close to the 10°C/min heating rate used in the present work. In Figure 5, the data of Berrueco et al. is compared to the original data of Figure 5.2.1.

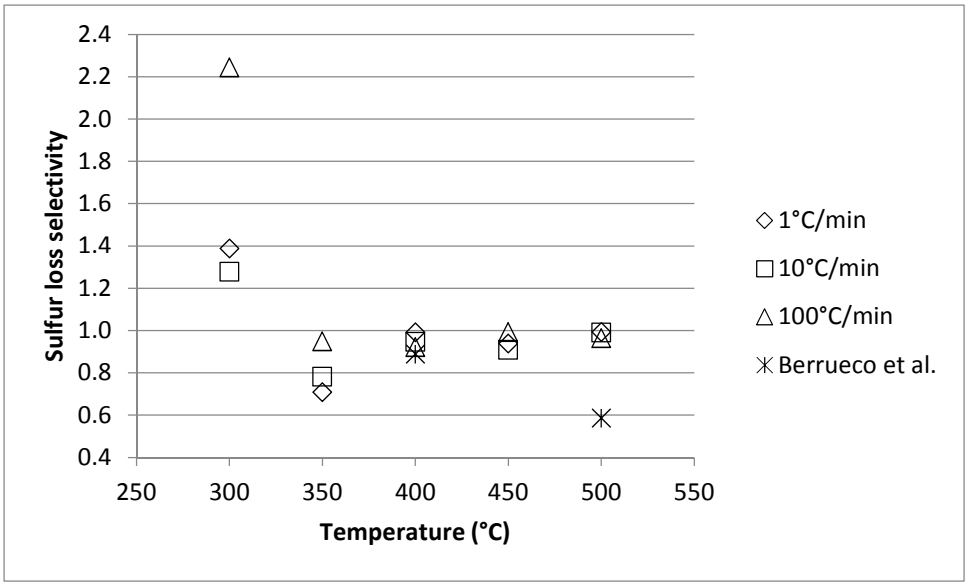

Figure 5.2.5. Sulfur loss selectivities: data from this work and data from [18].

At 400°C, even if there is a slight difference in the heating rate (15°C/min vs. 10°C/min) the ratios measured in the present study and reported by Berrueco et al. are very similar. This may suggest that the kinetics of iron sulfidation in the waste tire samples is somehow inhibited, but that zinc sulfidation may still happen. This may be due to two factors: temperature and limiting mass transfer. The rate of production of volatiles is relatively low, so H_2S partial pressure will also follow that trend. As well, solids porosity may not be very high as suggested in Section

5.2.4.1.3, which is suspected to have lowered the steel surface exposed to volatiles. It refers to equation (9).

There is a very low amount of sulfur present in the volatiles at 500°C for Berrueco et al. Assuming full ZnO conversion into ZnS, as done for original ratios in Figure 5.2.1, it would increase its selectivity, at 500°C, from **0.586** up to **0.836**. Because the value remains significantly lower than 1, it suggests that iron may have converted into iron sulfide (FeS), retaining more sulfur in the char phase than Zn could have done alone. As they performed static experiments, one can expect even more sulfur clustering in the char phase in continuously mixed systems. In mixed systems, steel filaments are partially grinded by attrition [12], which results in a significantly higher available surface for the sulfidation of iron. As a corollary, beds of powdered metals or metal oxides are nowadays used for desulfurization of biogas [26].

To validate the hypothesis of iron sulfidation, a kinetics model was developed for conditions used by Berrueco et al. Their experiments were considered as a batch iron sulfidation with variable H_2S partial pressure in a fixed bed. The pyrolysis volatiles volumetric flow was obtained by the authors during the whole batch time and it was assumed that gas composition was constant during the batch, with a known H_2S fraction. Nitrogen flow was also known and an average gas molecular weight was fixed (140 g/mol for volatiles). As the H_2S yields of Berrueco et al. are suspected to be biased by iron sulfidation, H_2S yields (wt %) were taken from Diez et al., for which it was obtained with Fe-free samples. The estimated H_2S partial pressure (atm) with time (minutes) is shown in Figure 5.2.6.

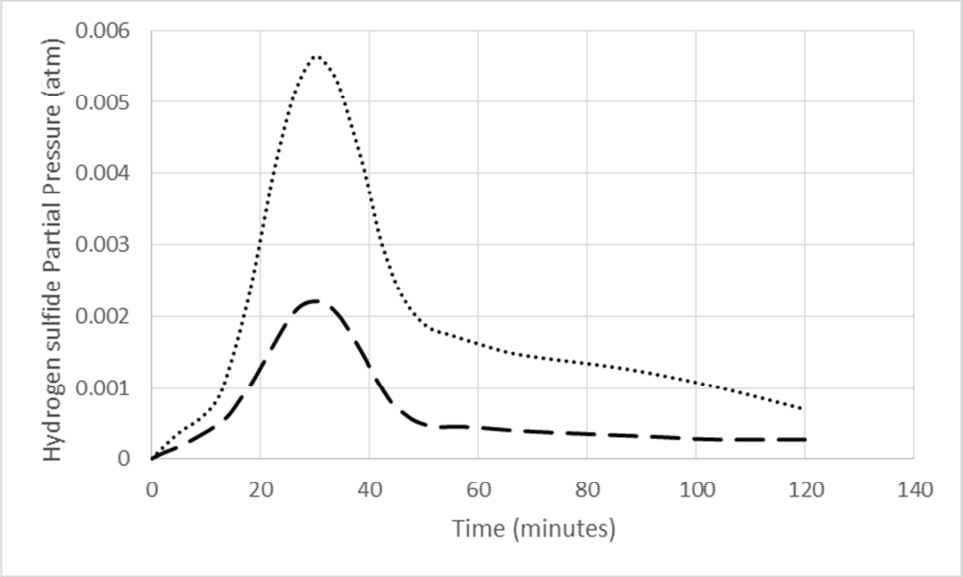

Figure 5.2.6. Hydrogen sulfide partial pressure (atm) as a function of time (minutes); Striped line: 400°C, Dotted line: 500°C. Estimated from data obtained [13] and [14].

The carbon steel fraction was assumed to be at 9.6 %wt (Laresgoiti et al., similar samples, no available value for Berrueco et al.) and the wire radius was estimated to be 250 µm. The carbon fraction in steel was neglected (~1 %wt). The iron sulfidation kinetics equation (rate of formation of 1st order) and kinetics constants were taken from Haugen and Sterten [27]:

$$\frac{d(FeS)}{dt} = k_f P_{H2S} - k_r P_{H2} \qquad (13)$$

At 400°C, the kinetics constant for the reverse reaction ($k_r P_{H2}$) is over 56,000 times slower than the forward reaction (sulfidation, $k_f P_{H2S}$) and at 500°C, it is 12,000 times slower. Hence, the reverse reaction was assumed to be negligible. Figure 5.2.7 shows the cumulative sulfidation (conversion) of Fe through time at both temperatures for a 300 g sample, as used by Berrueco et al.

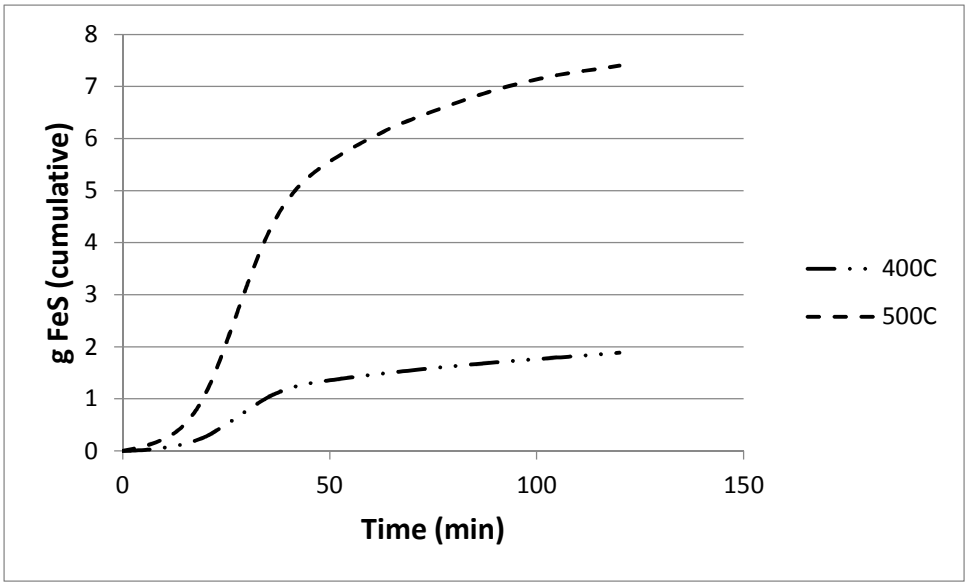

Figure 5.2.7. Simulated cumulative FeS production during pyrolysis at two temperatures, for 300 g of tire shreds.

Table 5.2.8 shows the overall sulfur distribution in light gases (as H_2S) for Berrueco et al. (original data and simulated H_2S production and zinc sulfidation) and Diez et al. Mass balance was recalculated as per simulation results.

Table 5.2.8. Sulfur distribution (% wt) with steel (Berrueco), without steel (Diez) and simulated sulfidation.

	With Fe (Berrueco)		Without Fe (Diez)		Simulation	
	400°C	**500°C**	**400°C**	**500°C**	**400°C**	**500°C**
char	67	70	64	55	70	65
oil	22	25	24	30	24	30
gas	11	5	12	15	7	5

The first observation is that iron sulfidation kinetics is fast enough to explain the very low sulfur loss selectivities obtained by Berrueco et al. Approximately 45 %wt of sulfur from the light gas fraction could have been retained as FeS at 400°C and it is 70 %wt retained at 500°C. At 400°C,

the simulated sulfidation is greater than expected. It is suspected less steel is swept by the gases due to a lower porosity of the system, which was not considered in the model.

The hydrogen sulfide consumption was well represented by the sulfidation model at 500°C. Nevertheless, there is still not enough sulfur retained in char in the simulation compared to Berrueco et al. (65 % wt in simulation vs. 70 % wt experimental). Sulfur in oil (condensables) was assumed to remain the same in the model, which might not be accurate. As shown in equation (10), iron sulfidation releases hydrogen. This hydrogen may have partially reacted with condensable volatiles to produce more H_2S, and then more FeS. Overall, it strongly indicates that iron sulfidation could influence sulfur distribution during pyrolysis.

Similarly to equation (13), the rate of iron sulfidation is written for sulfur loss selectivity, but in a compatible form with the unit system:

$$r_{FeS} = k_{FeS}(T)P_{H2S} \quad (14)$$

In the reaction rate equation, the apparent kinetics constant is $k_{FeS}(T)$ and the other term is the hydrogen sulfide partial pressure. At a temperature of 400°C and higher, the iron sulfidation rate of reaction is significant compared to the rate of decomposition of tires.

5.2.4.2.5 Developed form of the intrinsic sulfur loss selectivity

The temperature dependent intrinsic selectivity has been initially proposed to fix a reference value for the sulfur loss selectivity. In the limit case where no metals are present and that decomposition kinetics is dominant, the sulfur loss selectivity indeed converged to the value of 1 to confirm the hypothesis.

In the sections that followed, the other factors were characterized and two important phenomena were pointed out to make the sulfur loss selectivity diverge from 1, namely the solid matrix desulfurization and metals sulfidation. The former would contribute to increase the sulfur loss selectivity while it is the opposite for the latter.

Considering isothermal experiments, the hydrogen and hydrogen sulfide partial pressure are proportionally related to the rate of decomposition. Therefore, the global selectivity could be developed to obtain a form where the integrals can simplify and vanish. The resulting sulfur loss selectivity expression would then be an intrinsic selectivity. First, summarizing all the rates of reaction assumed accounting for the rate of sulfur loss, the selectivity becomes:

$$S_{SL/TWL} = \frac{\int_{t0}^{t} r_{SL} dt}{\int_{t0}^{t} r_{TWL} dt} = \frac{\int_{t0}^{t} (s_{SL/TWL}(T) r_{TWL} + r_{DESULF} - r_{ZnS} - r_{FeS}) dt}{\int_{t0}^{t} r_{TWL} dt} \quad (15)$$

The rate of volatiles loss has already been defined as the product of the sum of intrinsic selectivitiy for gas and oil and the rate of decomposition in equation (2). The other three rates of reaction in equation (15), r_{DESULF}, r_{ZnS} and r_{FeS}, must also be developed in order to simplify selectivity into an intrinsic form that would be only a function of temperature. First, the rate of desulfurization of the solid matrix was written in equation (11) as a function of hydrogen partial pressure. Assuming there is an intrinsic selectivity for the production of hydrogen during pyrolysis, the developed term becomes:

$$r_{DESULF} = k_{DESULF}(T) P_{H2} = k_{DESULF}(T) \frac{M_{H_2} RT}{m_{sulf_0} V_{cp(T)}} s_{H2} s_{gas} (-r_{pyrolysis}) \quad (16)$$

In equation (16), there is the molecular weight of hydrogen, the perfect gas constant and temperature, $M_{H2}RT$, the intrinsic selectivity for hydrogen (s_{H2}) within the pyrolysis non-condensable gas ($s_{gas}(-r_{pyrolysis})$). Both intrinsic selectivities are solely functions of

temperature. The rate depends also of the characteristic volume of the pores, since the reaction occurs on the internal surface of the particles. This parameter is assumed to be correlated with temperature. At low temperature, the total volume of the pores is very low and at the opposite, at high temperature, the volume is greater. The initial weight of sulfur in the system, m_{sulf_0}, rends the rate of reaction dimensionless, with the units percent sulfur loss within volatile per unit time.

The same development can be done for the rate of zinc sulfidation of equation (12). It then becomes:

$$r_{ZnS} = k_{ZnS}(T)P_{H2S} = k_{ZnS}(T)\frac{\alpha M_{H2S}RT}{m_{sulf_0}V_{cp(T)}}s_{H2S}s_{gas}(-r_{pyrolysis}) \quad (17)$$

All of the parameters in equation (17) are their equivalent in equation (16), but for hydrogen sulfide. The only addition is the constant α, which is the weight of sulfur per unit weight of zinc sulfide, to convert the units of the rate of zinc sulfidation in percent sulfur loss per unit time. For zinc sulfide, the total pore volume is also considered as a correlation with temperature.

Finally, the rate of iron sulfidation defined in equation (14) would have the same form as per equation (17):

$$r_{FeS} = k_{FeS}(T)P_{H2S} = k_{FeS}(T)\frac{\beta M_{H2S}RT}{m_{sulf_0}V}s_{H2S}s_{gas}(-r_{pyrolysis}) \quad (18)$$

The weight of sulfur per unit weight of iron sulfide is β. As iron or steel can react with hydrogen sulfide outside tire particles, the total free volume occupied by the pyrolysis gas is considered. As assumed in section 5.2.2, if an isothermal pyrolysis experiment is performed, the constant terms can be taken outside the integrals. The simplified global selectivity for sulfur is then obtained in its intrinsic form:

$$s_{SL/TWL} = s^{0}{}_{SL/TWL}(T) + k_{DESULF}(T)\frac{M_{H_2}RT}{(s_{gas}+s_{oil})m_{sulf_0}V_{cp}(T)}s_{H2}s_{gas} - k_{ZnS}(T)\frac{\alpha M_{H_2S}RT}{(s_{gas}+s_{oil})m_{sulf_0}V_{cp}(T)}s_{H2S}s_{gas} - k_{FeS}(T)\frac{\beta M_{H_2S}RT}{(s_{gas}+s_{oil})m_{sulf_0}V}s_{H2S}s_{gas} \quad (19)$$

What was first considered as the intrinsic sulfur loss selectivity, $s_{SL/TWL}$, is now considered as the reference intrinsic selectivity, $s^{0}{}_{SL/TWL}(T)$, with the influence of the other three reactions (desulfurization of the solid matrix and sulfidation of zinc and iron).

5.2.5 CONCLUSIONS

This investigation was initially justified by the lack of comprehensive studies on the behaviour of sulfur during the pyrolysis of tires, acknowledging that this issue is a major challenge to the profitability of industrial pyrolysis processes. To complement raw data found in literature, TGA experiments were performed with elemental analyses. In the absence of key parameters and reference values to study sulfur distribution within the pyrolysis products, a novel parameter was elaborated, namely the sulfur loss selectivity.

It emerged from the new TGA results that when decomposition kinetics is dominant, i.e. over 400°C, and without metals, this parameter should converge to the value of 1. The presence of iron and zinc, at a temperature over 350°C, and intrinsic mass transfer limitations, at a temperature below 350°C, the selectivity values would deviate from the reference value of 1. A developed form of the sulfur loss selectivity was expressed to account for these phenomena.

As industrial pyrolysis processes rarely produce results similar to small and medium scale set ups, key performance indicators must be created in order to characterize the productivity of those pyrolysis plants. The sulfur loss selectivity could be easily employed to diagnose abnormal operations or malfunctions. As well, it could be used to optimize the pyrolysis process and allow

clustering sulfur in the phase (gas, liquid or solid) which it would be the most efficiently and economically treated, if treatment is then required.

For example, tires could be torrefacted to first partly remove sulfur as H_2S, with limited global weight loss. Then, pyrolysis could be performed, producing volatiles containing potentially less sulfur. This would lighten the efforts in the post-processing of pyrolysis products. For other feedstock such as PVC, an expression for selectivity could be derived to optimize its pyrolysis and improve the understanding of the mechanisms of chlorine distribution within pyrolysis products.

5.2.6 Acknowledgements

The authors would like to extend their sincere thanks to the NSERC funding program that, in part, made this project successful.

5.2.7 References

[1] Justice Laws Website, *Sulphur in Diesel Fuel Regulations*, URL: http://laws-lois.justice.gc.ca/PDF/SOR-2002-254.pdf.

[2] United States Environmental Protection Agency Website, *Highway, Nonroad, Locomotive, and Marine Diesel Fuel Standards*, URL: http://www.epa.gov/otaq/standards/fuels/diesel-sulfur.htm.

[3] Aguado, R.; Olazar, M.; Velez, D.; Arabiourrutia, M.; Bilbao, J. Kinetics of scrap tyre pyrolysis under fast heating conditions. Journal of Analytical and Applied Pyrolysis 73(2) (2005) 290-298.

[4] Cunliffe, A.M.; Williams, P.T. Composition of oils derived from the batch pyrolysis of tyres. Journal of Analytical and Applied Pyrolysis 44(2) (1998) 131-152.

[5] Lopez, G.; Aguado, R.; Olazar, M.; Arabiourrutia, M.; Bilbao, J. Kinetics of scrap tyre pyrolysis under vacuum conditions. Waste Management 29 (2009) 2649-2655.

[6] Larsen, M.B.; Schultz, L.; Glarborg, P.; Skaarup-Jensen, L.; Dam-Johansen, K.; Frandsen, F.; Henriksen, U. Devolatilization characteristics of large particles of tyre rubber under combustion conditions. Fuel 85 (2006) 1335-1345.

[7] Williams, P.T.; Besler, S.; Taylor, D.T. Pyrolysis of scrap automotive tyres. The influence of temperature and heating rate on product composition. Fuel 69 (1990) 1474-1482.

[8] Martinez, J.D.; Veses, A.; Mastral, A.M.; Murillo, M.; Navarro, M.V.; Puy, N.; Artigues, A.; Bartroli, J.; Garcia, T. Co-pyrolysis of biomass with waste tyres: Upgrading of liquid bio-fuel. Fuel Processing Technology 119 (2014) 263-271.

[9] Mastral, A.M.; Callen, M.S.; Garcia, T.; Navarro, M.V. Improvement of liquids from coal-tire co-thermolysis. Characterization of the obtained oils. Fuel Processing Technology 64(1) (2000) 135-140.

[10] Ucar, S.; Karagoz, S.; Yanik, J.; Yuksel, M.; Saglam, M. Upgrading scrap tire derived oils using activated carbon supported metal catalysts. Energy Sources 29(4-8) (2007) 425-437.

[11] Murena, F. Kinetics of sulphur compounds in waste tyres pyrolysis. Journal of Analytical and Applied Pyrolysis 56 (2000) 195-205.

[12] Lanteigne, J.-R.; Laviolette, J.-P.; Tremblay, G.; Chaouki, J. Predictive kinetics model for an industrial waste tire pyrolysis process. Energy & Fuels 27 (2013) 1040-1049.

[13] Diez, C.; Martinez, O.; Calvo, L.F.; Cara, J.; Moran, A. Pyrolysis of tyres. Influence of the final temperature of the process on emissions and the calorific value of the products recovered. Waste Management 24 (2004) 463-469.

[14] Berrueco, C.; Esperanza, E.; Mastral, F.J.; Ceamanos, J.; Garcia-Bacaicoa, P. Pyrolysis of waste tyres in an atmospheric static-bed batch reactor: Analysis of the gases obtained. Journal of Analytical and Applied Pyrolysis 74 (2005) 257-269.

[15] Laresgoiti, M.F.; Caballero, B.M.; De Marco, I.; Torres, A.; Cabrero, M.A.; Chomon, M.J. Characterization of the liquid products obtained in tyre pyrolysis. Journal of Analytical and Applied Pyrolysis 7 (2004) 917-934.

[16] Barbooti, M.M.; Mohamed, T.J.; Hussain, A.A.; Abas, F.O. Optimization of pyrolysis conditions of scrap tires under inert gas atmosphere. Journal of Analytical and Applied Pyrolysis 72 (2004) 65-70.

[17] Luo, Y.-R. Handbook of bond dissociation energies in organic compounds (2003) 381 p.

[18] Moldoveanu, S. Analytical Pyrolysis of Organic Synthetic Polymers (2005) 714 p.

[19] Islam, M.R.; Haniu, H.; Fardoushi, J. Pyrolysis kinetics behavior of solid tire wastes available in Bangladesh. Waste Management 29 (2009) 668-677.

[20] Kyari, M.; Cunliffe, A.; Williams, P.T. Characterization of oils, gases, and char in relation to the pyrolysis of different brands of scrap automotive tires. Energy & Fuels 19 (2005) 1165-1173.

[21] Darmstadt, H.; Roy, C.; Kaliaguine, S. Inorganic components and sulfur compounds in carbon blacks from vacuum pyrolysis of used tires. Kautschuk Gummi Kunststoffe 47 (1994) 891-895.

[22] Westmoreland, P.R.; Gibson, J.B.; Harrison, D.P. Comparative kinetics of high temperature reaction between H2S and selected metal oxides. Environment Science & Technology 11(5) (1977) 488-491.

[23] Dravnieks, A.; Samans, C.H. Kinetics of reaction of steel with hydrogen sulfide-hydrogen mixtures. New Cathode Depolarizer Materials 105(4) (1958) 183-191.

[24] Lauretta, D.S.; Kremser, D.T.; Fegley, B. The rate of iron sulfide formation in the solar nebula. Icarus 122 (1996) 288-315.

[25] Efthimiadis, E.A.; Sotirchos, S.V. Reactivity evolution during sulfidation of porous zinc oxide. Chemical Engineering Science 48(5) (1993) 829-843.

[26] Abatzoglou, N.; Boivin, S. A review of biogas purification processes. Biofuels, Bioproducts & Biorefining 3 (2009) 42-71.

[27] Haugen, S.; Sterten, A. High-temperature linear kinetics of FeS formation and reduction in COS-CO-CO2 gas mixtures. Oxidation of Metals 3 (1971) 545-555.

CHAPITRE 6 DISCUSSION GÉNÉRALE

Dans un premier temps, la cinétique de pyrolyse des pneus a été modélisée et validée à l'aide de données provenant d'un réacteur de taille industrielle. Après vérification, les modèles tirés de la littérature ne permettaient pas de prédire avec précision la production du gaz non-condensable, de l'huile et du char. Soit les paramètres cinétiques étaient inadéquats, soit le modèle lui-même n'était pas en mesure de distinguer huile et gaz non-condensable.

Dans cette optique, une nouvelle approche a été privilégiée : une cinétique de décomposition unique combinée à des sélectivités intrinsèques pour le gaz, l'huile et le char. Les sélectivités sont définies uniquement comme des fonctions de la température. Cette hypothèse a été émise sachant que les conditions étudiées dans cet article favorisaient grandement le transfert de matière et une cinétique limitante.

Les simulations menées pour valider le modèle et tester ceux de la littérature étaient des batches industrielles. La production d'huile pyrolytique était mesurée en continu via le niveau dans le réservoir collecteur installé après les condenseurs.

La simulation était démarrée à température ambiante et le chauffage était réalisé jusqu'à ce que la production de volatiles soit complétée. Les modèles de la littérature ont soit produit l'huile beaucoup trop rapidement, soit ils n'ont produit que des traces de volatiles, démontrant que les énergies d'activation sont très sensibles à production d'huile. De même, pour les modèles prédisant indépendamment les cinétiques de production pour chacun des produits, un nombre élevé de paramètres à définir en ont significativement réduit la robustesse.

Une analyse de sensibilité complète aurait pu être menée, mais l'ampleur de cette analyse aurait difficilement permis de publier le modèle en un seul article. Quoi qu'il en soit, en confrontant les modèles à des batches où à la fois le taux de production d'huile et les profils de chauffage des

pneus variaient, leur robustesse a pu être étudiée. Il s'agissait de conditions d'extrapolation. Trois critères de robustesse ont été analysés, soit le moment de début de la production d'huile, le suivi de la production dynamique (temps de résidence) et enfin, le rendement cumulatif en huile obtenu après entière conversion des pneus. Seul le modèle développé dans la présente étude a su tenir compte de ces conditions et respecter les trois critères d'analyse de la robustesse. Le modèle pourra continuer d'être mis à l'épreuve en multipliant les tests en usine dans des conditions variées. Les paramètres variés sont toujours les mêmes : profil de température de batch, quantité de pneus et temps de résidence. Malgré tout, plusieurs changements individuels sur les paramètres de la cinétique et les sélectivités ont montré une sensibilité élevée et ont rendu le modèle imprécis, ce qui augmente le niveau de confiance pour les valeurs des paramètres identifiées.

Il s'agit d'une avancée importante pour la modélisation de la pyrolyse. Pour n'importe quelle matière à base de carbone, leur pyrolyse pourrait être modélisée à partir d'une cinétique de décomposition unique. En fonction des besoins, des sélectivités intrinsèques pourraient être définies pour les produits pyrolytiques sélectionnés. Par exemple, plutôt que de déterminer globalement une sélectivité pour l'huile, une sélectivité pourrait être déterminée spécifiquement pour le limonène, une des composés générés significativement lors de la pyrolyse des pneus, moyennant l'acquisition de données expérimentales suffisantes.

Le modèle a déjà pu démontrer son utilité. Dans un premier temps, il a servi à optimiser l'opération du procédé de pyrolyse et minimiser les durées de batch tout en maximisant la production d'huile. Sa principale contrainte était liée à la capacité de condensation. Dans un deuxième temps, le modèle a été implémenté dans le système de contrôle du réacteur, de sorte à automatiser la production et minimiser l'intervention de l'opérateur pendant l'opération.

Dans le deuxième objectif, l'enthalpie de pyrolyse était un autre point de contradiction retrouvé dans la littérature. Une majorité d'auteurs définissent l'enthalpie de pyrolyse comme étant

exothermique de par les résultats observés en DSC. Cela va à l'encontre de la définition même de la pyrolyse au point de vue théorique.

La capacité calorifique des solides lors de la pyrolyse a été étudiée. Le résultats montrent qu'elle diminue et atteint un minimum en cours de pyrolyse avant de remonter vers l'atteinte de l'équilibre thermodynamique.

Ces observations suggèrent fortement un biais dans les expériences en DSC. Le système de contrôle de l'appareil, lors du déclenchement de la pyrolyse, fournit à l'échantillon en continu un surplus de chaleur, qui cumulé en vient à faire grimper sa température à un taux supérieur à 10°C/min. En conséquence, le flux de chaleur mesuré devient artificiellement exothermique. Avec la remontée de la valeur de la capacité calorifique et l'intensification de la consommation d'énergie proportionnelle à la perte de masse de l'échantillon, le pic endothermique devient dominant.

Des données DSC, donc, seules les nouvelles données sur l'évolution de la capacité calorifique ont été conservées, car obtenues dans des conditions sans perte de masse significative. Elles ont été implémentées dans le bilan d'énergie élaboré dans cette étude avec des données provenant d'une batch industrielle.

Les mesures de température en continu dans cette batch ont confirmé l'absence de comportement exothermique lors de la pyrolyse des pneus, c'est-à-dire qu'il n'y a pas d'emportement de température malgré un chauffage continu et constant des pneus. Cette impression viendrait plutôt du fait que lors de la perte de masse intensive, le système devient plus facile à chauffer avec simultanément, une diminution de la capacité calorifique.

Les trois enthalpies identifiées ont pu être reliées, par ordre croissant de température où elles dominent, au bris intensif des liens soufrés présents dans la résine vulcanisée, à la perte de masse, ou de façon équivalente, à la production volatiles et enfin, à la stabilisation thermochimique du char en fin de pyrolyse. Une étude approfondie pourrait être menée, dans des conditions de torréfaction (basse température), pour identifier avec plus de certitude les réactions consommant de l'énergie en début de pyrolyse. De même, la robustesse du bilan d'énergie pourra être grandement augmentée en le confrontant à des données d'usine obtenues pour des batches opérées en conditions variables.

L'utilisation directe du bilan d'énergie permettra une prédiction plus juste de la température pendant la pyrolyse intensive, c'est-à-dire pendant la phase de perte de masse. Cette température est primordiale pour modéliser la cinétique de pyrolyse à l'aide du modèle développé lors du premier objectif spécifique. Les deux modèles (cinétique et bilan d'énergie) pourront être utilisés de façon combinée en un simulateur intégré.

Il s'agit donc d'une toute nouvelle méthodologie pour déterminer l'évolution de la capacité calorifique et des enthalpies en pyrolyse. L'utilisation de la DSC augmente la précision pour la détermination de la capacité calorifique alors que les données industrielles assurent une meilleure caractérisation des termes enthalpiques dominants vu l'incapacité actuelle de la DSC à le faire. Cette méthodologie pourrait être généralisée à n'importe quelle matière en pyrolyse et même à n'importe quel système où un solide se décompose pour générer des produits volatiles et laissant un résidu aux propriétés changeantes. Il s'agit d'une innovation qui permettra d'améliorer le design des réacteurs, en particulier du système de chauffage et de refroidissement qui est au cœur de ces procédés.

Le troisième objectif de ce projet doctoral était la compréhension du devenir des impuretés en pyrolyse. La littérature permet d'obtenir une certaine quantité de données brutes, mais il y a quasi-absence d'études sur les mécanismes de transfert de ces impuretés vers les produits

pyrolytiques. Pourtant, la rentabilité commerciale des procédés de pyrolyse est très fortement influencée par leur gestion des impuretés.

Afin de fournir des indicateurs permettant de caractériser et prédire le comportement des impuretés, un nouveau paramètre a été introduit, soit la sélectivité de la perte du soufre. Cette sélectivité intrinsèque aide à prédire la séquestration du soufre dans les volatiles et dans le char lors de la pyrolyse des pneus.

Afin d'assurer une fiabilité des résultats et des analyses, toutes les expériences ont été menées en triplicata et les analyses, en duplicata. Le peu de variabilité dans les valeurs obtenues confère un niveau de confiance élevé aux conclusions de cet objectif.

Le grand avantage de cette sélectivité est que l'influence du transfert de matière et des métaux sur le comportement du soufre ont été ramenés sous une forme entièrement dépendante de la température. De cette façon, il est maintenant de déterminer la distribution du soufre dans les produits pyrolytique en fonction des conditions d'opération d'un procédé industriel. Cette innovation ouvre la porte vers de nouveaux designs de procédés de pyrolyse plus adaptés aux impuretés des résidus afin de réduire les efforts de post-traitement des produits. Entre autres, cet outil pourrait être adapté au devenir du chlore lors de la pyrolyse du PVC, puisqu'il est chimiquement lié au polymère.

Sachant, par exemple, que les pneus libèrent beaucoup de soufre, mais peu de volatiles à basse température (< 300°C), il serait envisageable de torréfier les pneus afin de les pré-traiter avant la pyrolyse à haute température. Cette pyrolyse générerait alors des volatiles avec une teneur moindre en soufre et nécessitant un post-traitement moins intensif et moins coûteux.

CONCLUSION

Cette thèse a étudié trois aspects de la pyrolyse étant d'une importance majeure pour les procédés d'échelle industrielle.

Comme premier objectif, un nouveau modèle cinétique a été développé. Il est composé d'une cinétique de décomposition unique, à laquelle sont combinées les sélectivités intrinsèques pour chacun des trois produits pyrolytiques. En réduisant le nombre de paramètre cinétiques, la robustesse a été augmentée. Tout comme d'autres modèles cinétiques tirés de la littérature, ce modèle a été confronté à des données industrielles. Seul le présent modèle a pu prédire dynamiquement la production d'huile avec précision.

Dans le second objectif, la chaleur spécifique et l'enthalpie de pyrolyse ont été déterminées dans le cas des pneus. Au cours de cette étude, il a été démontré que la pyrolyse ne montrait pas de signes de comportement exothermique, mais qu'il s'agissait plutôt d'une illusion causée par la diminution simultanée de la chaleur spécifique de la masse pyrolysée. La modélisation du bilan d'énergie à l'aide de données industrielles a permis d'identifier trois enthalpies de pyrolyse : une pour le bris des liens soufrés de la vulcanisation, une étant dépendante de la perte de masse au cours de la pyrolyse et une enthalpie pour la stabilisation thermochimique du char en fin de pyrolyse.

Finalement, le troisième objectif de recherche s'est concentré sur l'étude de comportement du soufre lors de la pyrolyse des pneus. En l'absence de recherche étoffée sur les mécanismes dictant la distribution du soufre dans les produits de la pyrolyse, une nouvel indicateur a été développé pour prédire et caractériser la migration du soufre, nommément la sélectivité de la perte du soufre vers les volatiles. Cette sélectivité intrinsèque uniquement dépendante de la température, tient compte du transfert de matière et de l'influence du zinc et du fer sur la distribution du soufre. Dans le cas où la cinétique de pyrolyse est limitante et en l'absence de métaux, à température constante, la sélectivité devrait prendre la valeur de 1, c'est-à-dire que

proportionnellement en pourcentage massique, la perte de soufre est égale à la perte totale de masse (émission de volatiles).

BIBLIOGRAPHIE

Abatzoglou, N.; Boivin, S. (2009). A review of biogas purification processes. Biofuels, Bioproducts & Biorefining, 3, 42-71.

Aguado, R.; Olazar, M.; Velez, D.; Arabiourrutia, M.; Bilbao, J. (2005). Kinetics of scrap tyre pyrolysis under fast heating conditions. Journal of Analytical and Applied Pyrolysis, 73(2), 290-298.

Alizadeh, E.; Dubé, O.; Bertrand, F.; Chaouki, J. (2013). AIChE Journal, published online (DOI 10.1002/aic.13982).

Aylon, E.; Callen, M.S.; Lopez, J.M.; Mastral, A.M.; Murillo, R.; Navarro, M.V.; Stelmach, S. (2005). Journal of Analytical and Applied Pyrolysis, 74, 259-264.

Azargohar R, Dalai A (2006) Biochar as a precursor to activated carbon. Applied Biochemistry and Biotechnology, 131(1-3), pp. 762-773.

Babu B (2008, Sept/Oct) Biomass Pyrolysis: a state-of-the-art review. Biofuels, Bioproducts and Biorefining, 2(5), pp. 393-414.

Barbooti, M.M.; Mohamed, T.J.; Hussain, A.A.; Abas, F.O. (2004). Optimization of pyrolysis conditions of scrap tires under inert gas atmosphere. Journal of Analytical and Applied Pyrolysis, 72, 65-70.

Basu P (2010) Biomass Gasification and Pyrolysis: practical design and theory. Elsevier.

Beall, F.C. (1971). Differential calometric analysis of wood and wood components. Wood Science and Technology, 5, 159-175.

Berrueco, C.; Esperanza, E.; Mastral, F.J.; Ceamanos, J.; Garcia-Bacaicoa, P. (2005). Pyrolysis of waste tyres in an atmospheric static-bed batch reactor: Analysis of the gases obtained. Journal of Analytical and Applied Pyrolysis, 74, 257-269.

Bhattacharya P, Parthiban V, Kunzru D (1986, April) Pyrolysis of black liquor solids. Industrial Engineering & Chemistry, Process Design & Development, 25(2), pp. 420-426.

Boateng A, Daugaard D, Goldberg N, Hicks K (2007) Bench-scale fluidized-bed pyrolysis of switchgrass for bio-oil production. Industrial Engineering and Chemistry Research, 46, pp. 1891-1897.

Box, G. E. P.; Draper, N. R. (1987). Empirical Model Building and Response Surfaces, John Wiley & Sons, New York

Brazier, D.W.; Schwartz, N.V. (1978). Effect of heatimg rate on the thermal degradation of polybutadiene. Journal of Applied Polymer Science, 22, 113.

Brebu P, Ucar S, Vasile C, Yanik J (2010) Co-pyrolysis of pine cone with synthetic polymers. Fuel, 89(8), pp. 1911-1918.

Bridgwater A (2012, March) Review of fast pyrolysis of biomass and product upgrading. Biomass & bioenergy, 38, pp. 68-94.

Brown R, Stevens C (2011) Thermochemical processing of biomass: conversion into fuels chemicals and power. Wiley.

Chang YM (1996) On pyrolysis of waste tire: degradation rate and product yields. Resources, Conservation and Recycling, 17, pp. 125-139.

Chen G, Sjostrom K, Bjornbom E (1992) Pyrolysis/gasification of wood in a pressurized fluidized bed reactor. Industrial & Engineering Chemistry Research, 31(12), pp. 2764-2768.

Chen, J.H.; Chen, K.S.; Tong, L.Y. (2009). Journal of Hazardous Materials, B84, 43-55.

Cheung, K.Y.; Lee, K.L.; Lam, K.L.; Lee, C.W.; Hui, C.W. (2011). Fuel Processing Technology, 92, 856-863.

Cho MH, Jung SH, Kim JS (2010) Pyrolysis of mixed plastic wastes for the recovery of benzene, toluene, and xylene (BTX) aromatics in a fluidized bed and chlorine removal by applying various additives. Energy & Fuels, 24, pp. 1389-1395.

Clausthal University of Technology, Institute of Energy Process Engineering and Fuel Technology, Prof. Dr.-ing. Roman Weber, http://www.ievb.tu-clausthal.de.

Crocker M (2010) Thermochemical Conversion of Biomass to Liquid Fuels and Chemicals. Royal Society of Chemistry.

Cunliffe, A.M.; Williams, P.T. (1998). Composition of oils derived from the batch pyrolysis of tyres. Journal of Analytical and Applied Pyrolysis, 44(2), 131-152.

Danley, R.L. (2003). New heat flux DSC measurement technique. Thermochimica Acta, 395, 201-208.

Darmstadt, H.; Roy, C.; Kaliaguine, S. (1994). Inorganic components and sulfur compounds in carbon blacks from vacuum pyrolysis of used tires. Kautschuk Gummi Kunststoffe, 47,891-895.

Demirbas A (2009) Biorefineries: for Biomass Upgrading Facilities. London: Springer-Verlag.

Demirbas A (2004, June) Effect of initial moisture content on the yields of oily products from pyrolysis of biomass. Journal of Analytical and Applied Pyrolysis, 71(2), pp. 803-815.

Dravnieks, A.; Samans, C.H. (1958). Kinetics of reaction of steel with hydrogen sulfide-hydrogen mixtures. New Cathode Depolarizer Materials, 105(4), 183-191.

Diez, C.; Martinez, O.; Calvo, L.F.; Cara, J.; Moran, A. (2004). Pyrolysis of tyres. Influence of the final temperature of the process on emissions and the calorific value of the products recovered. Waste Management, 24, 463-469.

Dynamotive Energy. (2012). Corporate History. Consulted on March 1st, 2012, on Dynamotive, the evolution of energy: http://www.dynamotive.com/about/corporate-history/

Edwards W (1991) In D KLASS, Energy from biomass and wastes XV Chicago: Institute of gas technology, 503.

Efthimiadis, E.A.; Sotirchos, S.V. (1993).Reactivity evolution during sulfidation of porous zinc oxide. Chemical Engineering Science, 48(5), 829-843.

Fantozzi F, Colantoni S, Bartocci P, Desideri U (2007) Rotary kiln slow pyrolysis for syngas and char production from biomass and waste - Part II: Introducing product yields in the energy balance. Journal of Engineering for gas turbines and power, 129, 908-913.

Fiksel, J.; Bakshi, B.R.; Baral, A.;Guerra, E.;DeQuervain, B. (2011). Clean Technology Environment Policy, 13, 19-35.

Gasparovic L, Korenova Z, Jelemsky L (2010) Kinetic study of wood chips decomposition by TGA. Chemical Papers, 64(2), 174-181.

Gavrilescu D (2008, Sept/Oct) Energy from biomass in pulp and paper mills. Environmental Engineering and Management Journal, 7(5), 537-546.

Geldart D (1973, May) Types of gas fluidization. Powder Technology, 7(5), 285-292.

Bi H, Grace J, Zhu J (1995). Regime transitions affecting gas-solids suspensions and fluidized beds. Chemical Engineering Research and Design, 73(2), 154-161.

Harkin J, Rowe J (1971). Bark and its possible uses. U.S. Department of Agriculture, Forest Service, Madison, Wisconsin.

Haugen, S.; Sterten, A. (1971). High-temperature linear kinetics of FeS formation and reduction in COS-CO-CO2 gas mixtures. Oxidation of Metals, 3, 545-555.

He R, Ye X, English B, Satrio J (2009) Influence of pyrolysis condition on switchgrass bio-oil yield and physicochemical properties. Bioresource Technology, 100, 5305-5311.

Huber G, Iborra S, Corma A (2006) Synthesis of transportation fuels from biomass: chemistry, catalysts and engineering. Chemistry Review, 106, 4044-4098.

Imam T, Capareda S (2012) Characterization of bio-oil, syn-gas and bio-char from switchgrass pyrolysis at various temperatures. Journal of Analytical and Applied Pyrolysis, 93, 170-177.

Ingram L, Mohan D, Bricka M, Steele P, Strobel D, Crocker D, Mitchell B, Mohammad J, Cantrell K, Pittman Jr CU (2008) Pyrolysis of wood and bark in an auger reactor: Physical properties and chemical analysis of the produced bio-oils. Energy & Fuels, 22, 614-625.

Islam, M.R.; Haniu, H.; Fardoushi, J. (2009). Pyrolysis kinetics behavior of solid tire wastes available in Bangladesh. Waste Management, 29, 668-677.

Jiang G, Nowakowski DJ, Brigwater AV (2010) A systematic study of the kinetics of lignin pyrolysis. Thermochimica Acta, 498, 61-66.

Joung HT, Seo YC, Kim KH, Seo YC (2006) Effects of oxygen, catalyst and PVC on the formation of PCDDs, PCDFs and dioxin-like PCBs in pyrolysis products of automobile residues. Chemosphere, 65, 1481-1489.

Justice Laws Website, Sulphur in Diesel Fuel Regulations, URL: http://laws-lois.justice.gc.ca/PDF/SOR-2002-254.pdf.

Kamm B, Gruber P, Kamm M (2010). Biorefineries - Industrial Processes and Products. John Wiley & Sons.

Kanury A (1994). Combustion characteristics of biomass fuels. Combustion Science and Technology, 97(4-6), 469-491.

Khan M (1987). Production of high quality liquid fuels from coal by mild pyrolysis of coal/lime mixtures. Energy & Fuels, 5(2), 185-231.

Klason, P. Versuch einer Theorie der Trockendestillation von Hols. (1914). Journal fur Praktische Chemie, 90, 413.

Klass D (1998). Biomass for renewable energy, fuels, and chemicals. Academic Press.

Kunii D, Levenspiel O (1991). Fluidization Engineering (éd. 2nd). Butterworth-Heinemann.

Tillman D (1981). Wood combustion: principles, processes and economics. Academic Press.

Kothari A (1967). Master Thesis. Chicago, Illinois: Illinois Institute of Technology.

Koufopanos, C.A.; Papayannakos, N.; Maschio, G.; Lucchesi, A. (1991). Modelling of the pyrolysis of biomass particles. Studies on kinetics, thermal and heat transfer effects. Canadian Journal of Chemical Engineering, 69, 907-915.

Kyari, M.; Cunliffe, A.; Williams, P.T. (2005). Characterization of oils, gases, and char in relation to the pyrolysis of different brands of scrap automotive tires. Energy & Fuels, 19, 1165-1173.

Langholtz M, Carter D, Rockwood D, Alavalapati J (2007). The economic feasibility of reclaiming phosphate mined land with short rotation woody crops in Florida. Journal of Forest Economics, 12, pp. 237-249.

Lanteigne, J.-R.; Laviolette, J.-P.; Tremblay, G.; Chaouki, J. (2013). Predictive kinetics model for an industrial waste tire pyrolysis process. Energy & Fuels, 27, 1040-1049.

Laresgoiti, M.F.; Caballero, B.M.; De Marco, I.; Torres, A.; Cabrero, M.A.; Chomon, M.J. (2004). Characterization of the liquid products obtained in tyre pyrolysis. Journal of Analytical and Applied Pyrolysis, 7, 917-934.

Larsen, M.B.; Schultz, L.; Glarborg, P.; Skaarup-Jensen, L.; Dam-Johansen, K.; Frandsen, F.; Henriksen, U. (2006). Devolatilization characteristics of large particles of tyre rubber under combustion conditions. Fuel, 85, 1335-1345.

Lauretta, D.S.; Kremser, D.T.; Fegley, B. (1996). The rate of iron sulfide formation in the solar nebula. Icarus, 122, 288-315.

Leung, D.Y.C.; Wang, C.L. (1999). Energy & Fuels, 13, 421-427.

Li A, Li X, Li S, Ren Y, Shang N, Chi Y (1999). Experimental studies on municipal solid waste pyrolysis in a laboratory scale rotary-kiln. Energy, 24, 209-218.

Li, S.Q.; Ma, L.B.; Wan, W.; Yao, Q. (2005). Chemical Engineering Technology, 28(12), 1480-1489.

Lima I, Boateng A, Klasson K (2010). Physicochemical and adsorptive properties of fast pyrolysis bio-chars and their steam activated counterparts. Journal of Chemical Technology & Biotechnology, 85, 1515-1521.

Lin L, Khang S, Keener T (1997). Coal desulfurization by mild pyrolysis in a dual-auger coal feeder. Fuel Processing Technology, 53, 15-29.

Lopez, F.A.; Centeno, T.A.; Alguacil, F.A.; Lobato, B.; Urien, A. (2013). The GRAUTHERMIC-Tyres process for the recycling of granulated scrap tyres. Journal of Analytical and Applied Pyrolysis, 103, 207-215.

Lopez, G.; Aguado, R.; Olazar, M.; Arabiourrutia, M.; Bilbao, J. (2009). Kinetics of scrap tyre pyrolysis under vacuum conditions. Waste Management, 29, 2649-2655.

Luo, Y.-R. (2003). Handbook of bond dissociation energies in organic compounds, 381 p.

Mani T, Murugan P, Abedi J, Mahinpey N (2010). Pyrolysis of wheat straw in a thermogravimetric analyzer: Effect of particle size and heating rate on devolatilization and estimation of global kinetics. Chemical Engineering Research and Design, 88, 952-958.

Mansaray K, Ghaly A (1999). Kinetics of the thermal degradation rice husks in nitrogen atmosphere. Energy Sources, 21, 773-784.

Martinez, J.D.; Veses, A.; Mastral, A.M.; Murillo, M.; Navarro, M.V.; Puy, N.; Artigues, A.; Bartroli, J.; Garcia, T. (2014). Co-pyrolysis of biomass with waste tyres: Upgrading of liquid bio-fuel. Fuel Processing Technology, 119, 263-271.

Mastral, A.M.; Callen, M.S.; Garcia, T.; Navarro, M.V. (2000). Improvement of liquids from coal-tire co-thermolysis. Characterization of the obtained oils. Fuel Processing Technology, 64(1), 135-140.

Mellmann J (2001) The transverse motion of solids in rotating cylinders - forms of motion and transition behaviour. Powder Technology, 118, 251-270.

Mohan D, Pittman Jr C, Steele P (2006). Pyrolysis of wood/biomass for bio-oil: a critical review. Energy & Fuels, 20, 848-889.

Moldoveanu, S. Analytical Pyrolysis of Organic Synthetic Polymers (2005). 714 p.

Mujumdar A (2007) Handbook of industrial drying. CRC Press.

Mullen C, Boateng A, Mihalcik D, Goldberg N (2011). Catalytic fast pyrolysis of white oak wood in a bubbling fluidized bed. Energy & Fuels, 25, 5444-5451.

Murena, F. (2000). Kinetics of sulphur compounds in waste tyres pyrolysis. Journal of Analytical and Applied Pyrolysis, 56, 195-205.

National Agricultural Statistics Service (1995). Agricultural statistics. Washington D.C.: U.S. Department of Agriculture.

Olazar, M.; Lopez, G.; Arabiourrutia, M.; Elordi, G.; Aguado, R.; Bilbao, J. (2008). Journal of Analytical and Applied Pyrolysis, 81, 127-132.

Onay O, Beis S, Kockar O (2001). Fast pyrolysis of rape seed in a well-swept fixed-bed reactor. Journal of Analytical and Applied Pyrolysis, 58-59, 995-1007.

Pindoria R, Megaritis A, Messenbock R, Dugwell D, Kandiyoti R (1998). Comparison of the pyrolysis and gasification of biomass: effect of reacting gas atmosphere and pressure on Eucalyptus wood. Fuel, 77(11), 1247-1251.

Quek, A.; Balasubramanian, R. (2009). Journal of Hazardous Materials, 166, 126-132.

Ranz W (1952, May). Friction and transfer coefficients for single particles and packed beds. Chemical Engineering Progress, 48(5), 247-253.

Rao R, Sharma A (1998). Pyrolysis rates of biomass materials. Energy, 23(11), 973-978.

Rath, J.; Wolfinger, M.G.; Steiner, G.; Krammer, G.; Barontini, F.; Cozzani, V. (2003). Fuel, 82, 81-91.

Roberts AF (1970). A review of kinetics data for the pyrolysis of wood and related substances.Combustion and Flame, 14(2), 261-272.

Roberts, A.F.; Clough, G. (1963). Thermal Decomposition of Wood in an Inert Atmosphere. Ninth Symposium (International) Combustion, New York, 158.

Rodrigues I, Coelho J, Carvalho M (2012). Isolation and valorisation of vegetable proteins from oilseeds plants: methods, limitations and potential. Journal of Food Engineering, 109, 337-346.

Rubber Manufacturers Association, U.S. Scrap Tire Management Summary 2005-2009, RMA, October 2011.

Saft, R.J. (2007). Journal of Life Cycle Assessment, 12(4), 230-238.

Sanchez ME, Menendez JA, Dominguez A, Pis JJ, Martinez O, Calvo LF, Bernad PL (2009). Effect of pyrolysis temperature on the composition of the oils obtained from sewage sludge. Biomass and Bioenergy, 22, 922-940.

Senneca, O.; Salatino, P.; Chirone, R. (1999). Fuel, 78, 1575-1581.

Sircar, A.K.; Lamond, T.G. (1973). Carbon black transfer in blends of cis-poly(butadiene) with other elastomers. Journal of Applied Polymer Science, 17, 2569.

Sharma A, Rao R (1999). Kinetics of pyrolysis of rice husk. Bioresource Technology, 67, 53-59.

Singh R, Shadangi K (2011). Liquid fuel from castor seeds by pyrolysis. Fuel, 90, 2538-2544.

Solantausta, Y.; Bridgwater, A.T.; Beckman, D. (1995). Biomass & Bioenergy, 9(1-5), 257-269.

Sun S, Tian H, Zhao Y, Sun R, Zhou H (2010). Experimental and numerical study of biomass flash pyrolysis in an entrained-flow reactor. Bioresource Technology, 101, 3678-3784.

Thangalazhy-Gopakumar S, Adhikari S, Ravindran H, Gupta RB, Fasina O, Tu M, Fernando SD (2010. Physicochemical properties of bio-oil produced at various temperatures from pine wood using an auger reactor. Bioresource Technology, 101, 8389-8395.

Thomas, P.H.; Bowes, P.C. (1961). Some aspects of self-heating and ignition of solid cellulosic materials. British Journal of Applied Physics, 12, 222.

Ucar, S.; Karagoz, S.; Yanik, J.; Yuksel, M.; Saglam, M. (2007). Upgrading scrap tire derived oils using activated carbon supported metal catalysts. Energy Sources, 29(4-8), 425-437.

Unapumnuk, K.; Keener, T.C.; Lu, M.; Khang, S.J. (2006). Journal of the Air & Waste Management Association, 56(5), 618-627.

United States Environmental Protection Agency Website, Highway, Nonroad, Locomotive, and Marine Diesel Fuel Standards, URL: http://www.epa.gov/otaq/standards/fuels/diesel-sulfur.htm.

University of Manchester, Carbon steel thermal properties, URL: http://www.mace.manchester.ac.uk/project/research/structures/strucfire/, 2012.

US Department of Energy (2012). Feedstock types. Consulted on February 1st, 2012, sur http://www1.eere.energy.gov/biomass/feedstocks_types.html

USDA Forest Service (2007). Timber Product Output Database. Consulted on January 2012, on Forest Inventory Analysis: http://fia.fs.fed.us

Van der Drift A, Boerrigter H, Coda B, Cieplik M, Hemmes K (2004). Entrained flow gasification of biomass. ECN.

Varhegyi G, Bobaly B, Jakab E, Chen H (2011, January). Thermogravimetric study of biomass pyrolysis kinetics: a distributed activation energy model with prediction tests. Energy & Fuels, 25(1), 24-32.

Waldron K (2010). Bioalcohol production: biochemical conversion of lignocellulosic biomass. Taylor & Francis Group.

Wang H, Srinivasan R, Yu F, Steele P, Li Q, Mitchell B (2011). Effect of acid, alkali and steam explosion pretreatments on characteristics of bio-oil produced from pinewood. Energy & Fuels, 25, 3758-3764.

Watanabe I, Yong C, Hasatani M, Yushen X, Naruse I (1991). Gas to particle heat transfer in fast fluidized beds. Circulating Fluidized Bed Technology III, Pergamon Press, 283-287.

Weiland N, Means N, Morreale B (2012, April). Product distributions from isothermal co-pyrolysis of coal and biomass. Fuel, 94, 563-570.

Wendlandt W (1982, April). Thermal analysis. Analytical Chemistry, 54(5), 97R-105R.

Westmoreland, P.R.; Gibson, J.B.; Harrison, D.P. (1977). Comparative kinetics of high temperature reaction between H2S and selected metal oxides. Environment Science & Technology, 11(5), 488-491.

Williams, P.T.; Besler, S.; Taylor, D.T. (1990). Pyrolysis of scrap automotive tyres. The influence of temperature and heating rate on product composition. Fuel, 69, 1474-1482.

Yang, J.; Kaliaguine, S.; Roy, C. (1993). Improved quantitative determination of elastomers in tire rubber by kinetic simulation of DTG curves. Rubber Chemistry and Technology, 66, 213.

Yang, J.; Roy, C. (1996). A new method for DTA measurement of enthalpy change during the pyrolysis of rubbers. Thermochimica Acta, 288, 155-168.

Yang, J.; Roy, C. (1995). AIChe Journal, 41, 1500-1512.

Yang, J.; Tanguy, P.A.; Roy, C. (1995). Heat transfer, mass transfer and kinetics study of the vacuum pyrolysis of a large used tire particle. Chemical Engineering Science, 50(12), 1909-1922.

Yang WC (2003). Handbook of fluidization and fluid-particle systems (Chemical Industries). CRC Press.